ISSN 2636-8498

Environmental Research & Technology

Year 2023
Volume 6
Number 1

YTU PRESS

www.ert.yildiz.edu.tr

ISSN 2636-8498

Environmental Research & Technology

Volume 6 Number 1 Year 2023

ISSN 2636-8498

Environmental Research & Technology

Volume 6 Number 1 Year 2023

ISSN 2636-8498

Environmental Research & Technology

Volume 6 Number 1 Year 2023

CONTENTS

Research Articles

Environ Res Tec, Vol. 6, Issue. 1, pp. 1–7, March 2023

Environmental Research and Technology
https://ert.yildiz.edu.tr - https://dergipark.org.tr/tr/pub/ert
DOI: https://doi.org/10.35208/ert.1150621

Environmental Research & Technology

Research Article

Investigation into the possibility of using a novel ionic liquid leaching method to obtain vanadium from vanadium slag

Johannes Herman POTGIETER*[1,2], Samaneh TEIMOURI[1]

[1]*School of Chemical and Metallurgical Engineering, University of the Witwatersrand, Johannesburg, South Africa*
[2]*Department of Natural Sciences, Faculty of Science and Engineering, Manchester Metropolitan University, Chester Street, Manchester, UK*

ARTICLE INFO

Article history
Received: 15 August 2022
Revised: 06 December 2022
Accepted: 06 January 2023

Key words:
Vanadium slag; Ionic liquids; Vanadium extraction; Iron extraction; Pollution reduction

ABSTRACT

An environmentally friendly, novel method for extracting vanadium from slag with two imidazolium-based ionic liquids, namely1-butyl-3-methylimidazolium trifluoromethane sulfonate [$Bmim^+CF_3SO_3^-$], and 1-butyl-3-methyl-imidazolium hydrogen sulfate [$Bmim^+HSO_4^-$], before and after magnetic separation, was proposed in this study. The effect of the type of ionic liquid, the concentration of ionic liquid, temperature and liquid to solid ratio were examined. The optimum experimental condition after examining these influential factors was found to be: ionic liquid [$Bmim^+HSO_4^-$] 50% (v/v), a leaching temperature of 100 °C, and a liquid to solid ratio of 12 ml/g (12:1), at a leaching time of 90 min, with shaking speed of 250 rpm. The results indicated that a maximum vanadium extraction of 94.2% with 57.6% iron as an impurity could be achieved from the non-magnetic slag fraction. The kinetics of vanadium dissolution in 50% (v/v) [$Bmim^+HSO_4^-$] was governed by a surface chemical reaction with an estimated E_a= 65.5 kJ/mol.

Cite this article as: Potgieter JH, Teimouri S. Investigation into the possibility of using a novel ionic liquid leaching method to obtain vanadium from vanadium slag. Environ Res Tec 2023;6:1:1–7.

INTRODUCTION

Vanadium is one of the most important base metals and can be found in different primary and secondary resources worldwide [1]. The main raw material for the extraction of vanadium is titanomagnetite ore, which accounts for about 85% of vanadium production [2]. During the steelmaking process, vanadium is concentrated in a high-grade slag, which is a by-product of the process. The high-grade slag is widely used as a secondary raw material to extract vanadium [3]. The base metal is resistant to corrosion, has high fatigue resistance, and increases the hardness and tensile strength of steels to which it is added [4]. Therefore, vanadium has been used in the production of high-strength steels, as electrolytes in redox flow batteries, catalysts, and also in ferrous and non-ferrous alloys. In addition to these uses, vanadium as a critical raw material is used in electric mobility, defense and space applications. It also enables the transition to renewable energy sources by its use in long-duration energy storage (LDES) solutions [5].

***Corresponding author.**
*E-mail address: herman.potgieter@wits.ac.za

This paper has been presented at Sixth Symposium on Circular Economy and Urban Mining (SUM 2022)/Capri, Italy / 18–20 May 2022.

The commonly used process for the extraction of vanadium from both vanadium slag and titanomagnetite ore is the sodium roast-leach method. In some cases, a mixture of the three sodium salts (NaCl, Na_2CO_3, and Na_2SO_4) is added to the filtered cake and the mixture is fed to a rotary kiln to be roasted at a temperature range of 700–1200 °C. The roasted ore or slag is then leached using water to form the pregnant solution, from which vanadium can be precipitated as ammonium metavanadate (AMV), using ammonium sulphate ($(NH_4)_2SO_4$) [6]. This process is cost-effective, since the reagents used during the roasting stage are relatively cheap. Additionally, the sodium salt used in the process is selective towards vanadium in the ore or slag to form sodium metavanadate ($NaVO_3$), but some impurities i.e. Fe, S, K, Cr can also be extracted. Using water as a lixiviant gives the process the advantage of a relatively high vanadium extraction of 60–85% at a controlled pH of 5. To improve vanadium extraction during the leaching stage, water can be substituted by sulphuric acid [6].

Chen et al. [7] investigated roasting with NaOH molten salt for titaniferous magnetite ore. In the sodium roasting process, the sodium oxidation forms the vanadium oxides to water-soluble sodium vanadate and concurrently the reduction of iron oxides to metallic iron also occurred. Subsequently, water leaching achieved a satisfactory vanadium extraction of 84.5%, iron 89.4%, and titanium 95.6%. In another research, Zhang et al. [8] proposed substituting the sodium salts with calcium oxide for roasting at 850 °C for 2.5 h, followed by sulphuric acid leaching, precipitation, and calcination to recover vanadium pentoxide from the ore. The achieved vanadium extraction under these conditions was 93.3%.

Li [9] examined a calcium roasting method, followed by ammonium carbonate $(NH_4)_2CO_3$ leaching. The method succeeded to be selective towards vanadium, hence, reducing the amount of impurities, and AMV is formed directly during the leaching stage. A maximum vanadium extraction of 96.0% was obtained with this process. Li et al. [10] substituted sodium salts with potassium salts, followed by sulphuric acid leaching. The conditions were as follows: potassium salt roasting at a temperature of 900 °C for 1 h, 10% (v/v) sulfuric acid concentration, liquid to solid ratio of 3 ml/g, leaching temperature 95 °C, and leaching time 1.5 h, which yielded an extraction efficiency of 71.4% for vanadium. Liu & Meng [4] decreased the amount of impurities leached when using non-salt roasting, followed by alkaline leaching.

However, these modifications do not properly address the disadvantages of the roast-leach process, such as (a) emission of toxic and corrosive gases, i.e. hydrogen chloride (HCl), chlorine (Cl_2), and sulfur dioxide (SO_2) [1], (b) high energy consumption in the roasting step, (c) extraction of impurities i.e. S, K, Cr, during leaching which increase capital costs in the refinery stage [6–8].

To overcome these problems, this investigation aimed to examine the feasibility of imidazolium-based ionic liquids (ILs), such as 1-butyl-3-methylimidazolium trifluoromethane sulfonate [$Bmim^+CF_3SO_3^-$], and 1-butyl-3-methyl-imidazolium hydrogen sulfate [$Bmim^+HSO_4^-$], to extract vanadium efficiently from vanadium slag with high iron content, without including a roasting step. Some reports suggested [11] that imidazolium-based ionic liquids can decrease the reaction time and enhance the recovery yield. While the extraction of other metals such as gold, silver, copper, titanium, and aluminium by using the imidazolium-based ionic liquid (IL) have been investigated, few studies could be found in the literature on vanadium extraction by ILs. Only Bell & Castleman [12] reported an unsuccessful attempt to leach vanadium oxide using 1-butyl-3-methylimidazolium trifluoromethane sulfonate [$Bmim^+CF_3SO_3^-$]. This investigation focused to identify which IL results in the maximum extraction of vanadium from V-bearing slag before and after magnetic separation and to establish under which conditions it could be achieved. To this end, two different ILs, their varying concentrations, various liquid to solid ratios and a number of leaching temperatures were investigated. These two ILs were selected to examine the effect of ionic liquids having the same cationic part as [$Bmim^+$] and different anionic parts as [$CF_3SO_3^-$] and [HSO_4^-] to extract the target metals.

MATERIALS AND EXPERIMENTAL PROCEDURE

Materials

The vanadium slag containing a high metallic iron content was supplied by Powder Tech, a company located in Brits in South Africa. The ILs 1-butyl-3-methylimida-zolium trifluoromethane sulfonate [$Bmim^+CF_3SO_3^-$] (IL-A), 1-butyl-3-methyl-imidazolium hydrogen sulfate [$Bmim^+HSO_4^-$] (IL-B), and sulphuric acid (98%) were bought from ACE Chemicals (Pty.) Ltd. These two IL have been selected since other researchers used them in their work also, and that facilitates comparisons. Moreover, the IL-B [$Bmim^+HSO_4^-$], is able to act as a Brønsted acid by releasing proton [H^+] into an aqueous solution owing acidic properties [13].

Experimental Procedure

The slag was crushed using a jaw crusher and then milled into a fine powder using a Zieb pulverizing mill. The initial particle size of the slag was ~20 mm, then after crushing in the jaw crusher become ~1mm. To make the crushed material finer, they were put in the Zieb pulverizing mill which milled them to a fine powder with a particle size of D_{80}= 45 µm. The bulk chemical composition of the slag is presented in Table 1, as measured by X-ray fluorescence (XRF). XRF powder method was carried out on a Rigaku-ZSX Primus II instrument using SQX analysis software. The instrument settings during operation was 60 kV and 150 mA.

Table 1. Bulk chemical composition of vanadium slag (wt.% except V* in ppm)

Component	Fe_2O_3	SiO_2	TiO_2	MnO	Cr_2O_3	CaO	Al_2O_3	P_2O_5	V*	LOI
Content (wt.%)	46.03	17.94	13.38	10.91	1.61	1.53	1.25	0.12	163.04*	7.1

Table 2. Range of investigated experimental parameters

Parameters	Studied range				
Type of IL	[$Bmim^+CF_3SO_3^-$] (IL-A)			[$Bmim^+HSO_4^-$] (IL-B)	
IL concentration (v/v)	10%	20%	30%	40%	50%
Temperature (°C)	45	60	75	90	100
Liquid to solid ratio (ml/g)	5	6	8	10	12

Slag samples were treated in a magnetic separator to obtain a magnetic and non-magnetic fraction for further leaching. Sulphuric acid solutions with concentrations of 15%, 30%, 50% and 70% (w/w) were used for the initial leaching runs. A 10 ml volume of the different acid concentrations was mixed with 1 g of slag sample to ensure a liquid-to-solid ratio of 10 ml/g (10:1). These samples were leached under reflux condition with a condenser attached to the leaching flask stirring at a speed of 250 rpm, for 90 min at 100 °C. After 90 min, the mixture was filtered, and a 5 ml aliquot of the filtrate was pipetted into a 100 ml volumetric flask and made up to the mark. These diluted samples were analysed using atomic absorption spectrometry (AAS-Varian model A2000) to measure vanadium and iron content.

To investigate the effect of the IL concentration, a 10 ml IL/distilled water solution (IL-A and IL-B) with concentrations of 10%, 20%, 30%, 40% and 50% (v/v), was mixed with 1 g slag (magnetic and non-magnetic portion) with liquid to solid ratio (10:1). Then the samples were placed in the shaker with a speed of 250 rpm, at a temperature of 100 °C, for 90 min. The effect of varying temperatures on the leaching process was evaluated by using 10 ml 50% (v/v) solution of IL/distilled water mixed with 1 g slag sample to ensure a liquid to solid ratio of 10 ml/g. These samples were placed in the ultrasonic bath for 60 min at 60 °C, before they were leached at the following temperatures: 45, 60, 75, 90, 100 °C in the shaker with a speed of 250 rpm, for 90 min. To study the effect of the liquid to solid ratio on the V and Fe extraction, IL-A and IL-B with 50% (v/v) concentration was mixed with specific amount of the slag sample (magnetic and non-magnetic) to make different liquid to solid ratios of 5, 6, 8, 10, 12 ml/g. Table 2 listed the investigating parameters and their studied range. All experimental runs were carried out in duplicate to ensure good repeatability and average values are reported.

It was assumed that the total amount of vanadium and iron contained in the sample is the amount leached using 70% (w/w) sulphuric acid. Recoveries of each element were calculated as follows:

$$\%Vanadium\ Extraction = [V\ leached\ by\ IL/\ V\ leached\ by\ H_2SO_4] \times 100 \quad (1)$$

$$\%Iron\ Extraction = [\mathrm{Fe}\ leached\ by\ IL/\ \mathrm{Fe}\ leached\ by\ H_2SO_4] \times 100 \quad (2)$$

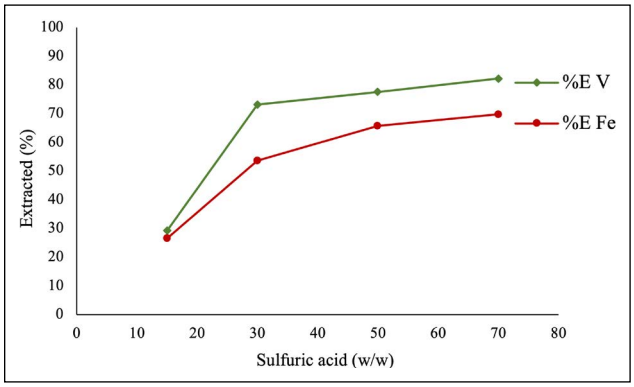

Figure 1. The effect of sulphuric acid concentration on V and Fe extracted from the vanadium slag sample. Conditions: liquid to solid ratio of 10 (mg/l), stirring speed 250 rpm, at 100 °C for 90 min.

RESULTS AND DISCUSSION

Vanadium and Iron Extraction Before Magnetic Separation

To determine the vanadium and iron before magnetic separation, sulphuric acid solutions with concentrations of 15%, 30%, 50% and 70% (w/w) were used for the initial leaching runs. A 10 ml aliquot of the different acid concentrations was mixed with 1 g of slag sample to ensure a liquid to solid ratio of 10 ml/g (10:1). These samples were leached for 90 min in a shaker, at a temperature of 100 °C. Then the mixture was filtered, and a 5 ml aliquot of the filtrate was pipetted into a 100 ml volumetric flask and made up to the mark. These diluted samples were analysed using AAS to measure vanadium and iron content. Figure 1 displays the results obtained in terms of the concentration of vanadium and iron contained in the solution when the slag sample was leached using sulphuric acid at different concentrations. The maximum amount of vanadium and iron was 61 mg/l, and 384 mg/l, respectively from the slag sample before magnetic separation with 70% sulphuric acid. These values were considered as the total amount of vanadium and iron in the slag and were used when calculating percentage recoveries.

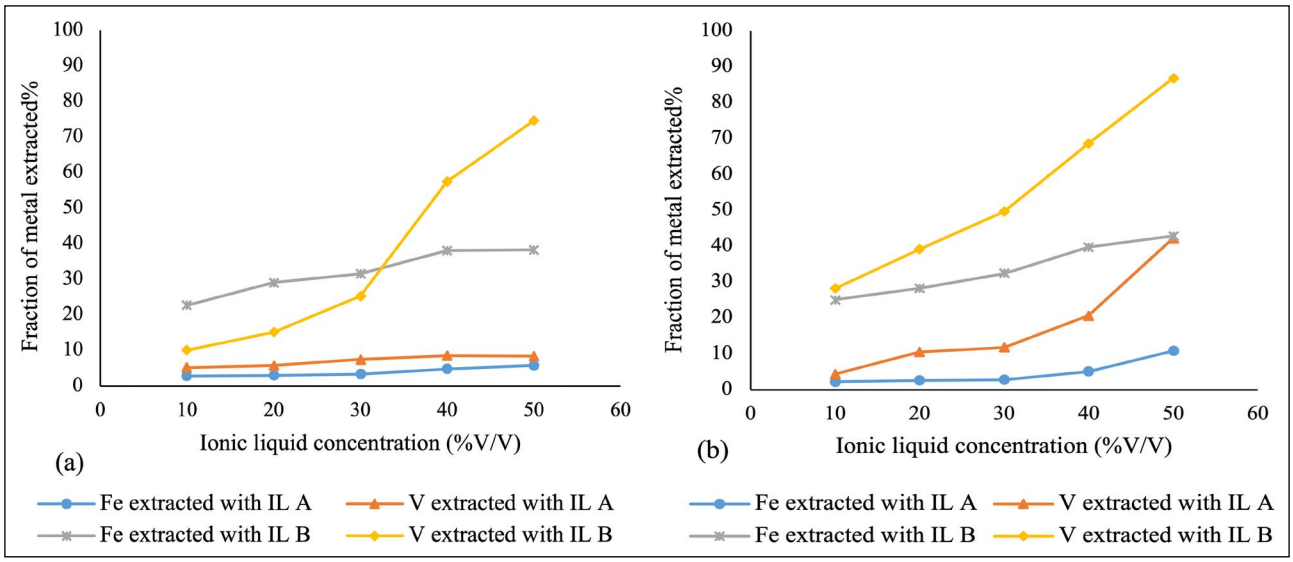

Figure 2. The effect of the IL (A & B) concentration on V and Fe extraction from **(a)** magnetic and **(b)** non-magnetic slag. Conditions: liquid to solid ratio of 10 (mg/l), stirring speed 250 rpm, at 100 °C for 90 min.

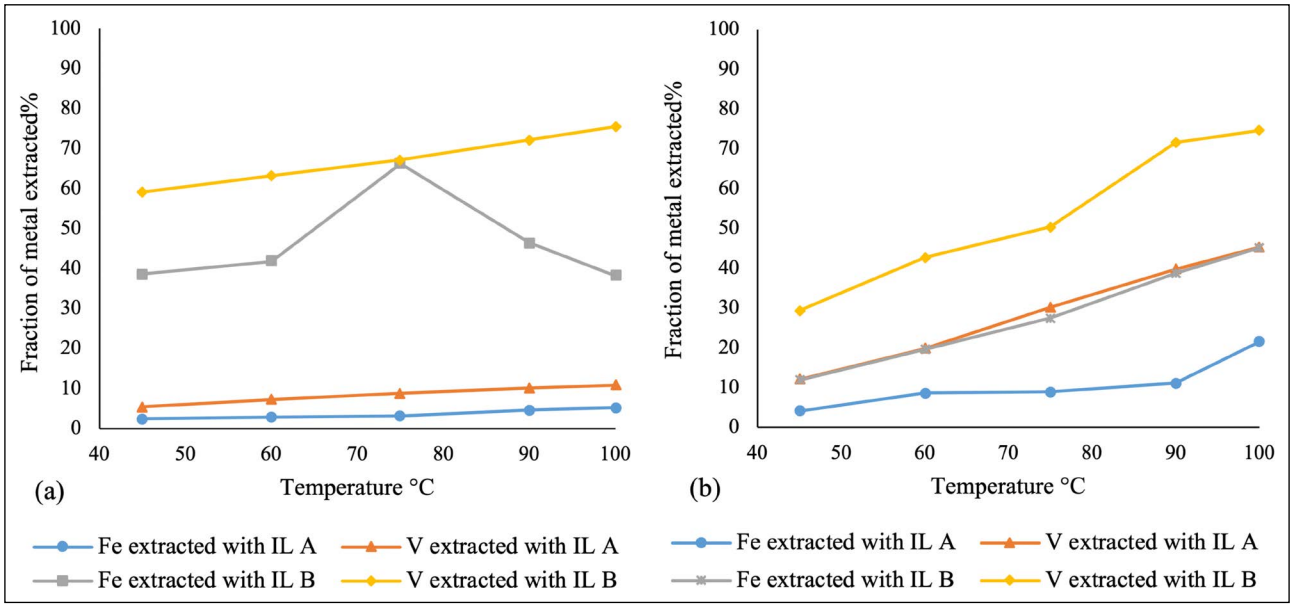

Figure 3. The effect of temperature from 45 to 100 °C on V and Fe extraction from **(a)** magnetic and **(b)** non-magnetic slag. Conditions: 10 ml IL (A & B) 50% (v/v) solution, liquid to solid ratio of 10 (mg/l), stirring speed 250 rpm, for 90 min.

Vanadium and Iron Extraction From the Magnetic and Non-Magnetic Slag Portions

Two different ILs were used to leach the magnetic and non-magnetic portions of the slag sample to investigate how the IL concentration, the liquid to solid ratio and the leaching temperature affect the recovery of vanadium and iron. Analyses indicated that the magnetic portion of the slag contained at least 10 times the amount (mass) of V compared to the non-magnetic portion, while the mass of Fe was at least twice as high in the magnetic portion as in the non-magnetic portion of the slag after separation.

The Effect of Ionic Liquid Concentration

Two different ILs [$Bmim^+CF_3SO_3^-$] (IL-A), and [$Bmim^+HSO_4^-$] (IL-B) were used to leach the magnetic and non-magnetic portions of the slag sample to investigate the effect of the IL concentration from 10% to 50% (v/v) on vanadium and iron extraction. The results are illustrated in Figure 2a, b. With 50% IL-B, 74.6% V and 38.7% Fe was extracted from the magnetic slag. It is evident that the magnetic separation increased the extraction of V to 86.9%, and Fe to 42.9% (Fig. 2b - non-magnetic slag). In comparison to IL-B, IL-A resulted in substantially less V and Fe with only 8.4% and 5.8% ex-

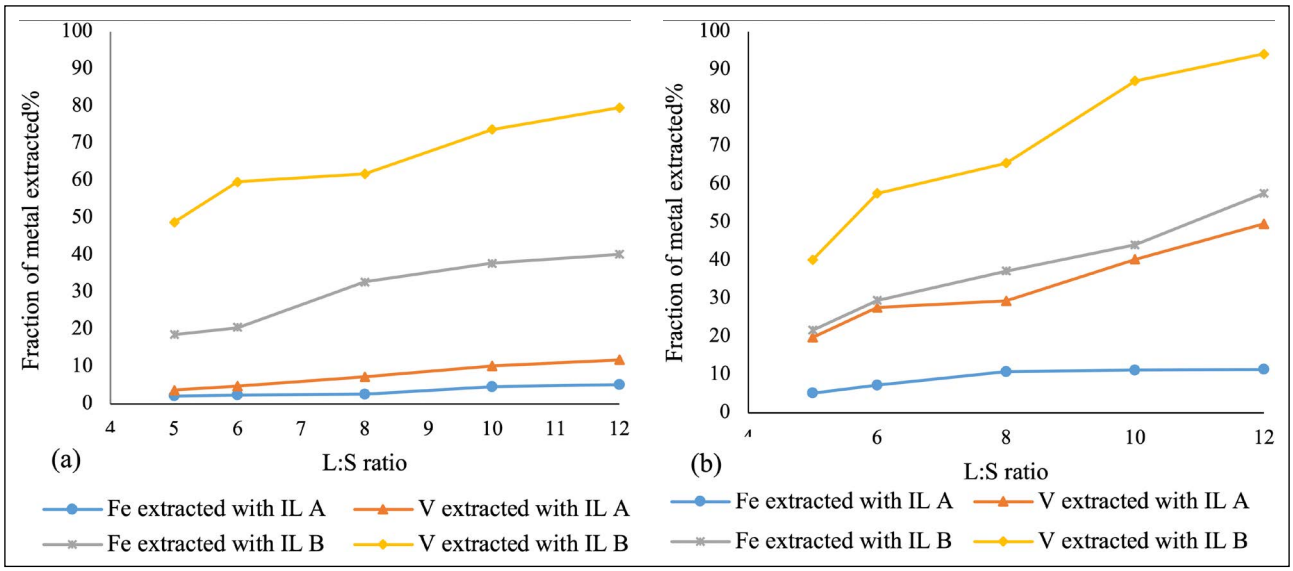

Figure 4. The effect of the solid-to-liquid ratio in the range of 5, 6, 8, 10, and 12 ml/g on V and Fe extraction from **(a)** magnetic and **(b)** non-magnetic slag. Conditions: 10 ml IL (A & B) 50% (v/v), stirring speed 250 rpm, at 100 °C for 90 min.

Table 3. Summary of V and Fe extraction with IL-B ($Bmim^+HSO_4^-$)

Studied factors	IL-B 50% (v/v)		Temperature 100 °C		L:S ratio (12:1)	
Extraction	%V	%Fe	%V	%Fe	%V	%Fe
Magnetic portion	74.6	38.3	75.5	38.2	79.6	40.2
Non-magnetic portion	86.9	42.9	74.6	45.1	94.2	57.6

traction, respectively from the magnetic slag portion. However, with IL-A, V and Fe extraction improved to 42.8% and 10.8%, respectively from the non-magnetic slag. Therefore, 50% (v/v) [$Bmim^+HSO_4^-$] (IL-B), was the better IL for V and Fe extraction from magnetic and non-magnetic slag portions.

The Effect of the Leaching Temperature

The effect of varying temperature on the leaching process was evaluated by using 10 ml of a IL at a concentration of 50% (v/v) with 1 g slag sample (magnetic and non-magnetic slag) to ensure a liquid to solid ratio of 10 ml/g. These samples were placed in the ultrasonic bath for 60 min at 60 °C, before they were leached at the following temperatures: 45, 60, 75, 90, 100 °C. As presented in Figure 3a, b, increasing the temperature generally leads to an increased V and Fe extraction for both the IL-A and IL-B. The reason is that, increasing the temperature improve the diffusion and the reaction rate leading to higher extraction. Thus, 100 °C was chosen as the optimum operating temperature. At 100 °C, IL-B extracted 75.5% V and 38.2% Fe from the magnetic portion of the slag. When considering the non-magnetic portion of the slag, the same IL-B achieved 74.6% V and 45.1% Fe at 100 °C. In contrast, IL-A extracted 10.8% V and 5.2% Fe from the magnetic slag, and 45.2% V and 21.5% Fe from the non-magnetic slag portions.

The Effect of Liquid-to-Solid Ratio

To examine the effect of the liquid-to-solid ratio, the IL-A and IL-B with 50% (v/v) concentration were mixed with a specific amount of the slag sample (magnetic and non-magnetic) to make different liquid-to-solid ratios of 5, 6, 8, 10, 12 ml/g. Figure 4a, b illustrates the effect of the solid-to-liquid ratio on V and Fe extraction from magnetic and non-magnetic slag. Generally, vanadium extraction increases with increasing the volume of the IL used for leaching. This is to be expected and in line with the mass transfer theory, which states that an increasing concentration gradient with an increasing liquid-to-solid ratio is the driving force for mass transfer [14]. A liquid-to-solid ratio of 12 ml/g (12:1) was therefore chosen as the optimum practical ratio. At this liquid-to-solid ratio IL-B yielded V and Fe of 94.2% and 57.6%, respectively from the non-magnetic portion of the slag (Fig. 4b), and slightly less from the magnetic portion (Fig. 4a) as 79.6% V and 40.2% Fe. With IL-A, 11.8% V and 5.2% Fe extraction were obtained from the magnetic slag, and it improved in the non-magnetic slag fraction to 49.6% V and 11.4% Fe.

A summary of the results on the optimum point for the studied factors with IL-B [$Bmim^+HSO_4^-$] which was the better IL for the magnetic and non-magnetic portion for V and Fe extraction is summarised in Table 3.

Kinetic Model

Leaching is a reaction between solid particles and liquid which is defined as a heterogeneous reaction. The reaction occurs at the interface of the leaching agent and a solid phase. The general leaching reaction can be defined as follow:

$$A_{(l)} + bB_{(S)} \rightarrow cC$$

Table 4. Shrinking core model equations as limiting step

	Limiting step	Equation	R^2	Rate constant
1	Diffusion through the product layer (SP)	$1 - 3(1 - X)^{2/3} + 2(1 - X) = k.t$	0.94	0.003
2	Diffusion through the product layer (CP)	$X + (1 - X)\ln(1 - X) = k.t$	0.95	0.004
3	Diffusion through the liquid film (SP)	$X = k.t$	0.99	0.009
4	Surface chemical reactions (CP)	$1 - (1 - X)^{1/2} = k.t$	0.99	0.006
5	Surface chemical reactions (SP)	$1 - (1 - X)^{1/3} = k.t$	0.98	0.004
6	New shrinking core model	$1/3\ln(1 - X) + [(1 - X)^{-1/3} - 1] = k.t$	0.87	0.001

*[SP = Spherical Particle & CP = Cylinder Particle]

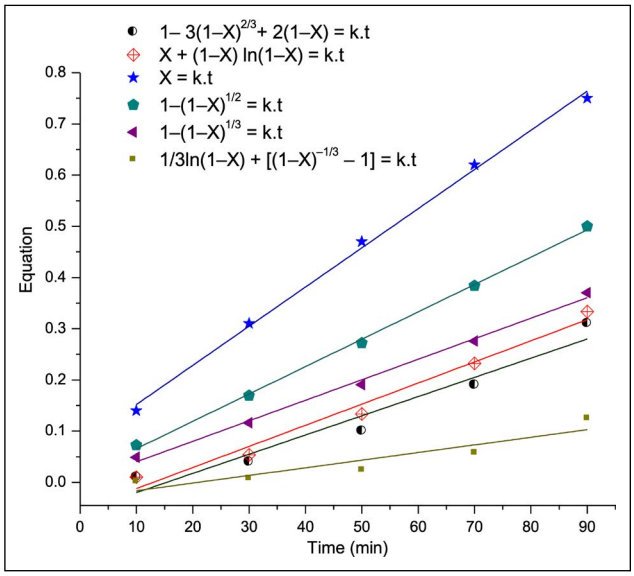

Figure 5. Different SCM model equation fittings.

Where A is the leaching agent (liquid), B is the solid phase (the particles), and C is the produced product(s). Typically, during leaching the following steps happen sequentially: diffusion of the leaching agent through the thin liquid film surrounding the solid particle, chemical reaction on the surface of the solid particle, and diffusion of the leaching agent through the product. The slowest step acts as a limiting step and controls the kinetics of dissolution [15].

To determine the kinetics of vanadium dissolution in 50% (v/v) IL-B ($Bmim^+HSO_4^-$), the experimental results at time intervals of 10, 30, 50, 70, and 90 min at 100 °C were evaluated using the shrinking core model. Considering the solid particles can be spherical and/or cylinder, the fitness of the different equations for diffusion, chemical reaction, and the new equation (mixed model) as a limiting step controlling the kinetics of vanadium dissolution were assessed.

To do so, the function of each equation versus time was plotted to obtain the correlation coefficient (R^2). Table 3 tabulated the list of the evaluated equations as a limiting step, the obtained correlation coefficient (R^2), and the rate constant. The trendline with R^2 close to one indicates the most suitable equation fitting to the experimental results. In this case, the surface chemical reaction (spherical and/or cylinder particles) controls the kinetics of vanadium dissolution in 50% (v/v) IL-B ($Bmim^+HSO_4^-$). Figure 5 illustrates the function and the fitness of each equation versus time.

Since the surface chemical reaction indicates the best fit of the results, the slope of the straight line presenting the functionality of the chemical reaction (Δ) in Figure 5, was taken as the rate constant (k) to estimate the activation energy as 65.5 kJ/mol. The value of the obtained activation energy is >40 kJ/mol, which is another indication that the surface chemical reaction is controlling the kinetics of the dissolution reaction [13].

CONCLUSIONS

The following conclusions can be drawn from this investigation:

- Of the two ILs which were used in this investigation, the aqueous solutions of the IL-B [$Bmim^+HSO_4^-$] emerged as a better extractant than the IL-A [$Bmim^+CF_3SO_3^-$].
- Magnetic separation concentrates the amount of vanadium and iron in the magnetic portion of the sample, leading to improved vanadium extraction, even though the recovery percentages of the non-magnetic fraction were higher than in the magnetic fraction.
- Under the investigated parameters, the optimum conditions for leaching were: IL-B [$Bmim^+HSO_4^-$] with 50% (v/v) concentration, a temperature of 100 °C, and L:S of 12:1.
- Maximum extraction of 94.2% V and 57.6% Fe was achieved from the non-magnetic portion of the slag sample.
- A surface chemical reaction controls the kinetics of vanadium dissolution in 50% (v/v) IL-B [$Bmim^+HSO_4^-$]
- The effectiveness of the different ionic liquids under different conditions to extract various amounts of V and Fe, coupled with magnetic separation of the material in two different fractions, offers the opportunity to design a process to separate the V and Fe in the slag for further recovery and purification.

- This study demonstrated the viability of a direct leaching method using imidazolium-based ILs to extract vanadium from the slag in yields comparable to traditional pyrometallurgical and hydrometallurgical means, with no emission of toxic gases, and considerably lower energy requirement compared to the conventional roast-leach method.

The study is incomplete in that it still needs to illustrate that:

- Recycling the ionic liquid to be reused in the extraction process would lead to less consumption than conventional acids in the leaching solution.
- Ionic liquids have large electrochemical "windows/ranges" which offer the potential for metal recovery and recycling after electrochemical recovery of V and/or Fe.

Follow-up work currently underway involves investigating the final separation of the V and Fe from the leach solution in such a way that the ionic liquid can be recycled. We also plan future work with other types of ionic liquids.

Acknowledgements
Ms. E. Matsobane and Ms K. Kebongile are acknowledged for their assistance with the experimental work.

DATA AVAILABILITY STATEMENT

The authors confirm that the data that supports the findings of this study are available within the article. Raw data that support the finding of this study are available from the corresponding author, upon reasonable request.

CONFLICT OF INTEREST

The authors declared no potential conflicts of interest with respect to the research, authorship, and/or publication of this article.

ETHICS

There are no ethical issues with the publication of this manuscript.

REFERENCES

[1] R. R. Moskalyk, and A. M., Alfantazi, "Processing of Vanadium: A review," Minerals Engineering, Vol. 16(9), pp. 793–805, 2003. [CrossRef]

[2] L. Zhang, and S. Zheng, "Acid leaching of calcined vanadium titanomagnetite with calcium compounds for extraction of vanadium," Chinese Journal of Process Engineering, Vol. 11(4), pp. 573–578. 2011.

[3] D. Huang, "Vanadium extraction & steelmaking," Metallurgy Industry Press, 2000.

[4] B. Liu, and L. Meng, "A novel method to extract vanadium from high-grade slag: Non-salt roasting and alkaline leaching," Physicochemical Problems of Mineral Processing, Vol. 54(3), pp. 657–667, 2018.

[5] R. Navarror, "Vanadium recovery from oil fly ash by precipitation and solvent extraction processes," Waste Management, Vol. 27(3), pp. 114–119, 2007. [CrossRef]

[6] S. Nkosi, and N. Dire, "A comparative study of vanadium recovery from titaniferous magnetite using salt, sulphate, and soda ash roast-leach processes," In: 3rd Young Professionals Conference: Innovation Hub. Pretoria: The Southern African Institute of Mining and Metallurgy, pp. 191–200, 2017.

[7] D. Chen, L. Zhao, and Y. Liu, "A novel process for recovery of iron, titanium and vanadium from titanomagnetite concentrate: NaOH molten salt roasting and water leaching," Journal of Hazardous Materials, Vol. 244–245, pp. 588–595, 2013. [CrossRef]

[8] J. Zhang, W. Zhang, and L. Zhang, "Mechanism of vanadium slag roasting with calcium oxide," International Journal of Mineral Processing, Vol. 138, pp. 20–29, 2015. [CrossRef]

[9] H. Li, K. Wang, and W. Hua, "Selective leaching of vanadium in calcification-roasted vanadium slag by ammonium carbonate," Hydrometallurgy, Vol. 160, pp. 18–25, 2016. [CrossRef]

[10] R. Li, T. Liu, and Y. Zhang, "Efficient extraction of vanadium from vanadium- titanium magnetite concentrate by potassium salt roasting additives," Minerals, Vol. 8(25), pp. 1–14, 2018. [CrossRef]

[11] T. Welton, "Ionic liquids in catalysis. coordination chemistry reviews," Vol. 248(21–24), pp. 2459–2477, 2004. [CrossRef]

[12] R. Bell, & A. W. Castleman, "Vanadium oxide complexes in room-temperature chloroaluminate molten salts," Inorganic Chemistry, Vol. 38, pp. 5709–5715, 1999. [CrossRef]

[13] C. L. Aguirre, N. Toro, N. Carvajal, H. Watling, and C. Aguirre, "Leaching of chalcopyrite (CuFeS2) with an imidazolium-based ionic liquid in the presence of chloride," Minerals Engineering, Vol. 99, pp. 60–66, 2016. [CrossRef]

[14] R. Treybal, "Mass transfer operations," McGraw-Hill, 1955.

[15] F. Faraji, and A. Alizadeh, F. Rashchi, and N. Mostoufi, "Kinetics of leaching: A review," Reviews in Chemical Engineering, Vol. 1, pp. 1–36, 2020.

Environ Res Tec, Vol. 6, Issue. 1, pp. 8–12, March 2023

Environmental Research and Technology
https://ert.yildiz.edu.tr - https://dergipark.org.tr/tr/pub/ert
DOI: https://doi.org/10.35208/ert.1208362

Environmental Research & Technology

Research Article

Chemical disinfectants detoxify wastewater containing various organic substances

Sarwoko MANGKOEDIHARDJO[*1], Latifa Mirzatika AL-ROSYID[1,2]

[1]*Department of Environmental Engineering, Institut Teknologi Sepuluh Nopember, Surabaya, Indonesia*
[2]*Universitas Muhammadiyah Jember, Jember, Indonesia*

ARTICLE INFO

Article history
Received: 22 November 2022
Revised: 27 December 2022
Accepted: 01 February 2023

Key words:
Diseases; Healthy; Microorganisms; Mixed organic matter; Toxicity effect; Zebrafish

ABSTRACT

The use of disinfectants is intensive and widespread during the pandemic. Disinfectants are mixed with various organic wastewater substances, and also resuspend from the soil surface during the rainy season, which are eventually discharged into river waters. This study aimed to assess the potential of alcohol in detoxifying wastes containing organic substances so as to secure their disposal into water bodies. Preparation of organic substance solutions, aquatic test biota, and measurement of substance concentration parameters, as well as substance toxicity to biota, were all carried out using international standard laboratory protocols. In addition, real wastewater containing various organic substances was also investigated. It was revealed that the toxicity rating of organic substances to microbes was in line with their toxicity rating to zebrafish aquatic biota indicator. The toxicity rating of organic substances to microbes was expressed in the ratio of biological to chemical oxygen demand. The acute lethal concentration of half the number of zebrafish was a rating of the toxicity of organic substances to aquatic biota. Both of these toxicity measures were closely related to the solubility properties of substances in organic matter, which were expressed as octanol-water partition coefficient values. A very important finding was the potential of alcohol to detoxify wastewater containing mixed organic substances to secure its discharge into water bodies. This supports the continued use of alcohol disinfectants as a health protocol in daily life.

Cite this article as: Mangkoedihardjo S, Al-Rosyid LM. Chemical disinfectants detoxify wastewater containing various organic substances. Environ Res Tec 2023;6:1:8–12.

INTRODUCTION

The use of disinfectants is indefinite and without limitations on environmental health conditions. Disinfectants in various forms have been formed to eliminate disease-causing microbes. Sunlight is one of the physical disinfectants that have formed naturally, which we know existed before human life on earth. The development of human life and disease problems has broadened and deepened knowledge to produce various disinfectants, both physical and chemical forms. Responding to the problem of the COVID-19 pandemic, chemical disinfectants have become one of the health protocols for everyone around the world. Various formulations of chemical disinfectants are available and used. Of particular concern are glycerol [1], isopropyl alcohol [2], and ethanol [3]. The use of disinfectants is predicted

***Corresponding author.**
*E-mail address: prosarwoko@gmail.com

to continue even after the pandemic ends. The consequence is the enrichment of organic matter in wastewater, both from personal hygiene and existing wastewater production [4] and treatment processes [5].

Meanwhile, the wastewater generated in daily life also contains various types of organic substances. More attention to organic substances in daily wastewater is the content of oxalic acid, acetic acid, lactose, sucrose, glucose, and formaldehyde. Oxalic acid is a cleaning agent for laundry and household appliances from stains on metal [6]. Acetic acid is one of the common fermented food products in addition to many organic substances sourced from foodstuffs, which are generally lactose, sucrose and glucose [7]. Often foods contain naturally occurring formaldehyde, which is intentionally added as a preservative even though its use must be limited [8]. All existing organic matter content and new enrichment in wastewater becomes an urgency for its treatment [9] discharge into water bodies [10], as well as evaluation of existing wastewater plans [11].

Therefore, this research was carried out with a new approach in the form of alcohol disinfectant as a detoxification of organic wastewater. The first objective was to obtain a rating of the toxicity of organic substances to microbes and to freshwater indicator biota. The second objective was to determine the potential of alcohol-type disinfectants to secure waste disposal into freshwater bodies.

MATERIALS AND METHODS

The following organic substances were of pro-analytical quality for laboratories, i.e., lactose, sucrose, glucose, oxalic acid, acetic acid, formaldehyde, glycerol, isopropyl acid, and ethanol. The first six organic substances were solution materials as a simulation of organic wastewater. The next three organic substances were alcohol disinfectants. Each organic matter solution was measured for biological oxygen demand (BOD) and chemical oxygen demand (COD) content based on [12, 13]. and prepared in various concentrations of 10 mg/L, 100 mg/L, and 1,000 mg/L.

The aim was to rank the BOD/COD ratio as a measure of the level of toxicity of organic substances to microbes. Each organic substance was also measured in terms of octanol water partition (Pow) based on [14] to assess the lipophilic properties of the substance. Each substance parameter was measured in three replications, thus, the data obtained were nine measurements of the concentration of each organic substance. The result of which was the average.

Furthermore, each organic substance underwent an acute toxicity test for 96 h on the indicator biota of zebrafish *Brachydanio rerio* to secure the discharge of effluent into freshwater bodies. Probit statistical analysis was used to determine the lethal concentration of the substance on biota [15].

The mixture of organic substances in simulated wastewater was proportional to the volume and its toxicity against *B. rerio* was calculated using the following equations:

$$\boldsymbol{M = \sum_{i=1}^{n} TUi} \quad (1)$$

Where *TUi* was equal to the sum of the toxicity units of each substance [16]. The toxicity unit (*TU*) was the reciprocal of the lethal concentration of the substance to 50% of the test biota (*LC-50*).

$$\boldsymbol{TU = \left(\frac{1}{LC-50}\right)} \quad (2)$$

The Equation 2 was derived from researchers [16–19] and has been used by other researchers [20].

The mixed effect can be evaluated according to the values of *M* and *Mo* under the following arrangements:

$$\boldsymbol{Mo = \left(\frac{M}{maxTUi}\right)} \quad (3)$$

The mixed effect assessment was stated as follows:

$M < 1$:	Synergistic
$M = 1$:	Simple additive
$M = Mo$:	Independent
$M > Mo$:	Antagonism
$Mo > M > 1$:	Partial additive

The mixture of organic substances simulating wastewater that has synergistic toxicity properties then undergoes the addition of an alcohol disinfectant. In this mixture of wastewater and disinfectant, BOD and COD measurements were carried out as well as a 96 h acute toxicity test for *B. rerio*. This mixture is to assess the antagonistic toxicity properties, which indicates the potential of alcohol as detoxification of organic wastewater.

Wastewater samples in the field which actually contain various organic substances are taken from the residential landscape of domestic activities and where the wastewater is discharged into rivers [21, 22]. Real wastewater samples were tested to assess their suitability with the simulation results of the organic matter mixture. The selected wastewater samples were those containing BOD and COD of less than 1,000 mg/L in accordance with the limits of the concentration of the tested organic substances.

RESULTS

The results of the measurement of the parameters of organic substances in the wastewater simulation group were presented in Table 1. Specifically, the BOD/COD ratio was simply the calculation of the results of the two parameters, and the *TU* was calculated using Equation 2.

Based on the TU results in Table 1, a mixture of all wastewater organic substances in equal volume proportions yields M < 1 (Equations 1 and Equation 3). This means that any mixture of organic substances has the potential for a syner-

Table 1. Organic matter parameters and toxicity to *B. rerio*

Organic matter solution	BOD (mg/L)	COD (mg/L)	BOD/COD	Pow	LC-50-96 h-*B. rerio* (mg/L)	TU of substance
Lactose	7.7–750.7	8.3–962.0	0.8–0.9	0.7–0.8	851	0.0012
Sucrose	5.7–495.3	7.3–954.0	0.5–0.8	0.7–1.4	685	0.0015
Glucose	4.2–452.0	6.3–899.0	0.4–0.7	0.7–1.1	372	0.0027
Oxalic acid	0.8–114.7	7.7–796.0	0.1–0.3	1.1–2.3	42	0.0238
Acetic acid	1.7–158.7	6.7–792.0	0.2–0.4	0.7–1.6	30	0.0333
Formaldehyde	0.8–98.7	5.3–123.0	0.1–0.2	0.7–4.5	24	0.0417

Table 2. Lethal concentration of mixed organic matter by addition of alcohol to *B. rerio*

A mixture of substances in equal volume proportions	BOD (mg/L)	COD (mg/L)	BOD /COD	LC-50-96 h- B. rerio (mg/L)	Toxicity properties of the mixture
Sucrose+Acetic acid+Glycerol	11.8–814.7	15.3–1,051.0	0.8–0.8	205	Antagonistic due to Glycerol
Acetic acid+Formaldehyde+Isopropyl alcohol	0.8–52.9	1.4–98.8a	0.5–0.6	191	Antagonistic due to Isopropyl alcohol
Oxalic acid+Formaldehyde+Ethanol	0.7–83.5	2.0–299.0	0.3–0.4	59	Antagonistic due to Ethanol

Table 3. Toxicity of real wastewater contains a variety of organic substances

Samples	BOD (mg/L)	COD (mg/L)	BOD/COD	LC-50-96 h- *B. rerio* for real wastewater
Household wastewater	108.0	200.0	0.54	188
Laundry and textile washing wastewater	446.0	960.0	0.46	78

gistic effect, which increases its toxicity to *B. rerio*. Therefore, the results of this experiment deliberately divided the toxicity of organic substances at the LC-50 limit of 100 mg/L. In this case, the low toxicity was LC-50 >100 mg/L, and the high toxicity was LC-50 < 100 mg/L, for both microbes and *B. rerio*.

With the LC-50 limit, further experiments were carried out for mixtures of low and high toxicity organic substances, and mixtures of high toxicity organic substances with the addition of alcohol disinfectant. In the settings, glycerol was added to the mixture of sucrose (LC-50 > 100 mg/L) and acetic acid (LC-50 < 100 mg/L), all of which were in the same volume proportion. Likewise, for mixing organic substances that have an LC-50 < 100 mg/L with the addition of isopropyl alcohol and ethanol. The results of the measurement of BOD, COD, and toxicity parameters of the mixture were presented in Table 2.

Table 2 showed the addition of alcohol to wastewater containing a mixture of organic substances produces an antagonistic effect that reduces its toxicity to *B. rerio*. Therefore, these disinfectants are capable of detoxifying organic matter, which protects the life of biota in water bodies.

The results of the real wastewater toxicity study were presented in Table 3. The Pow parameter of the real wastewater was of course not measured. This was because the content of organic substances was not specific apart from being a mixture of various organic substances. The LC-50-96 h results against *B. rerio* were for real wastewater that has been enriched with alcohol disinfectant during the pandemic.

DISCUSSION

The results of the study of single organic substances Table 1 shows the BOD/COD ratio in the range of easily biodegradable (more than 0.5) and non-biodegradable, or toxic to microbes (less than 0.5). As the results of previous studies [23], the range of the BOD/COD ratio was closely related to the Pow range, where biodegradable organic substances have a Pow smaller than the Pow of non-biodegradable substances. The Pow results show that biodegradable organic substances were hydrophilic, whereas non-biodegradable organic substances were lipophilic, which easily accumulates into the biomass of biota. Thus, the lipophilic nature of the organic substance explains its toxicity to microbes.

Similarly, the results of LC-50-96 h-*B. rerio* for non-biodegradable organic substances showed less than biodegradable organic substances. This indicates that non-biodegradable organic substances become more toxic to *B. rerio*.

Again, the toxicity of organic substances to *B. rerio* is due to the lipophilic nature of organic substances, which easily accumulate into *B. rerio*.

The association of Pow with the toxicity of organic substances to microbes and *B. rerio* has been in line with and confirms the results of previous studies by other researchers [24–26]. All of them use different organic substances from each other, thus strengthening the correlation between Pow, accumulative properties of substances, and toxicity of substances to biota.

The aforementioned results of the laboratory studies can be applied to respond to the use of disinfectants that enrich the quality of wastewater and even to runoff during the rainy season. Especially for wastewater containing BOD and COD of not more than 1,000mg/L, people need not worry too much about the effects of discharging disinfectant-rich wastewater into fresh water bodies as previously designed and practiced. This was evidenced by the results of research for real wastewater in Table 3, which shows a fairly high ratio of BOD/COD and LC-50-96 h. Both were considered biodegradable and less toxic to aquatic biota. During this three-year pandemic, there have been no reports of damage to water quality and aquatic biota with the exception of microbes.

However, careful attention needs to be paid to wastewater that has a BOD and COD concentration of more than 1,000 mg/L, such as leachate from the degradation of solid waste in landfills. In this condition, other detoxification methods are needed that are able to reduce BOD and COD below 1,000 mg/L, such as wetland treatment involving a variety of plants [27]. Plants are resistant to alcohol disinfectants [28].

CONCLUSIONS

The first objective of this study has been achieved by showing that the toxicity rating of organic substances to microbes is the same as their toxicity rating to zebrafish. The second but more important objective is the toxicity of alcohol disinfectants to microbes but has the potential to reduce the toxicity of organic mixtures to zebrafish. This is a representation of the potential ability of alcohol disinfectants to detoxify organic wastewater that is safely discharged into water bodies. Therefore, the use of alcohol as a microbial disinfection does not worsen the chemical quality of the environment and its effect on macro biota.

The limitation of this research was the mixture of organic substances based on the same volume proportion. The concentration of each organic substance was a maximum of 1,000 mg/L. Therefore, further research is needed regarding the proportion of the mixture of organic substances, which optimally reduces its toxicity to zebrafish. In addition, the concentration of organic matter should be increased to more than 1,000 mg/L.

Acknowledgements
The authors gratefully acknowledge financial support from the Institut Teknologi Sepuluh Nopember for this work, under project scheme of the Publication Writing and Intellectual Property Rights Incentive Program (PPHKI) 2023.

DATA AVAILABILITY STATEMENT

The authors confirm that the data that supports the findings of this study are available within the article. Raw data that support the finding of this study are available from the corresponding author, upon reasonable request.

CONFLICT OF INTEREST

The authors declared no potential conflicts of interest with respect to the research, authorship, and/or publication of this article.

ETHICS

There are no ethical issues with the publication of this manuscript.

REFERENCES

[1] K. Abuga and N. Nyamweya, "Alcohol-based hand sanitizers in COVID-19 prevention: A multidimensional perspective," Pharmacy, Vol. 9(1), Article 64, 2021. [CrossRef]

[2] W. A. Rutala, and D. J. Weber, "Guideline for Disinfection and Sterilization in Healthcare Facilities, 2008," Healthcare Infection Control Practices Advisory Committee HICPAC, Vol. 2019, pp. 163, 2019.

[3] World Health Organization, "Cleaning and disinfection of environmental surfaces in the context of COVID-19, Interim Guidance," World Health Organization, 2020. [CrossRef]

[4] M. Razif, V. E. Budiarti, and S. Mangkoedihardjo, "Appropriate fermentation process for tapioca's wastewater in Indonesia," Journal of Applied Sciences, Vol. 6(13), pp. 2846–2848, 2006. [CrossRef]

[5] S. Mangkoedihardjo, "Physiochemical performance of leachate treatment, a case study for separation technique," Journal of Applied Sciences, Vol. 7(23), pp. 3827–3830, 2007. [CrossRef]

[6] J. Cui, N. Zhu, D. Luo, Y. Li, P. Wu, Z. Dang, and X. Hu, "The role of oxalic acid in the leaching system for recovering ındium from waste liquid crystal display panels," ACS Sustainable Chemistry & Engineering, Vol. 7(4), pp. 3849–3857, 2019. [CrossRef]

[7] O. J. Odell, T. Podlogar, and G. A. Wallis, "Comparable exogenous carbohydrate oxidation from lactose or sucrose during exercise," medicine and science in sports and exercise, Vol. 52(12), pp. 2663–2672, 2020. [CrossRef]

[8] F. Nowshad, M. N. Islam, and M. S. Khan, "Concentration and formation behavior of naturally occurring formaldehyde in foods," Agriculture & Food Security, Vol. 7(1), pp. 1-8, 2018. [CrossRef]

[9] S. Mangkoedihardjo, "Individual or communal sanitation services?: Decision based on wastewater storage capacity," Advances in Natural and Applied Sciences, Vol. 4(3), pp. 226–228, 2010.

[10] G. Samudro and S. Mangkoedihardjo, "Urgent need of wastewater treatment based on BOD footprint for aerobic conditions of receiving water," Journal of Applied Sciences Research, Vol. 8(1), pp. 454–457, 2012.

[11] S. Mangkoedihardjo, "A new approach for the Surabaya sewerage and sanitation development programme 2020," Advances in Natural and Applied Sciences, Vol. 4(3), pp. 233–235, 2010.

[12] APHA 5210, "Biochemical oxygen demand (BOD)," APHA, 2017.

[13] APHA 5220, "Chemical oxygen demand (COD)," APHA, 2017.

[14] OECD, "Test no. 123: Partition coefficient (1-Octanol/Water): Slow-stirring method. Paris: Organisation for Economic Co-operation and Development," 2022. Available at: https://www.oecd-ilibrary.org/environment/test-no-123-partition-coefficient-1-octanol-water-slow-stirring-method_9789264015845-en Accessed on Sep 17, 2022.

[15] OECD, "Test no. 203: Fish, acute toxicity test. Paris: Organisation for Economic Co-operation and Development, 2019. Available at: https://www.oecd-ilibrary.org/environment/test-no-203-fish-acute-toxicity-test_9789264069961-en Accessed on Sep 17, 2022.

[16] Y. Dong, Z. Fang, Y. Xu, Q. Wang, and X. Zou, "The toxic effects of three active pharmaceutical ingredients (APIs) with different efficacy to Vibrio fischeri," Emerging Contaminants, Vol. 5, pp. 297–302, 2019. [CrossRef]

[17] K. Fischer, S. Sydow, J. Griebel, S. Naumov, C. Elsner, I. Thomas, A. A. Latif, and A. Schulze, "Enhanced removal and toxicity decline of diclofenac by combining uva treatment and adsorption of photoproducts to polyvinylidene difluoride," Polymers, Vol. 12(10), Article 2340, 2020. [CrossRef]

[18] S. H. Lee, I. Kim, K. W. Kim, and B. T. Lee, "Ecological assessment of coal mine and metal mine drainage in South Korea using Daphnia magna bioassay," SpringerPlus, Vol. 4(1), pp. 1–13, 2015. [CrossRef]

[19] A. Qiu, Q. Cai, Y. Zhao, Y. Guo, and L. Zhao, "Evaluation of the treatment process of landfill leachate using the toxicity assessment method," International Journal of Environmental Research and Public Health, Vol. 13(12), Article 1262, 2016. [CrossRef]

[20] F. Gholami-Borujeni, F. Nejatzadeh-Barandozi, and H. Aghdasi, "Data on effluent toxicity and physicochemical parameters of municipal wastewater treatment plant using Daphnia Magna," Data in Brief, Vol. 19, pp. 1837–1843, 2018. [CrossRef]

[21] H. Samudro, G. Samudro, and S. Mangkoedihardjo, "Prevention of indoor air pollution through design and construction certification: A review of the sick building syndrome conditions," Journal of Air Pollution and Health, Vol. 7(1), pp. 81–94, 2022. [CrossRef]

[22] H. Samudro and S. Mangkoedihardjo, "Indoor phytoremediation using decorative plants: An overview of application principles," Journal of Phytology, Vol. 13(6), pp. 28–32, 2021. [CrossRef]

[23] L. M. Al-Rosyid and S. Mangkoedihardjo, "Relationship between BOD/COD ratio and octanol/water partition coefficient for glucose, lactose, sucrose, formaldehyde, acetic acid and oxalic acid," International Journal of Civil Engineering and Technology, Vol. 10(1), pp. 691–696, 2019.

[24] S. Afida and G. Razmah, "Partition coefficient, water solubility and aquatic toxicity of short-chain palm fatty acids," Journal of Oil Palm Research, Vol. 27(1), pp. 75–81, 2015.

[25] C. D. Schönsee and T. D. Bucheli, "Experimental determination of octanol–water partition coefficients of selected natural toxins," Journal of Chemical & Engineering Data, Vol. 65(4), pp. 1946–1953, 2020. [CrossRef]

[26] A. T. N. Do, Y. Kim, Y. Ha, and J. H. Kwon, "Estimating the bioaccumulation potential of hydrophobic ultraviolet stabilizers using experimental partitioning properties," International Journal of Environmental Research and Public Health, Vol. 19(7), 2022. [CrossRef]

[27] G. Samudro and S. Mangkoedihardjo, "Mixed plant operations for phytoremediation in polluted environments – a critical review," Journal of Phytology, Vol. 12, pp. 99–103, 2020. [CrossRef]

[28] Y. Ludang, HP. Jaya, and S. Mangkoedihardjo, "Potential applications of land treatment systems for disinfectant-rich wastewater in response to the COVID-19 health protocol: A narrative review," Journal of Environmental Health and Sustainable Development, Vol. 7(1), pp. 1525–1535, 2022. [CrossRef]

Environ Res Tec, Vol. 6, Issue. 1, pp. 13–20, March 2023

Environmental Research and Technology
https://ert.yildiz.edu.tr - https://dergipark.org.tr/tr/pub/ert
DOI: https://doi.org/10.35208/ert.1204883

Environmental Research & Technology

Research Article

Microplastic pollution in a small fishing port in Zonguldak/Türkiye

Gülçin DEMİREL BAYIK*, Elif AYDEMİR

Department of Environmental Engineering, Zonguldak Bülent Ecevit University, Zonguldak, Türkiye

ARTICLE INFO

Article history
Received: 15 November 2022
Revised: 03 January 2023
Accepted: 01 February 2023

Key words:
Blacksea; Microplastic pollution; Microplastic risk assessment; Sea pollution

ABSTRACT

In this study, the occurrence and morphology of microplastics in a small fishing port in the Black Sea were determined by bulk sampling and visually analyzed by a stereo microscope. Three sampling campaigns were carried out, two of which were after the opening of the legal fishing season. The average abundance of the microplastics was found to be 3417+1401 items/m^3. The determined microplastic concentration was 1.43 times higher on the day of the most intense fishing activities. No statistically significant differences were observed for the different sampling locations (coast, middle, and seaside). The most frequent microplastic colors observed were blue, followed by black, green, red, white and grey, while fibers represented the dominant shape. The prevalent size of microplastics was <50 µm which makes it easy to ingest by even the smaller fishes and introduce into the food chain as well. However the NP value which shows the bioavailability of microplastic was calculated as 0.72 indicating a low bioavailability (≤2).

Cite this article as: Demirel Bayık G, Aydemir E. Microplastic pollution in a small fishing port in Zonguldak/Türkiye. Environ Res Tec 2023;6:1:13–20.

INTRODUCTION

Plastic debris is described as "any persistent solid material that is manufactured or processed and directly or indirectly, intentionally or unintentionally, disposed of or abandoned into the marine environment or the Great Lakes" in UNEP Regional Seas Reports and Studies [1]. Plastics are exposed to the action of biological organisms and exogenous agents like solar radiation, wind, and waves after they are spread in the environment, which speeds up degradation through thermal, photo-oxidative, and mechanical stimuli. The breakdown of these plastic items creates microplastics (plastics< 5 mm; MPs). Microplastics (MPs) have now been discovered in almost every component of the aquatic environment, including seawater, lake water and beach and bottom sediments. Additionally, MPs have been found in a variety of aquatic animals, including mussels and fish, and it has been shown that they can transfer within the planktonic food web [2].

The diversity and composition of microplastics match consumption trends for plastic goods quite well. Primary microplastics are produced in tiny sizes and can be employed either directly, as the microbeads in toothpaste, soap, and facial cleansers, or as precursors in industrial production [3]. Anthropogenic activities, the hydrodynamic regime, and regional characteristics are linked to the spatial distribution and composition profile of microplastics. Areas with a lot of anthropogenic activity, such as those with industry, tourism, aquaculture, and residential processes, are high in

***Corresponding author.**
*E-mail address: gulcin.demirel@beun.edu.tr

microplastic concentration [4]. Aquacultural and fishing activities are one of the important anthropogenic sources in ponds, lakes and surface waters. Plastic ropes, nets, fences, boats, floats, cages, impermeable membranes, feeders, oxygenators, and packaging materials used during these activities are linked to the high abundance of microplastics in the marine environment [5]. Microplastics may be transported and deposited differently in coastal and marine environments due to hydrodynamic characteristics such as current velocity, turbidity, turbulence, and residual circulation [6]. The study of Liu et al. [4] reported that microplastic abundance was significantly influenced by the human population density, waste management efficiency, maritime activity and hydrodynamic conditions. In particular, the ratio of tidal range to average water depth showed a significantly negative correlation with microplastic abundance ($P<0.01$), whereas river plastic emissions and aquaculture production were significantly positively correlated with microplastic abundance ($P<0.01$). The methodological decisions, such as the pore size of filter paper (PSFP), density separation (DS), drying temperature (DT), sample depth (SD), identification method (IM), and digesting method (DM), had a significant impact on microplastic abundance as well ($P<0.05$). The mesh size of the filter is an important parameter when performing in situ monitoring because only particles larger than the mesh size are retained, the smallest microplastics are therefore missed and not counted. These small particles make up a significant portion of the total mass and the total number of microplastic particles expressed per volumetric unit [7]. It was discovered that the mean concentrations were two orders of magnitude higher when using a mesh size of 50 μm than when using a sample net of 330 μm. [8]. Microplastic transport is also influenced by the materials' own characteristics, such as particle size and surface modification, as well as other environmental factors (e.g., pH, light and dissolved organic matter) [4]. MPs consist of heterogeneous polymer mixtures of various shapes and sizes, and they can be unevenly distributed in the aquatic environment. Overall, plastics with a higher density than water, like polyesters (PES, 1.2–2.3 g/cm^3) or polyvinylchloride (PVC, 1.2–1.6 g/cm^3), are more prone to sink to the bottom [9]. In turn, the most produced polymers, such as polypropylene (PP), polyethylene (PE), and polystyrene (PS), have a density lower than or similar to that of water (0.9–1.1 g/cm^3), and they are more likely to disperse from their sources [2].

Large efforts have been undertaken to gather data on the prevalence of plastic in shorelines and the open sea, but few studies have concentrated on peculiar maritime habitats, such as ports. The port areas are constantly subjected to intense anthropogenic pressures that significantly degrade their quality. They serve as a source for spreading contaminants (including plastics) originating from land by connecting to the open sea [9]. Indeed, plastics entering the port region may be carried by water currents outside the basin but may also be impacted by sinking processes, just as in any other marine ecosystem [10]. Due to the regular dredging operations that result in silt resuspension from the bottom, ports are a peculiar example of a marine environment [11]. In addition to land inputs, ports are characterized by the high presence of boats and vessels, which can work as sources of plastics and microplastics (MPs) [12].

In the present study, MP contamination in a fishing port was investigated by in situ bulk sampling. Three sampling campaign was carried out, two of which is after the start of the fishing season. The abundance of microplastics was calculated and classified according to their size, shape and color. Microplastic bioavailability was calculated by the Nemerow Pollution Index (NPI).

MATERIALS AND METHODS

Study Area

The sampling was carried out in a small fishing port, shown in Figure 1, used mainly by small boats for fishing activities. The port is in the city of Zonguldak/Türkiye located in the western Anatolian part of the Black Sea. It is 390 m in wide and 170 m in length with a varying depth of 7–10 m. It is not used for commercial sea transportation and there are approximately 110–120 boats of different sizes registered. The sampling area was divided into 3 regions; the coast, middle and seaside. Four samples were collected at each region and a total of 12 samples were collected in each sampling campaign. Sampling was carried out on three different days in 2020 as; August 28, September 3 and September 21. A notable point in the sampling dates is that September 1 is the beginning of the legal fishing season in Türkiye.

Sampling and Analysis

Bulk surface water samples were collected from 0–60 cm depth with a metal bucket suspended from a fishing boat. The sampling method was adopted from literature studies with a modification of sample size [13, 14] Before sampling, all the materials were rinsed with first tap water then distilled water and then seawater (for each sampling point). A fisherman's boat was used to reach sampling points. At each sampling point, a metal bucket was immersed in water and 15 L sample was collected. Then it was passed through a 5 mm and 0.045 mm stainless steel sieve respectively. Bigger particles remaining on the 5 mm sieve were removed and the materials remaining on the 0.045 mm sieve were washed into glass jars with distilled water and stored at +4°C until analysis.

Pre analysis methods were carried out based on previous studies [15–17] At the laboratory, organic material was removed from the samples by acid ingestion. For this purpose, 10–25 ml of 30% Hydrogen Peroxide (H_2O_2) was added to the samples and were shaken at 80 rpm for 2 days. Mixing was

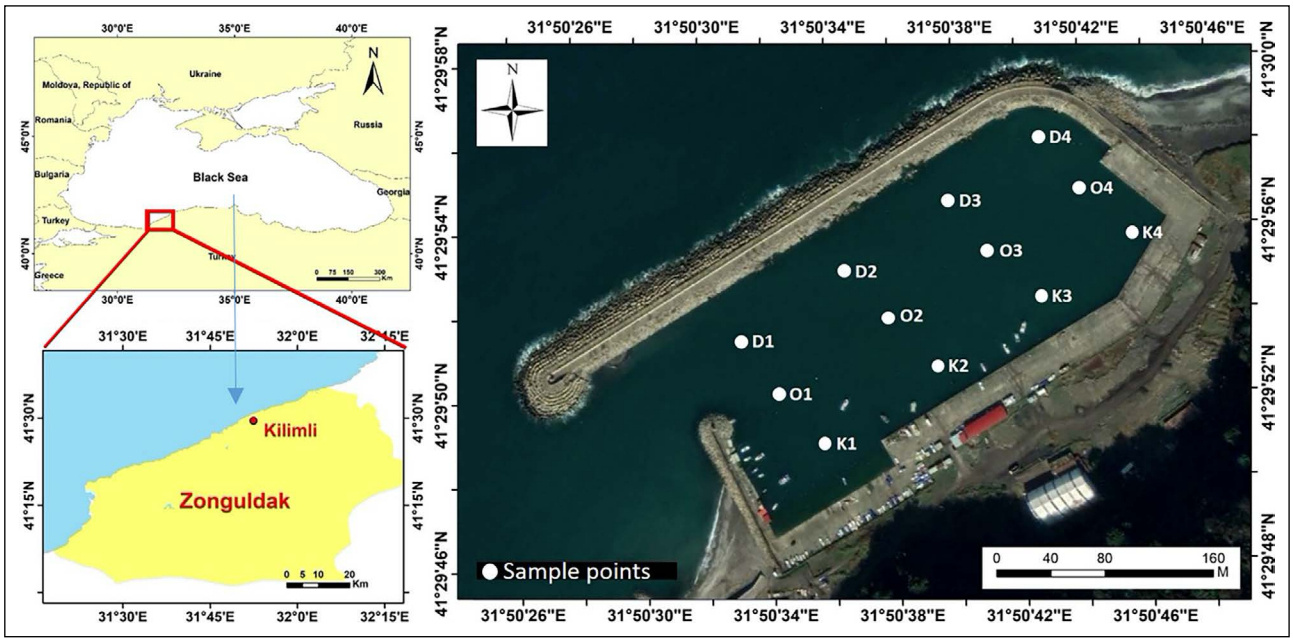

Figure 1. Sampling area and sampling points.

carried out at 40 °C to accelerate the reaction if necessary. The density separation was provided by adding saturated sodium chloride solution to the sample and by keeping it overnight. After filtering through a Whatman GF/C filter the samples were ready for visual analysis. Visual analyses were performed by Euromex NZ.1903-P stereo microscope equipped with ImageFocus Alpha software and a camera attached to it. The number, color (red, blue, green, black, yellow, white, transparent and others), shape (fiber, fragment, pellet, foam), and size of all detected microplastics were recorded.

Microplastic Bioavailability

Currently, no standardized procedure has been developed to assess the potential environmental risk of MPs exposure. However, the bioavailability of the microplastics in the port was calculated as in the study of Liu et al. [4] (2022) using Nemerow Pollution Index (NPI) by Equation 1.

$$NPI = \sqrt{\frac{\left(\frac{Ci}{Si}\right)max^2+\left(\frac{Ci}{Si}\right)ave^2}{2}} \quad (1)$$

where Ci represents the measured MP abundance and Si refers to the maximal regulatory abundance for regulatory standard [4] Si value was taken as 6650 particles /m^3 seawater [18]. When the NPI value is ≤2 the bioavailability level is low and if it is >2 then the bioavailability is high.

Statistical Analyzes

SPSS 15.0 was used to summarize the basic statistics and analyze the differences between the groups. The statistical significance of the difference between the sampling campaigns was evaluated by non-parametric statistical tests. Although parametric tests are more powerful tools to explain the differences between the groups, in cases where parametric test assumptions are not met, non-parametric tests can be used to examine these differences.

Table 1. Basic statistical results of microplastic abundance

Date	Statistical parameter (items/m^3)			
	Mean	Min.	Max.	Std. Dev.
Augu 28	2800	1200	5600	1393
Sept 3	3425	1400	5300	1404
Sept 21	4017	2500	5900	1239
Total	3417	1200	5900	1401

RESULTS AND DISCUSSION

Abundance of Microplastics

Microplastics were detected in all water samples collected from the Kilimli port and basic statistics are given in Table 1. A total of 1847 MP were determined at the end of three sampling campaigns (505 MP in August, 619 MP in September 3 and 723 MP in September 21) with an average of 3400±1400 items/m^3 and a range of 1200 to 5860 items/m^3. The average abundance of microplastics in the first and second sampling were 2800±1400 and 3400±1400 items/m^3 while it was determined slightly higher in the third sampling campaign as 4000±1230 items/m^3.

In this study, since the number of samples is small (<30) and the data is not normally distributed for each group

Table 2. Normality test and differences between the groups

Sampling date	Shapiro-Wilk			Friedman test	
	Statistic	df	Sig.	Mean rank	
Augu 28	0.810	12	0.012	1.50	Chi-Square: 6.00
Sept 3	0.908	12	0.199	2.00	Df :2
Sept 21	0.910	12	0.213	2.50	Asymp.Sig.: 0.05

Figure 2. Boats in the port on a routine day (top photos) and on September 21 (photo below).

(Shapiro-Wilk test), the Friedman test, which is the non-parametric equivalent of the one-way analysis of variance, was used to explain the differences between the groups (Table 2). In Table 2, it can be seen that the data of the second (Sept 3) and third (Sept 21) sampling campaigns shows a normal distribution ($p>0.05$), while the August sampling campaign did not ($p<0.05$). The difference between the groups was evaluated from the result of the Friedman test which indicates a significant difference between the three sampling dates ($p=0.05$). The mean rank column shows the order of the mean values where the MP abundance is the highest on the 3rd date, followed by the 2nd and the first date. The evidence about the impact of human activities on the presence of microplastics can be observed in the data. As mentioned before the first of September is the opening of the legal fishing season in Türkiye. After that day fishermen start heavy fishing activities using larger fishing nets instead of angling. Furthermore, even larger boats from other cities of the Black Sea participate in fishing activities in the port from time to time which was also encountered in the third sampling campaign of our study (Fig. 2).

The main sources of plastic pollution in the port are varying solid wastes arriving from owners of the boats and locals as a result of human activities. An unusual increase in human activities can also be associated with an increase in the amount of MP. Here, a prediction can be made about this relationship, but the effect of fishing activities on MP concentration can be proved by a more detailed sampling study. The big boats anchored in the port at the

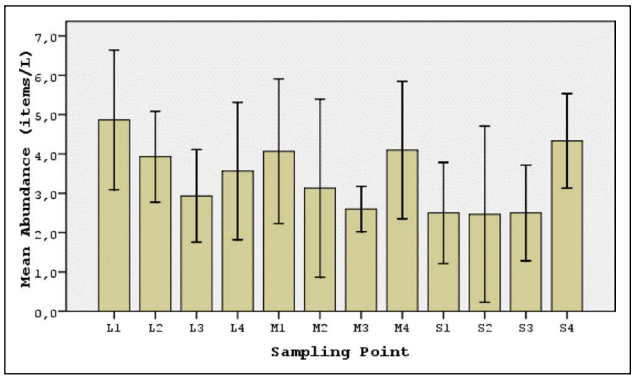

Figure 3. Microplastic distribution at sampling points along the port.

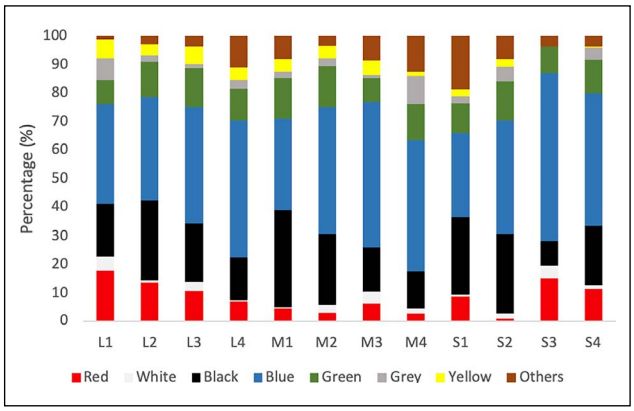

Figure 4. Color distribution of microplastics.

third sampling date were stuffing the fish into the crates and transporting them to trucks over a belt. This activity can be considered one of the unusual activities that may increase MP concentrations. In the field observations, plastic bottles, packaging wastes and styrofoam particles were recorded in addition to polypropylene grass carpets and piles of tools used in the fishing activities. All these wastes can act as microplastic sources degrading by sunlight, waves, and wind.

The distribution of MP along the sampling points given in Figure 3 shows that microplastic abundances were higher in land sampling points but the difference between the land, middle and seaside sampling points was not statistically significant ($p>0.05$). The maximum abundance of MP was 5900 items/m^3 at sampling point L1 and an average of 3800±1320 items/m^3. Because the boats are tied to the coast and launched to the sea from this region, there are lots of plastic sources like ropes, spherical plastic pontoons, and various plastic junk. The average number of microplastics in the middle and seaside samples were 3500±1430 and 3000±1400 items/m^3. It is difficult to compare the results of different microplastic studies because there is no uniform standard for recording microplastic data. Sampling methodologies, concerning particle size, time and date of sampling, and even quantification units differ for various studies [19]. The first study on MP pollution on the Anatolian coast of the Blacksea was conducted by Aytan et al. [20] (2016) on the southeastern coast of the region. Average microplastic abundance was 1.2±1.1 $\times$ 10^3 items/m^3 in November and 0.6±0.55 $\times$ 10^3 items/m^3 in February. The primary shapes were fibers (49.4%) followed by plastic films (30.6%) and fragments (20%), and no microbeads were found. In the study of Terzi et al. [21] (2022) MP concentration along the whole Anotalian part ot the blacksea was investigated. They reported a mean abundance of 18.68±3.01 items/m^3 and furthermore they concluded that the highest MP abundances were gathered from some of the sampling points at the western and Marmara region. The study of Sönmez and Sivri has reported a 0 to over 1 items/m^3 MP in İstanbul with a dominant size of 249–100 µm and color of transparent [22]. As can be seen microplastic concentrations fluctuate over a wide range of studies all over the world. The heterogeneity in the reported MP concentrations could be related to several factors as mentioned before. First of all, every sampling area/region is unique in terms of meteorological, hydrological, and hydrodynamic parameters in addition to the presence and diversity of natural and anthropogenic sources. Secondly, the lack of a standardized protocol for sampling and analysis is still a handicap in the field of microplastic research. While Egessa et al. reported 0.73 items/m^3 in Lake Victoria, a range of 21000–49000 items/m^3 were addressed in Manas River Basin, China [17, 23]. Filtering or digestion of organic materials could also affect the identified MPs. When considering the sampling location; the distance from the coast and the influence of hydrodynamic properties such as currents, up and downwelling, gyres and fronts could also be responsible for the heterogeneity in MPs concentrations [24]. Desforges et al. [25] reported 4–27 times greater microplastic concentrations at the nearshore sampling sites than the offshore in the ME Pacific Ocean. They also reported increased plastic sizes from coast to the offshore. A study by Garces-Ordonez et al. [26] 2022 investigates the effect of sampling depth, distance from river mouth and distance from population centers to microplastic concentrations. Although no relationship was reported for water depth, the microplastic concentration significantly decreases by distance to the river mouth and population center.

In our study, a small mesh size of 45 µm has resulted in relatively higher concentrations when compared to most of the studies. Schönlaua and friends investigated the microplastic concentration in open surface waters by using a manta trawl and in-situ filtering pump. They reported a higher concentration of microplastic particles in pump samples compared to trawl sampling. Moreover using a smaller mesh size of 0.05 mm has also resulted in higher concentrations [27].

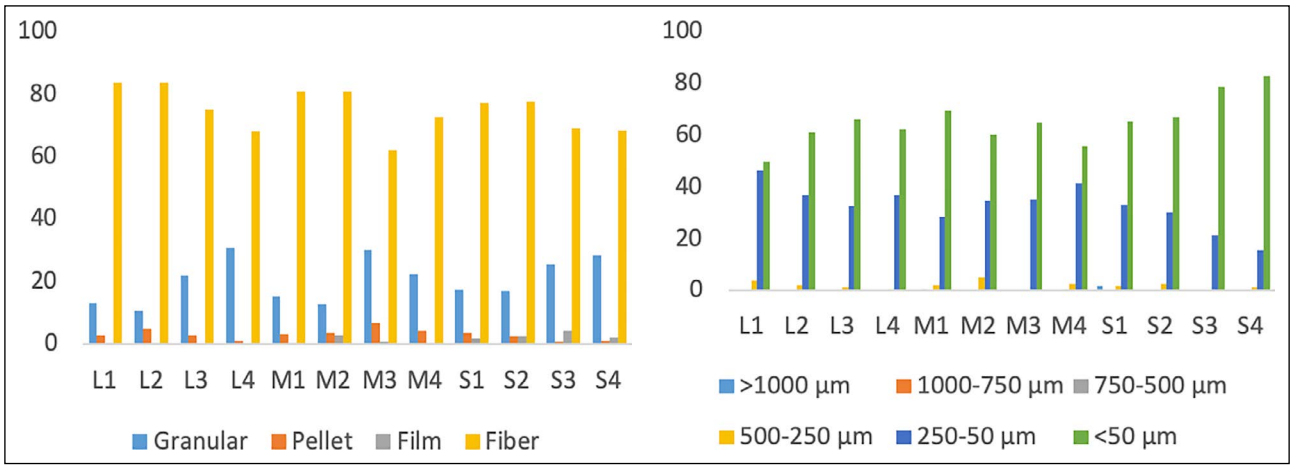

Figure 5. Shape and size distribution of microplastics.

Morphological Properties of Microplastics

Eleven different microplastic colors were observed under the microscope as; black, white, red, blue, green, grey, yellow, orange, purple, transparent and brown as shown in Figure 4. The dominant color was blue, followed by black, green, red, white and grey. The remaining colors were determined in a small number of samples so they were classified as others.

The shape and size distribution of the microplastics are presented in Figure 5. The most common forms of microplastics were fibers which are mostly blue in color and are over 60% in all sampling points. These fibers are thought to arrive from intense fishing activities by abrasion of fishing nets and lines. These results are consistent with field observations where blue fishing nets were recorded. The abundance of granular microplastics is between 12–31% followed by pellets 0.8–7% and films 0.46–4.42%.

The prevalent size of microplastics is <50 µm, followed by 50–250 µm and 250–500 µm. Microplastic with a size of >1000 µm, 750–1000 and 500–750 were detected in only one sample during the all sampling campaigns. The smaller size of determined microplastics can be suspected to be ingested by smaller fishes.

Bioavailability

The interacting of organisms with microplastics increases as a result of increasing environmental concentrations. It is well known that microplastics are available for ingestion by marine biota due to their small sizes. Microplastics can collect in the gut, the digestive gland, the gills, or the liver of some organisms after consumption or they can be moved along the digestive system until elimination [28]. Microplastics can have negative impacts on aquatic species when they are ingested or adsorbed to them. It can affect the number of species or their biomass at the population level and can have an impact on survival, reproduction, growth, feeding, emergence, embryonic development and photosynthetic effectiveness at the individual level. The severity of the effects varies depending on the properties of the microplastics, their concentrations and the exposure time [29]. Microplastic ingestion mainly depends on bioaccessibility. The NP value which shows the bioavailability of microplastic was calculated as 0.72 in our study which indicates a low bioavailability (≤2). High levels of bioavailability were reported for Beibu Golf and Sanggou Golf with NPI values being 8.48 and 4.42 respectively.

Energy and nutrient flow via both individual species and ecological networks may be affected by plastics. For that reason, it is crucial to understand the entry and transfer pathways of plastics through food webs. Jams and his friends have researched the relationship between the body length of an animal and ingested plastic size from published literature. They reported that animal body length alone explains 42% of the variation in the length of plastic an animal may ingest, resulting in a size ratio of about 20:1 between animal body length and the largest plastic the animal may ingest [30]. Their study has reported the relationship between ingested plastics and a minimum plastic size of 0.2 mm and a maximum of approx. 800 mm. Plastic sizes between 0.2 mm and 1 mm can be ingested by animals with a body length of 6–200 mm. Black Sea meets 76% of Türkiye's fish production. Of the fish caught from the Black Sea, 61.5% is anchovy, 26% is sprat, 4.3% is Black Sea horse mackerel and 2% is bonito. Their average body length is approx. 120, 130, 250 and 350 mm so these are susceptible to MP exposure. The study of Aytan et al. [20] proves the presence of MP in these species where they investigated the occurrence of MP in seven commercial fish species of the Black sea. They reported a 0.81±1.42 mean number of plastic particles per fish. Plastics were detected in 190 of the 650 fish analyzed of which 93.2% were micro (<5 mm), 6.5% meso (5–25 mm) and 0.3% were macroplastics (>25 mm). Fibers were the most frequent type of plastic (68.5%), followed by films (19%), fragments (11.9%), foams (0.3%), and microbeads

(0.3%). Black (39.3%) and blue (19.5%) were the most popular plastic colors, followed by transparent (18.1%). The length of plastics ranged from 0.05 to 26.5 mm with an average of 1.84±2.80 mm. The plastic occurrence was highest in bonita (plastic in 70% of the analyzed individuals [31].

Conclusion and prospects

This study was conducted to investigate microplastic pollution in a small fishing port, which can be considered as a closed marine environment. Our study has reported preliminary evidence about the effect of increasing fishing activities on microplastic abundance. The Black Sea has twice as much floating macro litter, mostly plastic, than the Mediterranean, according to a study on the environment funded by the European Union and the United Nations Development Programme (UNDP) [32]. The average abundance of MP was 3417+1401 items/m^3. A slight increase observed after the fishing season and between the two different fishing days shows the influence of fishing activities.

Further study is required that includes identification of the polymer types, the prevalence in the biota and indeed sediment samples. It is also necessary to evaluate the daily habits of the fisherman and test their awareness regarding the factors.

Acknowledgements
This study was funded by Bulent Ecevit University Scientific Research Funding Program with the project number of 2019-77047330-03. Authors would like to thank to Assoc. Dr. Çağlar BAYIK, Mr. Oral ERGÜL and diving supervisor Mr. Mustafa EKICI for their assistance during the sampling procedures.

DATA AVAILABILITY STATEMENT

The authors confirm that the data that supports the findings of this study are available within the article. Raw data that support the finding of this study are available from the corresponding author, upon reasonable request.

CONFLICT OF INTEREST

The authors declared no potential conflicts of interest with respect to the research, authorship, and/or publication of this article.

ETHICS

There are no ethical issues with the publication of this manuscript.

REFERENCES

[1] G. Macfadyen, T. Huntington, and R. Cappell, "Abandoned, lost or otherwise discarded fishing gear," United Nations Environment Programme Food and Agriculture Organization of The United Nations, 2009.

[2] M. Viitala, Z. Steinmetz, M. Sillanpää, M. Mänttäri, and M. Sillanpää, "Historical and current occurrence of microplastics in water and sediment of a Finnish lake affected by WWTP effluents," Environmental Pollution, Vol. 314, Article 120298, 2022. [CrossRef]

[3] D. Zhang, Y. Cui, H. Zhou, C. Jin, X. Yu, Y. Xu, Y. Li, and C. Zhang, "Microplastic pollution in water, sediment, and fish from artificial reefs around the Ma'an Archipelago, Shengsi, China," Science of The Total Environment, Vol. 703, Article 134768, 2020. [CrossRef]

[4] D. Liu, Z. F. Guo, Y. Y. Xu, F. K. S. Chan, Y. Y. Xu, M. Johnson, and Y. G. Zhu, "Widespread occurrence of microplastics in marine bays with diverse drivers and environmental risk," Environment International, Vol. 168, Article 107483, 2022. [CrossRef]

[5] X. Xiong, S. Xie, K. Feng, and Q. Wang, "Occurrence of microplastics in a pond-river-lake connection water system: How does the aquaculture process affect microplastics in natural water bodies," Journal of Cleaner Production, Vol. 352, Article 131632, 2022. [CrossRef]

[6] L. Zhang, S. Zhang, J. Guo, K. Yu, Y. Wang, and R. Li, "Dynamic distribution of microplastics in mangrove sediments in Beibu Gulf, South China: Implications of tidal current velocity and tidal range," Journal of Hazardous Materials, Vol. 399, Article 122849, 2020. [CrossRef]

[7] K. Enders, R. Lenz, C. A. Stedmon, and T. G. Nielsen, "Abundance, size and polymer composition of marine microplastics ≥10 μm in the Atlantic Ocean and their modelled vertical distribution," Marine Pollution Bulletin, Vol. 100(1), pp. 70–81, 2015. [CrossRef]

[8] J. H. Kang, O. Y. Kwon, K. W. Lee, Y. K. Song, and W. J. Shim, "Marine neustonic microplastics around the southeastern coast of Korea," Marine Pollution Bulletin, Vol. 96(1-2), pp. 304–312, 2015. [CrossRef]

[9] A. Reboa, L. Cutroneo, S. Consani, I. Geneselli, M. Petrillo, G. Besio, and M. Capello, "Mugilidae fish as bioindicator for monitoring plastic pollution: Comparison between a commercial port and a fishpond (north-western Mediterranean Sea)," Marine Pollution Bulletin, Vol. 177, Article 113531, 2022. [CrossRef]

[10] M. Mali, D. Malcangio, M.M. Dell' Anna, L. Damiani, and P. Mastrorilli, "Influence of hydrodynamic features in the transport and fate of hazard contaminants within touristic ports. Case study: Torre a Mare (Italy)," Heliyon, Vol. 4(1), Article e00494, 2018. [CrossRef]

[11] F. Preston-Whyte, B. Silburn, B. Meakins, A. Bakir, K. Pillay, M. Worship, S. Paruk, Y. Mdazuka, G. Mooi, R. Harmer, D. Doran, F. Tooley, T. Maes, "Meso- and microplastics monitoring in harbour environments: A case study for the Port of Durban, South Africa," Marine Pollution Bulletin, Vol. 163, Article 111948, 2021. [CrossRef]

[12] H. A. Nel, J. W. Hean, X. S. Noundou, and P. W. Froneman, "Do microplastic loads reflect the population demographics along the southern African coastline?," Marine Pollution Bulletin, Vol. 115, pp. 115–119, 2017. [CrossRef]

[13] F. Dubaish, and G. Liebezeit, "Suspended Microplastics and Black Carbon Particles in the Jade System," Southern North Sea, Water, Air, & Soil Pollution," Vol. 224, Article 1352, 2013. [CrossRef]

[14] L. Lahens, E. Strady, T. C. Kieu-Le, R. Dris, K. Boukerma, E. Rinnert, J. Gasperi, and B. Tassin, "Macroplastic and microplastic contamination assessment of a tropical river (Saigon River, Vietnam) transversed by a developing megacity," Environmental Pollution, Vol. 236, pp. 661–671, 2018. [CrossRef]

[15] J. Zhang, H. Chen, H. He, X. Cheng, T. Ma, J. Hu, S. Yang, S. Li, and L. Zhang, "Adsorption behavior and mechanism of 9-Nitroanthracene on typical microplastics in aqueous solutions," Chemosphere, Vol. 245, Article 125628, 2020. [CrossRef]

[16] P. Wu, Y. Tang, M. Dang, S. Wang, H. Jin, Y. Liu, H. Jing, C. Zheng, S. Yi, and Z. Cai, "Spatial-temporal distribution of microplastics in surface water and sediments of Maozhou River within Guangdong-Hong Kong-Macao Greater Bay Area," Science of The Total Environment, Vol. 717, Article 135187, 2020. [CrossRef]

[17] G. Wang, J. Lu, Y. Tong, Z. Liu, H. Zhou, and N. Xiayihazi, "Occurrence and pollution characteristics of microplastics in surface water of the Manas River Basin, China," Science of The Total Environment, Vol. 710, Article 136099, 2020. [CrossRef]

[18] G. Everaert, L. Van Cauwenberghe, M. De Rijcke, A. A. Koelmans, J. Mees, M. Vandegehuchte, and C. R. Janssen, "Risk assessment of microplastics in the ocean: Modelling approach and first conclusions, Environmental Pollution," Vol. 242, pp. 1930–1938, 2018. [CrossRef]

[19] E. D. Osorio, M. A. N. Tanchuling, and M. B. L. D. Diola, "Microplastics Occurrence in Surface Waters and Sediments in Five River Mouths of Manila Bay," Frontiers in Environmental Science, 9, pp. 1–14, 2021. [CrossRef]

[20] U. Aytan, A. Valente, Y. Senturk, R. Usta, F.B. Esensoy Sahin, R.E. Mazlum, and E. Agirbas, "First evaluation of neustonic microplastics in Black Sea waters," Marine Environmental Research, Vol. 119, pp. 22–30, 2016. [CrossRef]

[21] Y. Terzi, K. Gedik, A. R. Eryasar, R. C. Ozturk, A. Sahin, and F. Yilmaz, "Microplastic contamination and characteristics spatially vary in the southern Black Sea beach sediment and sea surface water," Marine Pollution Bulletin, Vol. 174, Article 113228, 2022. [CrossRef]

[22] V. Z. Sonmez, C. Akarsu, and N. Sivri, "Impact of coastal wastewater treatment plants on microplastic pollution in surface seawater and ecological risk assessment," Environmental Pollution, Vol. 318, Article 120922, 2023. [CrossRef]

[23] R. Egessa, A. Nankabirwa, H. Ocaya, and W. G. Pabire, "Microplastic pollution in surface water of Lake Victoria," Science of The Total Environment, Vol. 741, Article 140201, 2020. [CrossRef]

[24] M. Kazour, S. Jemaa, C. Issa, G. Khalaf, and R. Amara, "Microplastics pollution along the Lebanese coast (Eastern Mediterranean Basin): Occurrence in surface water, sediments and biota samples," Science of The Total Environment, Vol. 696, Article 133933, 2019. [CrossRef]

[25] J. P. W. Desforges, M. Galbraith, N. Dangerfield, and P. S. Ross, "Widespread distribution of microplastics in subsurface seawater in the NE Pacific Ocean," Marine Pollution Bulletin, Vol. 79(1-2), pp. 94–99, 2014. [CrossRef]

[26] O. Garcés-Ordóñez, J.F. Saldarriaga-Vélez, L. F. Espinosa-Díaz, A. D. Patiño, J. Cusba, M. Canals, K. Mejía-Esquivia, L. Fragozo-Velásquez, S. Sáenz-Arias, T. Córdoba-Meza, and M. Thiel, "Microplastic pollution in water, sediments and commercial fish species from Ciénaga Grande de Santa Marta lagoon complex," Colombian Caribbean, Science of The Total Environment, Vol. 829, Article 154643, 2022. [CrossRef]

[27] C. Schönlau, T. M. Karlsson, A. Rotander, H. Nilsson, M. Engwall, B. van Bavel, and A. Kärrman, "Microplastics in sea-surface waters surrounding Sweden sampled by manta trawl and in-situ pump," Marine Pollution Bulletin, Vol. 153, Article 111019, 2020. [CrossRef]

[28] K. L. Kaposi, B. Mos, B. P. Kelaher, and S. A. Dworjanyn, "Ingestion of microplastic has limited impact on a Marine Larva," Environmental Science & Technology, Vol. 48(3), pp. 1638–1645, 2014. [CrossRef]

[29] A. A. Koelmans, P. E. Redondo-Hasselerharm, N. H. M. Nor, V. N. de Ruijter, S. M. Mintenig, and M. Kooi, "Risk assessment of microplastic particles," Nature Reviews Materials, Vol. 7, pp. 138–152, 2022. [CrossRef]

[30] I. B. Jâms, F. M. Windsor, T. Poudevigne-Durance, S. J. Ormerod, and I. Durance, "Estimating the size distribution of plastics ingested by animals," Nature Communications, Vol. 11, Article 1594, 2020. [CrossRef]

[31] U. Aytan, F. B. Esensoy, Y. Senturk, E. Arifoglu, K. Karaoglu, Y. Ceylan, and A. Valente, "Plastic occurrence in commercial fish species of the Black Sea," Turkish Journal of Fisheries and Aquatic Sciences, Vol. 22(12), 2021. [CrossRef]

[32] United Nations Development Programme, "Black Sea twice as polluted by marine litter as Mediterranean Sea – EU project's survey," 2019. https://www.undp.org/ukraine/press-releases/black-sea-twice-polluted-marine-litter-mediterranean-sea-%E2%80%93-eu-project%E2%80%99s-survey Accessed on Feb 6, 2023.

Environ Res Tec, Vol. 6, Issue. 1, pp. 21–34, March 2023

Environmental Research and Technology
https://ert.yildiz.edu.tr - https://dergipark.org.tr/tr/pub/ert
DOI: https://doi.org/10.35208/ert.1188385

Environmental Research & Technology

Research Article

Diallyl dimethyl ammonium chloride (DADMAC) and acrylic acid (AAc) embedded nonwoven irradiated polyethylene fabric as efficient adsorbent to separate U(VI) from aqueous solution

Shahnaz SULTANA[*1], Nazia RAHMAN[1], Md. RAZZAK[2], Md. Nabul SARDAR[1]

[1]Nuclear and Radiation Chemistry Division, Institute of Nuclear Science and Technology, Atomic Energy Research Establishment, Bangladesh Atomic Energy Commission, Savar, Dhaka, Bangladesh
[2]Instituteof Radiation and Polymer Technology, Atomic Energy Research Establishment, Bangladesh Atomic Energy Commission, Savar, Dhaka, Bangladesh

ARTICLE INFO

Article history
Received: 17 October 2022
Revised: 11 January 2023
Accepted: 01 February 2023

Key words:
Adsorption capacity; Grafted polymeric adsorbent; Uranium; Wastewater

ABSTRACT

Selective isolation of uranium (VI) from wastewater is now a subject of concern due to its damaging effect on living beings. In this study, the pre-irradiation technique was used to prepare grafted polymeric adsorbent by diallyl dimethyl ammonium chloride (DADMAC) and acrylic acid (AAc) onto nonwoven polyethylene fabric (PE) and the grafted adsorbent was applied for uranium (VI) adsorption from aqueous solution by batch method. After irradiation of the non-woven polyethylene fabrics with 50 kGy radiation dose, the grafting reaction was carried out at 80 °C with a monomer solution consisting of 20 g DADMAC and 20 g AAc to 110 mL deionized water. The prepared adsorbent was characterized by Fourier Transform Infrared (FTIR), Scanning Electron Microscopy (SEM), and Thermo-gravimetric Analysis (TGA). After treatment with NaOH solution, the adsorption study was analyzed by pH, initial metal ion concentrations, contact time, and temperature on the adsorption of U(VI). The highest graft yield was achieved at 598%. The maximum adsorption capacity achieved at 160 mg/g was found by treating with 0.1M NaOH for 4 minutes with an initial concentration of 1000 ppm, pH 3.3, and a contact time of 48 hours at room temperature (25 °C). Kinetic adsorption data fitted better with the pseudo-second-order equation and a good correlation of experimental data with the Langmuir isotherm model suggested monolayer adsorption. Langmuir equation showed that the maximum adsorption capacity for U(VI) was 333.333 mg/g. The study depicted good results on the desorption and reuse of the adsorbent.

Cite this article as: Sultana S, Rahman N, Razzak M, Sardar MN. Diallyl dimethyl ammonium chloride (DADMAC) and acrylic acid (AAc) embedded nonwoven irradiated polyethylene fabric as efficient adsorbent to separate U(VI) from aqueous solution. Environ Res Tec 2023;6:1:21–34.

INTRODUCTION

Uranium (U) is a naturally occurring primordial radioactive element with atomic number 92. It has three major isotopes such as ^{234}U, ^{235}U, and ^{238}U with a natural abundance of 0.0050–0.0059%, 0.7198–0.7202% and, 99.2739–99.2752%, respectively. All these isotopes follow radioactive decay by releasing alpha particles along with weak gamma

***Corresponding author.**
*E-mail address: shahnazju32@gmail.com

radiation and they exist ubiquitously in nature such as in soil, rock, and water with low concentrations [1]. However, due to anthropogenic activities, a significant portion of U is accumulated in the environment. First of all, in the past, several serious nuclear power plant accidents took place such as the Fukushima nuclear disaster (2011), the Chornobyl disaster (1986), the Three Mile Island accident (1979), and the SL-1 accident (1961) [2–5]. Secondly, various radiological incidents occurred in the world such as the Kyshtym disaster, the Windscale fire, the radiation accident in Morocco, the Goiania accident, the radiation accident in Mexico City, and the Mayapuri radiological accident in India [6–8]. Thirdly, some major nuclear submarine accidents happened including the K-19 (1961), K-11 (1965), K-27 (1968), K-140 (1968), K-429 (1970), K-222 (1980), K-431 (1985) accidents [9–14]. Finally, U-containing wastewater is discharged by the processing of mining and ore industries [15]. Due to all these phenomena, air, soil, and particularly water is prone to be a major source of U contamination. In radioactive wastewater, U is present with the principal valence states U(IV) and U(VI) depending on the redox environment [16]. However, U(VI), in the form of uranyl ion (UO_2^{2}+) and with multi complexes, is more soluble and widely present in radioactive wastewater and seawater for its highly migratory performance [17]. Thus, U(VI) can arrive at the top of the food chain where it is consumed by humans. Since all isotopes of U have mutagenic and carcinogenic properties, they are responsible for harmful effects on the human body such as liver damage, skin problem, kidney damage and even death [18–22]. Not only they are detrimental to human beings but also, they can cause significant damage to the aquatic environment. Thus, to protect humans and the biodiversity of the ecosystem, effective recovery of U by selective isolation of U(VI) from aqueous solution and sea water is of immense importance.

In the past, many approaches were applied to uptake the U(VI) from an aqueous solution, such as solvent extraction, chemical precipitation, flotation, ion exchange processes, biological treatment, and adsorption [23–34]. Among these techniques, adsorption is one of the most effective methods for U(VI) removal from wastewater and seawater because of its excellent efficiency, cost-effectiveness, and simple operation, and hence, the technique has gained much attention [35–40]. So far, several ligands such as imidazole, amidoxime, and phosphoryl groups were studied [41–46]. These organic ligands enhance adsorption selectivity and capacity towards uranyl ions which are tightly bonded or chemically grafted into adsorbents. However, the solid carriers are also vital parts of adsorbents besides these ligands because in unfavorable conditions like extreme pH, temperature, and radiation dose they must be survived entirely. Furthermore, these polymers should have suitable surface area and structure so that active groups could be covalently connected on their structures. In recent times, graft polymer becomes a great blessing in the field of removal of heavy metals from aqueous solution [47–50]. In this case, the adsorbent has a higher value of adsorption capacity, and its ability to reuse reduces the probability of secondary pollution. In this method, functional monomers are covalently bonded onto the parent polymer chain. The reason for being most successful method of this is that this technique allows the blending of various functions of the grafted monomer to the parent polymer without disturbing the mechanical properties of the parent polymer [51–53]. Along with the other methods for initiating graft copolymerization like plasma treatment, decomposition of chemical initiators, ionizing radiation, ultraviolet light, and oxidation of polymers, the radiation-induced grafting technique is advantageous. To some extent, it is more suitable for its extensive penetration into the polymer chain and its rapid and uniform formation of radicals [54]. Available methods of radiation polymerization involve direct irradiation of fiber in monomer solution, vapor phase irradiation method, and pre-irradiation [50].

Many researchers have reported the elimination of toxic and heavy metals by radiation-grafted polyethylene covalently bonded with single or binary monomers (PE) [55–59]. Guo et al. [60] developed a facile route for the fabrication of polyethyleneimine-functionalized reduced graphene oxide/molybdenum disulfide composition aerogels (PEI-rGO/MoS2 CAs) and applied them to adsorb U(VI) from aqueous solutions successfully. In another investigation, Das et al. [61] showed graft polymerization of acrylonitrile and vinyl-phosphonic acid onto polyethylene fiber is a good candidate to adsorb U(VI) from seawater. In the present study, the preparation of a new adsorbent to remove U(VI) ion based on nonwoven PE fabric was attempted by pre-irradiation grafting. Non-woven polyethylene (PE) fabric is known for its excellent mechanical and thermal properties and low cost. Grafting was carried out by binary monomers of acrylic acid (AAc) and diallyl dimethyl ammonium chloride (DADMAC). The grafted polymer was characterized by employing Fourier Transform Infrared Spectroscopy (FTIR), Scanning Electron Microscopy (SEM), and Thermogravimetric Analysis (TGA).

MATERIALS AND METHOD

Materials and Reagents

The mother polymer of non-woven polyethylene (PE) fabric used for preparing grafted adsorbent was collected from Kurashiki Textile Manufacturing Co. Ltd., AAc (99%) and DADMAC (65% in water) were procured from Sigma Aldrich (USA) and Fluka Chemie AG CH-9470 Buchs respectively utilized as monomers to graft onto PE. NaOH, NaCl, and HCl were supplied by Merck, Germany. Uranyl nitrate [$UO_2(NO_3)_2.6H_2O$] was supplied by BDH Chemicals Pvt. Ltd., England and Arsenago III was supplied by Fluka, Switzerland.

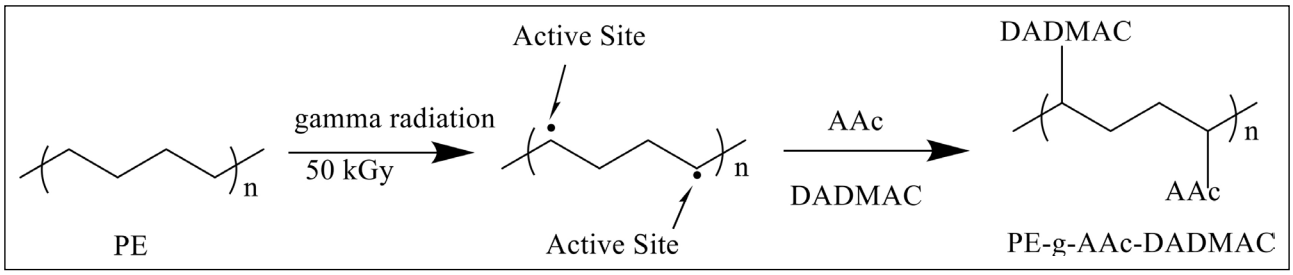

Figure 1. Reaction pathways for grafted PE-AAc-DADMAC formation.

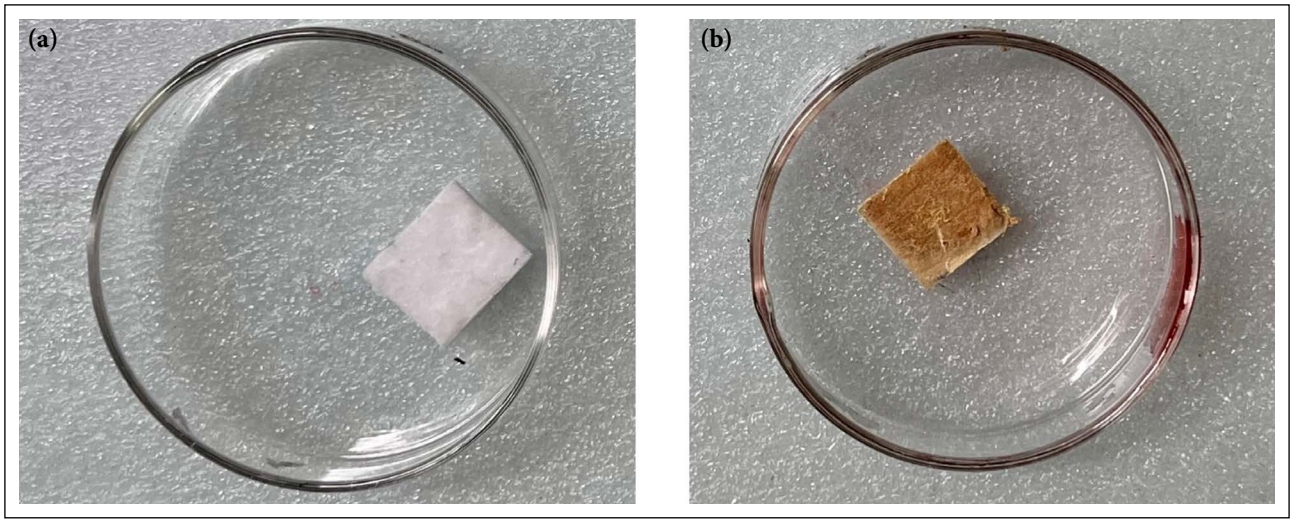

Figure 2. PE- g-AAc-DADMAC polymer before adsorption **(a)** and PE- g-AAc-DADMAC polymer after adsorption with U(VI) **(b)**.

Instruments and Apparatus

The irradiation of PE was conducted by the Co-60 gamma-irradiator (Panoramic Irradiator of 90 kCi Batch Type collected from BRIT, India) from Institute of Food and Radiation Biology (IFRB), Atomic Energy Research Establishment, Savar, Dhaka, Bangladesh. IR Prestige-21, supplied by Shimadzu Corporation, Japan, was used to investigate FTIR-ATR in the wave number range of 700–4000 cm^{-1}. U(VI) ion concentration from the aqueous solution was analyzed by UV-VIS spectrophotometer (Model: UV2401PC from SHIMADZU, Japan). Scanning electron microscopy (Model JSM-6490LA, JEOL) was used to measure the change in surface morphology after grafting.

Preparation of Grafted Polymeric Adsorbent

In this study, non-woven polyethylene sheets were cut into pieces with 10 cm in length and 2 cm in width and put into airtight packets. Then these non-woven PE films were irradiated with 50 kGy radiation dose at ambient temperature. The irradiator activity was 50 kCi at the time of irradiation and the dose rate used was 13 kGy/h. As soon as the irradiation was completed, the irradiated PE films were preserved quickly under dry-ice condition until use. The monomer solution was prepared by the addition of 30 g DADMAC and 30 g AAc to 150 mL distilled water. The monomer solution was taken into a beaker and heated at 70 °C on a hot plate for half an hour to make a clear solution. Then the solution was placed in the gas-passing bottle where argon gas was passed for 40 minutes. The monomer solution was bubbled with argon gas to remove dissolved oxygen. The previously preserved irradiated nonwoven PE films were taken into tubes and immediately the deaerated monomer solution was poured into the tubes. When the tube was fulfilled with monomer solution, it was securely closed with a lid to escape the invasion of oxygen from the air into the monomer solution as soon as possible. Afterward, the grafting reaction was carried out in a water bath at a temperature of 80 °C for 4 hours. Then, the grafted PE fabric was washed properly to remove the remaining monomers and homopolymers. Finally, upon washing and drying, it was ready to be used in the experiment. Schematic diagram is presented in the Scheme 1. The degree of grafting was determined by the following formula:

$$DG(\%) = \frac{W_1 - W_0}{W_0} \times 100 \ldots\ldots\ldots\ldots (1)$$

Where, DG(%) = Degree of grafting

W_1(g) = Weight of the PE fabric after grafting

W_0(g) = Weight of the PE fabric before grafting

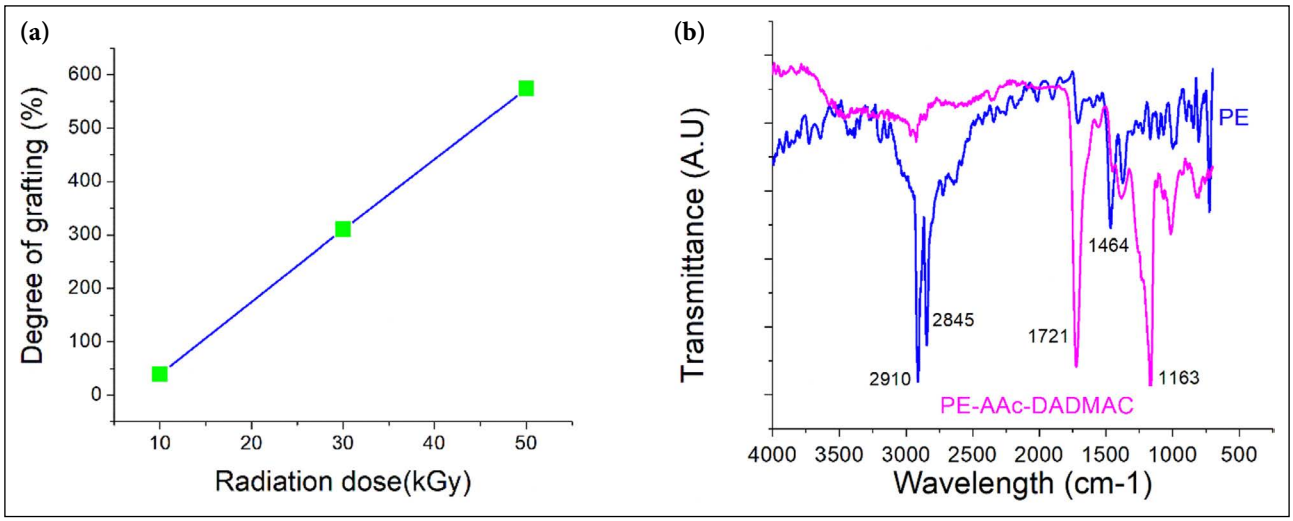

Figure 3. Radiation dose vs degree of grafting **(a)** and FTIR spectrum of PE and PE-g-AAc-DADMAC films **(b)**.

U(VI) Adsorption by DADMAC and AAc onto Nonwoven Irradiated Polyethylene Fabric

Adsorption criteria were studied by changing contact time, concentration, pH, alkali treatment, and temperature of the U(VI) solution to notice the effect of the adsorption process. A constant weight of absorbent was kept in a beaker inside the U (VI) solution. After adsorption, the white adsorbent depicted in Figure 1a turned yellow shown in Figure 1b and the U concentrations before and after absorption were determined by the Arsenazo-III spectrophotometry method [62]. To measure U(VI) concentration, UV-Vis spectrophotometer color complex formation is vital. Thus, 4 mL of U (VI) solution was taken into a 50 mL volumetric flask and added 0.5 mL of 1M HCl, 5 mL of 0.01% Arsenago and then filled the volumetric flask up to the mark with deionized water. Then sample concentration was determined by UV-Vis spectroscopy at the wavelength of 652 nm. Using the following formula adsorption capacity of the adsorbent was calculated,

$$Q_0 = \frac{C_1 - C_2}{W} \times V \ldots\ldots\ldots\ldots (2)$$

Here,

Q_0 = Adsorption capacity of the adsorbent (mg/g)

W = Mass of dry adsorbent (g)

V = Volume of Metal ion solution (L)

C_1 = Initial concentration of metal ion before adsorption (mg/L)

C_2 = Final concentration of metal ion after adsorption (mg/L)

Desorption of U(VI) Ion and Reuse of the Adsorbent

U(VI) was desorbed from the adsorbent by treating it with HCl. After adsorption, the adsorbent was placed into 20 ml of 1M HCl solution in a beaker. The yellow color of the adsorbent turned into white quickly. After 5 hours the solution of U(VI) was separated from adsorbent. The formula used to calculate desorption percentage is given below:

$$\text{Percentage of desorption} = \frac{\text{Desorbed ions (mg)}}{\text{Adsorbed ions (mg)}} \times 100 \ldots\ldots\ldots\ldots (3)$$

After desorption of the metal ion, the adsorbent was again capable for reuse to remove U(VI) by the same method.

RESULTS AND DISCUSSION

Degree of Grafting with Radiation Dose

There was a strong relationship between the degree of grafting of the adsorbent with radiation dose represented in Figure 2a. When the radiation dose increased from 10 kGy to 50 kGy, the degree of grafting climbed linearly from 50% to 598% which was the maximum degree of grafting. Hence, for the experimental works, 50 kGy grafted PE was selected to be used.

FTIR Analysis

Figure 2b shows the FTIR spectrum of PE and PE-g-AAc-DADMAC films. The FTIR pattern of PE showed the main characteristic peaks at about 2910 cm^{-1}, and 2845 cm^{-1} were resulted from C-H asymmetric and symmetric stretching vibrations from methylene groups, respectively. The bands at 1464 cm^{-1} and 1373 cm^{-1} were observed due to the symmetric and asymmetric bending vibrations of the C-H bond the methylene group. Besides, Figure 2b also demonstrated the band at 1721 cm^{-1} due to the carbonyl bond of AAc, and another peak at 1163 cm^{-1} was seen due to the C-N fundamental vibration of DADMAC. Hence, the above analysis confirms the addition of DADMAC and AAc on the PE sheet.

SEM Analysis of the Adsorbent

To relate the physical characteristic of nonwoven bare PE with PE-g-AAc-DADMAC scanning electron microscopy of nonwoven PE and grafted PE were analyzed. The SEM image of the bare nonwoven PE fabrics showed the trans-

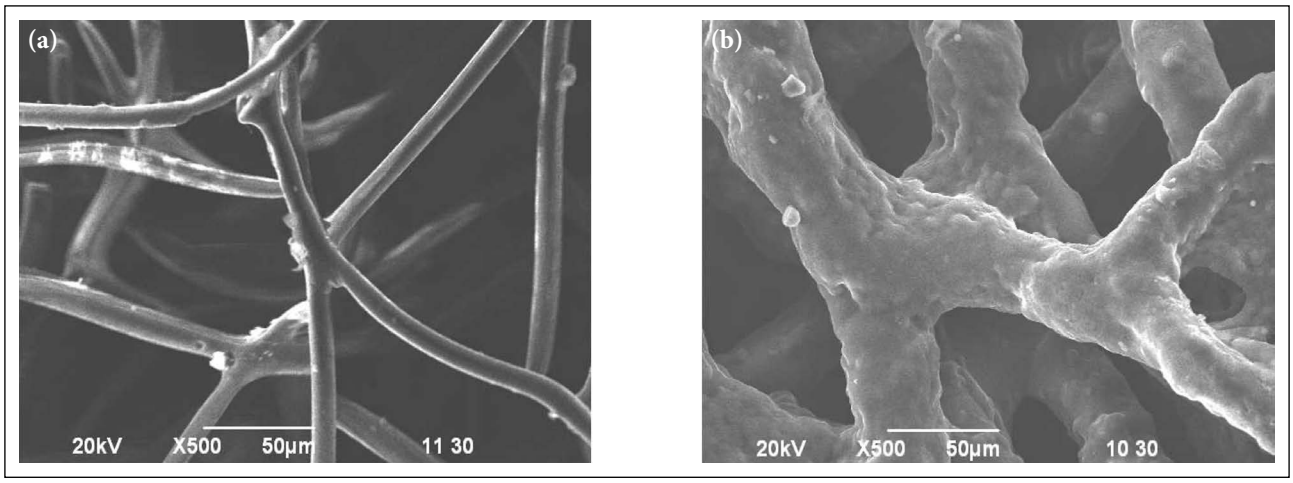

Figure 4. SEM images of PE **(a)** and grafted PE films **(b)**.

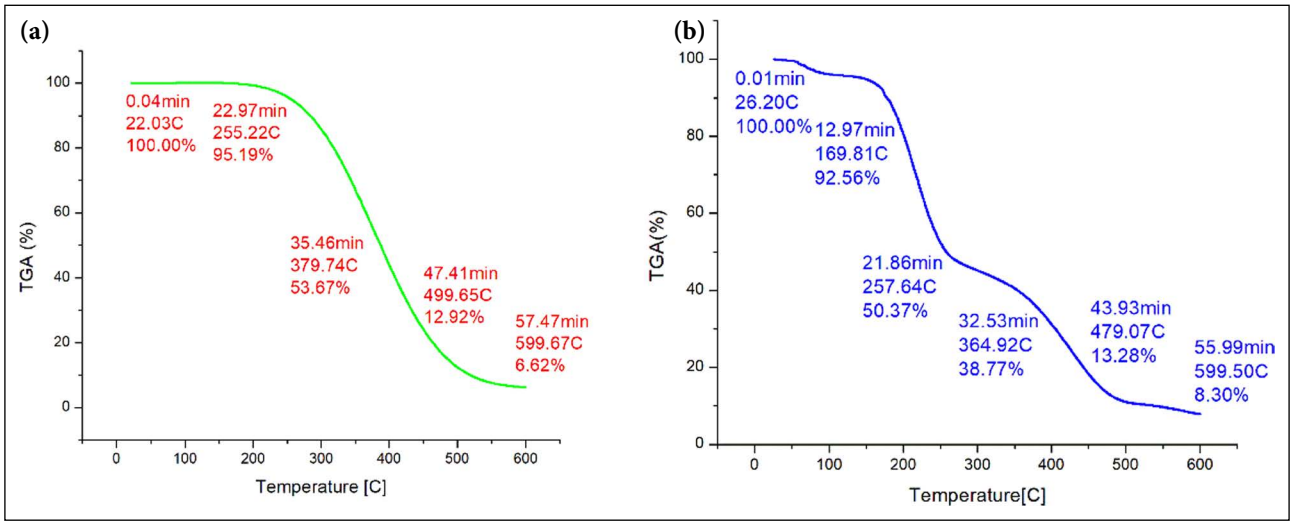

Figure 5. TGA of PE **(a)** and grafted PE films **(b)**.

formation of the physical appearance after grafting with DADMAC and AAc. A layer of grafted chains covering the surface of PE film could observe after grafting with monomers, which was also seen in another study [63]. The SEM image of non-woven bare PE film is shown in Figure 3a and the SEM image of DADMAC and AAc grafted PE is shown in Figure 3b. The average diameter of fibers increases slightly and distributes more closely which indicates the additional surface due to grafting.

TGA Analysis of the Adsorbent

The thermogravimetric analysis (TGA) thermograms for PE film with DADMAC and AAc grafted PE adsorbent are shown in Figure 4 to understand thermal stability and decomposition and present clear differences in thermal stability between them. The original PE film in Figure 4a showed thermal stability up to 220 °C and above 220 °C it started to be decomposed. It showed two decomposition steps, i.e., 220 °C–540 °C and above 540 °C. On the other hand, grafted PE film in Figure 4b decomposed more quickly than bare PE film and started weight loss (5%) at 50 °C due to the loss of moisture absorbed from the air. Then it followed four weight loss stages 50 °C–170 °C, 170–257 °C, 257–479 °C, and above 479 °C which were for degradation of grafted chain and degradation of the PE backbone. Above 479 °C the grafted PE film decomposed more than 90%. The thermal stability of DADMAC and AAc grafted PE film was lower than that of the original PE film might be due to the less thermal stability of monomers.

Effect of Treatment of the Adsorbents with NaOH Solution

The adsorbents were treated with NaOH solution to observe the effect of the adsorption capacity of grafted film of the PE-AAc-DADMAC sheet. The prepared adsorbents were sunk into 40 mL of NaOH solution with three different concentra-

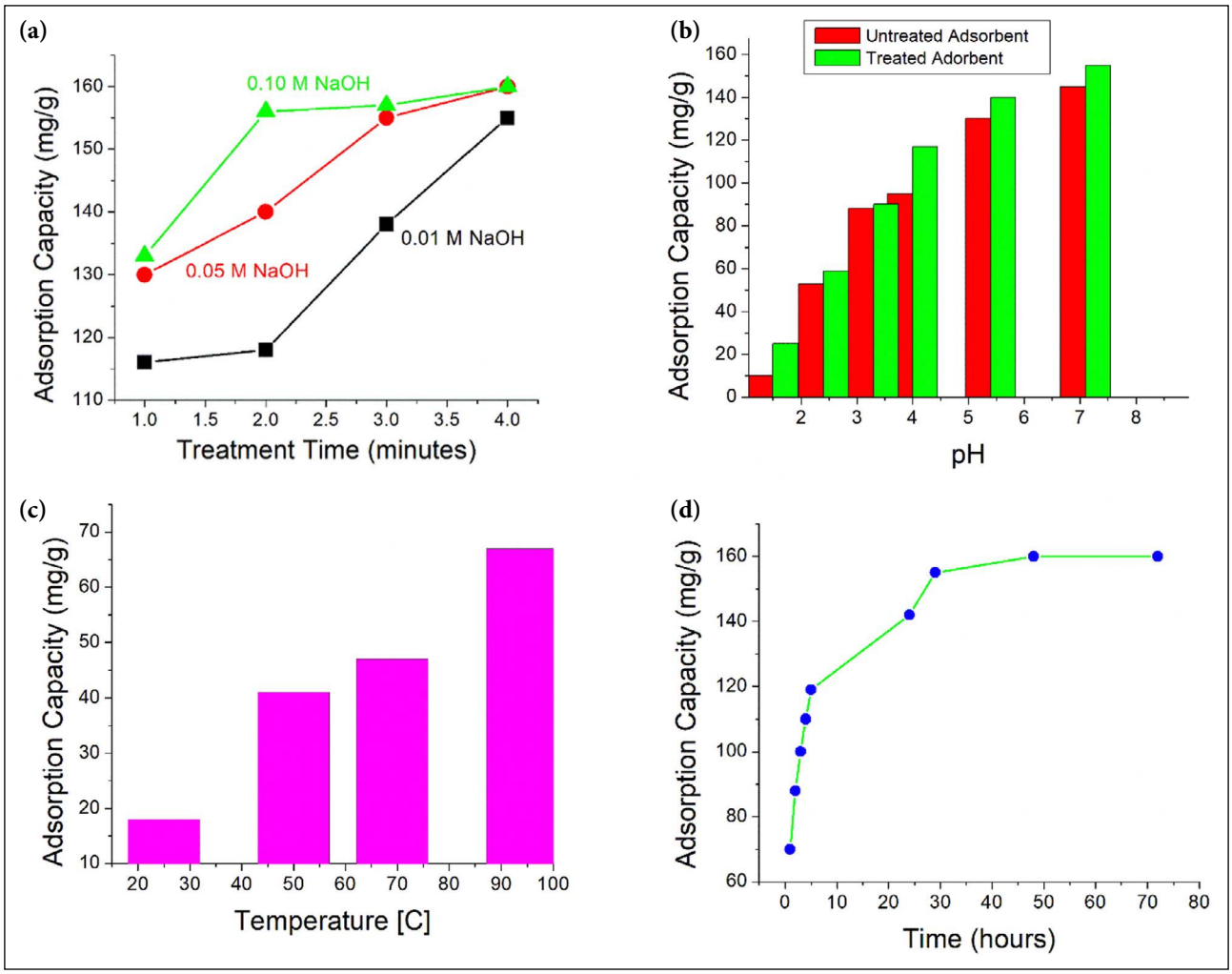

Figure 6. Treatment effect of the adsorbent **(a)**; adsorption capacity vs pH **(b)**; capability of adsorption vs temperature **(c)**; Effect of contact time on U(VI) adsorption capacity with pH 3.2 and initial U(VI) concentration 1000 ppm **(d)**.

tions such as 0.01M NaOH, 0.05M NaOH, and 0.1M NaOH. The adsorbents were dipped in each solution with constant stirring for 1, 2, 3 and 4 minutes respectively and washed immediately after the said times. These phenomena are graphically represented in Figure 5a. The adsorption capacity of the prepared adsorbents increased when treating with higher concentrations of NaOH solutions. However, above the concentration of 0.01M NaOH, the adsorbents swelled much, and degradation was observed. A 1000 ppm 10 mL solution of U(VI) was taken, and adsorption capacity was measured. It was found that the adsorption capacity was 100 mg/g for the untreated sample and 155 mg/g for the treated samples (treated with 0.01 M NaOH for 4 minutes stirring). Therefore, in this study for all experiments, the adsorbents were treated with 0.01M NaOH solution for 4 minutes.

U(VI) Adsorption Effect with pH of the Solution

The adsorption capacity of the prepared composite grafted film of PE-AAc-DADMAC sheet was studied with 800 ppm of U(VI) solution of pH 1.5 to 8.5 shown in Figure 5b. The pH of the U(VI) solution was adjusted by different concentrations of HCL and NaOH solutions. From the graph, it is shown that the effect of pH on U(VI) adsorption was significant for both samples of treated (with 0.01M NaOH solution) and untreated adsorbents. The pH of the mother solution showed acidic (pH=3.3) and in this condition, the adsorption capacity was found to be 80 mg/g and 90 mg/g for untreated and treated adsorbents respectively. However, for both the cases, adsorption capacity increased with increasing pH values from 1.5 to 7.1. Less adsorption capacity was measured below pH 3.3. However, when the pH of the solution increased, the uptake of metal ions enhanced and hence the higher adsorption capacity was observed. At low pH levels, protonated functional groups increased which repulsed the positively charged U(VI) ions resulting the reduction of adsorption of U(VI) cations. On the other hand, higher adsorption capacity was found at higher pH. At higher pH, number of hydroxyl ions increased. As a result,

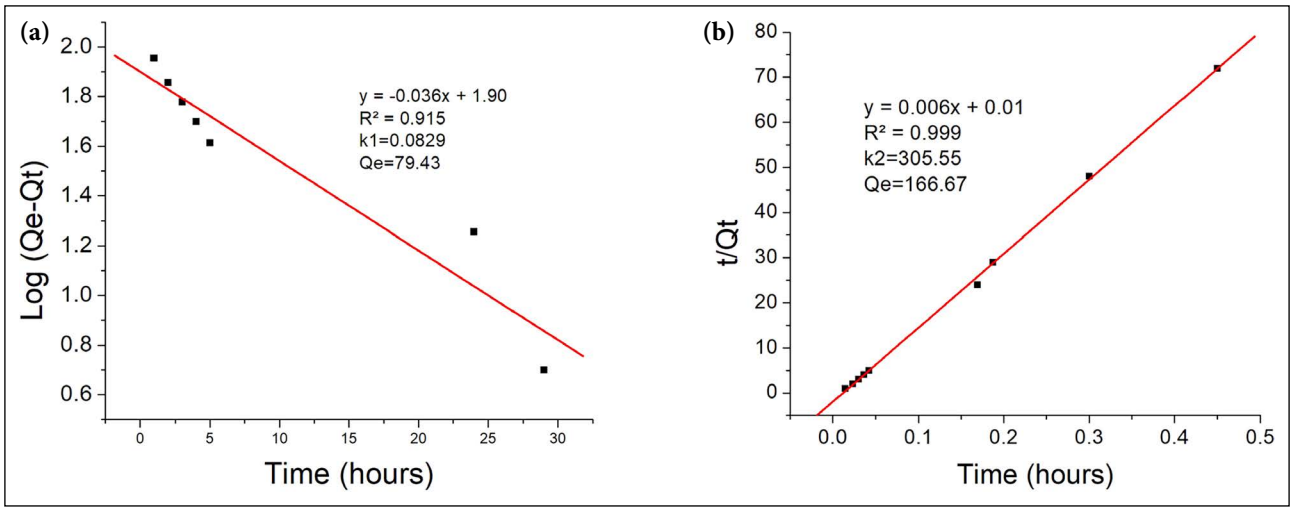

Figure 7. Adsorption kinetic model **(a)** Pseudo-first order **(b)** Pseudo-second order.

Table 1. The parameters of adsorption kinetics and adsorption isotherms

	Kinetic models					Isotherm models			
Pseudo	K_1	Q_e	K_2	R^2		Q_0	n	K_f	R^2
Order -1st	0.083	79.430		0.915	Langmuir	333.333			0.993
Order -2nd		166.660	305.550	0.999	Freundlich		1.46	2.328	0.983

the proton's competitive action on the metal ion decreased [31, 45]. In a previous study, Sun et al. [17] found that adsorption capacity increased when pH was increasing from 2 to 7. But at higher pH, U(VI) solutions became more turbid because of the precipitation formation of U complex [64]. pH 3.3 was set fixed for all the parameters of this study.

U(VI) Adsorption Effect by Temperature

To understand the effect of temperature, the adsorption capacity was studied with different temperatures such as 25 °C, 50 °C, 69 °C, and 94 °C with 200 ppm U(VI) solution. The solutions were heated for 4 hours except for the 25 °C while maintaining a constant pH. From the graph, it is seen that temperature plays an important role in the adsorption capacity of the adsorbent. This phenomenon is observed in Figure 5c where the adsorption capacity enhanced with increasing temperature. At 25 °C, adsorption capacity was only 18 mg/g, on the other hand, it raised to 67 mg/g at 94 °C. It suggested that the adsorption exhibited an endothermic behavior. It also indicated that the adsorption process is more effective at higher temperature because it needed sufficient energy to decompose U(VI) hydration [31]. The trend was similar with the other studies such as Yuan et al. [46].

U(VI) Adsorption by DADMAC and AAc Grafted PE Film with Standing Time (hr)

There is a relationship that has been established between contact time on U(VI) adsorption from aqueous solution which is depicted in Figure 5d. The grafted-PE films were treated with 40 mL of 0.1 N NaOH solution and kept into the aqueous solutions of U(VI) and maintained the solution with constant pH (pH 3.3) and initial metal ion concentration of1000 ppm at room temperature (25 °C). The concentrations of U(VI) ions in aqueous solution were measured at a regular time intervals. From the process, it was seen that, at the initial stage, the U(VI) adsorption rate was rapid and after that the adsorption reached gradually toward equilibrium. After 29 hours, 96.87% adsorption was completed with the adsorption capacity of 155 mg/g, and after 48 hours, the adsorption capacity reached to an equilibrium and the value was 160 mg/g. This trend is similar to another study where 70–90% Cu (II) adsorption completed within 120 minutes and, after that, the adsorption rate became slower till equilibrium [65]. The experimental data are presented graphically in Figure 5d.

To get deeper understanding of U(VI) adsorption, the measured data of adsorption were analyzed using pseudo 1st and pseudo 2nd order kinetic model. The linear mathematical forms of these models are shown by equations (4) – (5), respectively

$$\log(Q_e - Q_t) = -\left(\frac{K_1}{2.303}\right) \times t + \text{Log } Q_e \ldots\ldots\ldots\ldots (4)$$

$$\left(\frac{t}{Q_t}\right) = \left(\frac{1}{(K_2 \times Q_e)^2}\right) + \frac{t}{Q_e} \ldots\ldots\ldots (5)$$

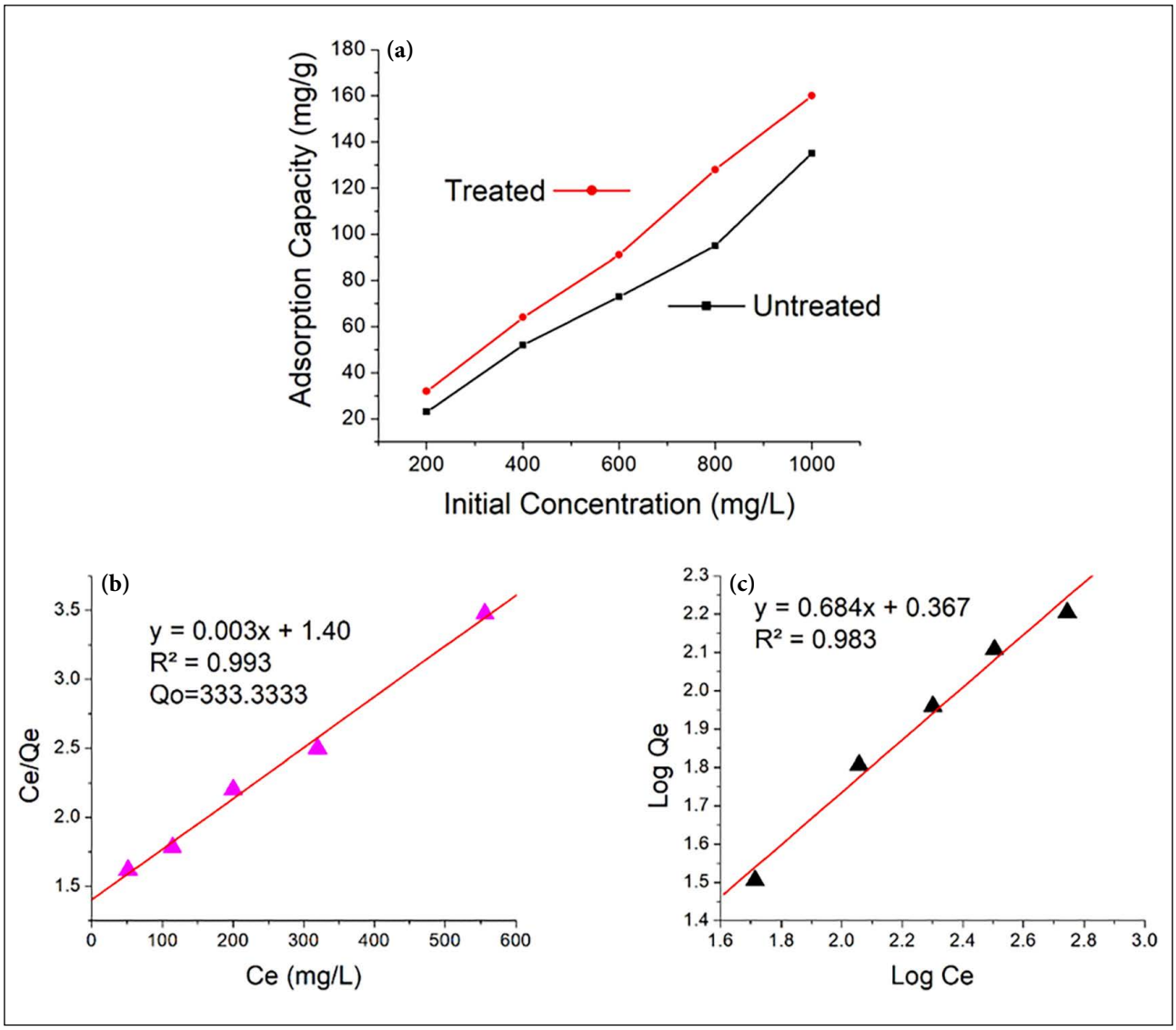

Figure 8. **(a)** Adsorption capacity variation with initial concentration of metal ions; adsorption isotherm model **(b)** the Langmuir **(c)** the Freundlich.

Where Q_e (mg/g) represents adsorption capacity at equilibrium and Q_t (mg/g) indicates adsorption capacity at time t (h), K_1(/h) and K_2 (g/mg/h) denote the first and second-order kinetic constants, respectively. The rate constant for the pseudo first-order kinetic model could be determined by plotting log (Q_e–Q_t) versus t as shown in Figure 6a and the values of K_1 and Q_e can be calculated from the slope and intercept of the line graph. The values of K_1, Q_e, R^2 (correlation coefficient) for U(VI) adsorption are presented in Table 1. Results revealed that the experimental Q_e value (160 *mg/g*) and Q_e value (79.43 *mg/g*) measured from the first-order kinetic model were different from each other.

Further, the pseudo-second-order rate constant can be determined from the graph of $\frac{t}{Q_e}$ against t shown in Figure 6b. The values of K^2, Q_e, and R^2 are shown in Table 1. It is observed that the experimental Q_e value (160 *mg/g*) and the Q_e value (166.67 *mg/g*) measured from the pseudo-2nd-order kinetic model match with each other and the R^2 value (0.99) was relatively higher and very close to unity compared to the pseudo-first-order kinetic model (R^2= 0.91). Hence, the adsorption process of U(VI) uptake followed the pseudo 2nd order equation and might be regarded as chemisorption process with chelation and electron transfer between U(VI) and organic monomers which is similar with Li et al. [36]. In that study, pseudo-2nd-order kinetic model fitted better at low pH. Since the adsorption followed the pseudo 2nd order model, therefore, the intra-particle diffusion process might have happened in the rate-determining step [65]. Moreover, the maximum adsorption capacity for U(VI) removal of this study was compared with previous studies which are shown in Table 2.

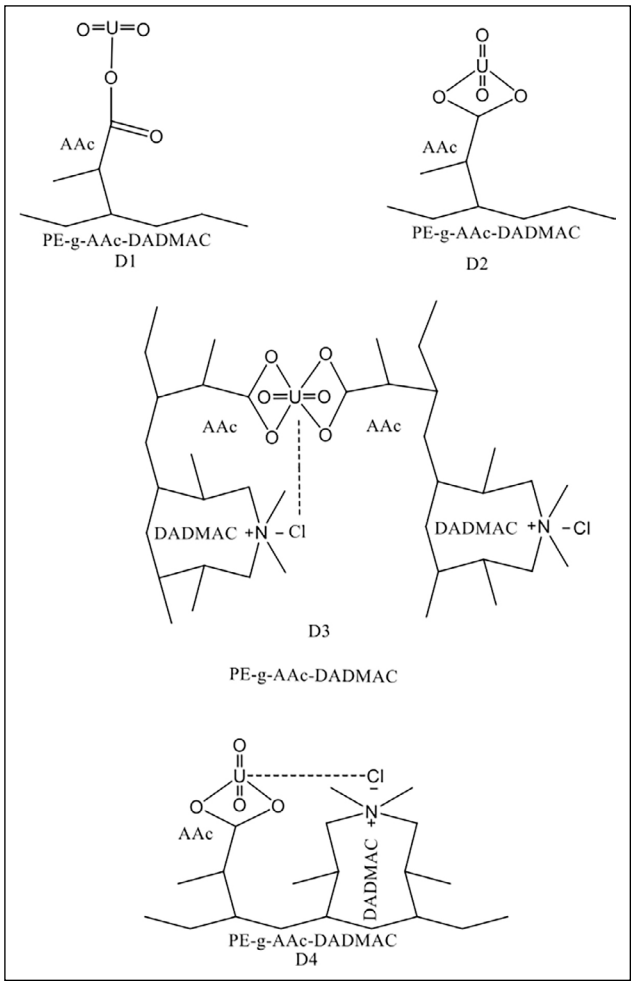

Figure 9. Proposed binding motifs of PE- g-AAc-DADMAC with uranyl summarized in the literatures. Solvent molecules adding sixth, seventh and/or eight coordination sites on the uranyl cation are not shown.

Adsorption Capability with Initial Concentration of Metal Ions

Figure 7a shows the relationship between the initial concentration of metal ions (200 mg/L–1000 mg/L) and the adsorption capacity. This figure depicts that the adsorption of metal ions increased with increasing initial metal ion concentrations up to 1000 mg/L for both the cases of treated with 0.01 N NaOH and untreated adsorbents. When the concentrations of U(VI) ions increased the probability of interaction between adsorbate and adsorbent enhanced. This interlinkage prompted adsorption capacity [35].

Adsorption Isotherm Models

The adsorption isotherm defines surface metal–ligand interaction processes. The Langmuir and the Freundlich adsorption isotherms are usually applied for better understanding of adsorption isotherm. The main difference between the Freundlich and the Langmuir adsorption isotherms is that Freundlich adsorption isotherm is empirical, whereas Langmuir adsorption isotherm is theoretical. The homogeneous method of Langmuir adsorption is demonstrated by the following linear equation:

Table 2. Adsorption capacity of different adsorbents for U (VI) ion removal

Adsorbents	Adsorption capacity (mg/g)	Ref.
Flax fiber	40.9*	[68]
Silicon dioxide nano-powder	10.15***	[69]
Nano-goethite powder	104.22*	[70]
Commercial ceramic	11.43**	[71]
Flower-goethite (TDFLG)	48.24**	[72]
Flower-goethite (MTDFLG)	112.35**	[72]
PE-g-AAc-DADMAC film [This study]	160*	
PE-g-AAc-DADMAC film [This study]	333.33**	

Ref: References; *: Maximum adsorption capacity from experimental value; **: Maximum adsorption capacity from Langmuir isotherm model; ***: Maximum adsorption capacity from Pseudo-second-order kinetic model.

$$\frac{C_e}{Q_e} = \frac{C_e}{Q_o} + \frac{1}{(Q_o b)} \ldots\ldots\ldots (7)$$

Where C_e (mg/L) and Q_e (mg/g) are the concentration of the metal ion and capacity of the adsorption at equilibrium, Q_o (mg/g) represents the saturation adsorption capacity and b (L/mg) is the Langmuir adsorption constant. Q_o and b can be calculated by the slope and intercept of the plot of $\frac{C_e}{Q_e}$ vs C_e of the treated samples, which is shown in Figure 7b and summarized in Table 1. The value of maximum adsorption capacity, Q_o was found to be 333.33 mg/g, which is very similar to another study of U(VI) adsorption, where Q_o was 333.13 mg/g [66]. The dimensionless separation factor, R_L, is an important characteristic in Langmuir adsorption isotherm, can be expressed as,

$$R_L = \frac{1}{(1 + Q_o b)} \ldots\ldots\ldots (8)$$

Where Q_o is the maximum adsorption capacity, b (L/mg) is the Langmuir adsorption constant. The value of R_L indicates the type of isotherm to be either unfavorable ($R_L > 1$), favorable ($0 < R_L < 1$), linear ($R_L = 1$) and irreversible ($R_L = 0.00$).

By following Langmuir equation, the values of Q_o [=333.333 (mg/g)], R_L (0.19) and R^2 (0.993) indicated that the adsorption data was well-fitted with the Langmuir adsorption isotherm model.

The Freundlich isotherm illustrates multilayer adsorption on heterogeneous surface and expressed by the linear Equation:

$$log\ Q_e = \ln K_f + \frac{1}{n}\ (\log C_e) \ldots\ldots\ldots (8)$$

Here, the Freundlich constants, which are represented by K_f (mg/g) and n (L/mg) calculated from the intercept and slope of the plot of $log\ Q_e$ vs $log\ C_e$ of the treated samples, are shown in Figure 7c and summarized in Table 1. n represents good, moderately difficult, and poor adsorption characteristics when the values of n are in the range of 2–10, 1–2, and less than 1 respectively. From the slope, the value of n was found to be 1.46. Thus, by analyzing the values of n and R^2, it is understandable that the adsorption process is more compatible with the Langmuir adsorption isotherm model than the Freundlich adsorption isotherm model, indicating that PE-g-AAc-DADMAC implemented the specific homogenous sites and provided monolayer surface [46].

Adsorption Mechanism

Based on the results discussed above, mostly, the binding motifs of uranyl moiety with grafted PE-AAc-DADMAC in Scheme 2 were suggested where D1, D2, D3 and D4 binding motifs are presented. Binding motifs shown in D1 and D2 are U-O monodentate and bidentate covalent coordinate bond formation with coordination number three and four respectively [67]. Also, from the scheme, in D3 and D4, the electrostatic interactions between UO_2^+ and the DADMAC moiety and/or Cl^- ions stabilized the complex further. From the adsorption isotherm (pseudo-second order) and Langmuir adsorption isotherm model, the maximum adsorption capacity is determined to be 333.33 mg/g. This result indicated that both chelation and electrostatic interactions might be operating to reach a maximum adsorption due to the available binding sites. It should be mentioned that there are other probable binding motifs that may exists which could be responsible for the remaining adsorption. Although it is worthwhile to state that, understanding the interaction between uranyl moiety with grafted PE-AAc-DADMAC is uncertain [36].

Comparison of PE-g-AAc-DADMAC with Other Adsorbents

The U(VI) adsorption capacity (mg/g) of radiation-grafted adsorbent of DADMAC and AAc onto nonwoven PE fabric was compared with those of the other adsorbents reported in other studies, as shown in Table 2. In the present work, the maximum adsorption capacity was found to be 160 mg/g with an initial U(VI) concentration of 1000 ppm at room temperature and undisturbed pH of the solution. Also, according to Langmuir isotherm, the adsorption capacity for the grafted PE was 333.33 mg/g. From the experiment (Table 2), the adsorption capacity of flax fiber showed 40.9 (mg/g) where PE-g-AAc-DADMAC demonstrated 160 mg/g. Further, flower-goethite (MTDFLG) and nano-goethite powder had adsorption capacity 112.35 mg/g and 104.22 mg/g respectively from Langmuir isotherm model. However, adsorbent from this study showed 333.33 mg/g using the same model. Since the adsorption capacity was found to be higher in this experiment, it could be said that the adsorbent which were fabricated had a great affinity to adsorb U(VI) from aqueous solution.

Desorption and Reuse Study

After adsorption, adsorbents were sunk into 20 ml of 1M HCl solution for 5 hours with constant stirring for desorption. It was observed that the desorption was found to be 98%. Furthermore, after desorption, the adsorbents were used for recycling. The adsorbents were treated with 40 mL of 0.01M NaOH for 4 minutes and placed into 1000 ppm U(VI) solution to adsorb as the same process as earlier. In that condition, the maximum adsorption capacity was found to be 150 mg/g, which indicated that the adsorbents could be reused efficiently. Thus, this phenomenon demonstrated that the prepared adsorbent was suitable for recycling and reusing which are very beneficial to lower the cost of overall adsorption process.

CONCLUSIONS

Diallyl dimethyl-ammonium chloride (DADMAC) and acrylic acid (AAc) grafted PE adsorbent was fabricated effectively by the pre-irradiation technique. The prepared adsorbent was characterized by employing FTIR, TGA, and SEM techniques. The radiation dose was optimized to 50 kGy because in that dose, maximum degree of grafting (598%) was achieved. The prepared adsorbent was engaged in adsorbing U(VI) from various aqueous solutions. To complete the adsorption process, it took 48 hours while maintaining pH 3.3 as an optimum condition. The adsorption capacity was found to be 90 mg/g for the treated sample which was higher than the untreated counterpart (80 mg/g). At ambient temperature, the highest adsorption capacity was found to be 160 mg/g in 1000ppm metal solution. Adsorption capacity increased for both the initial metal ion concentrations and the temperature of the aqueous solution. Pseudo-second-order kinetic and Langmuir isotherm models fitted better with U(VI) adsorption. The maximum adsorption capacity was found to be 333.333 mg/g from the Langmuir isotherm model and 160 mg/g from the experiment. Desorption of metal ions and recycling of the adsorbents also showed promising results. To conclude, since the newly prepared grafted polymer was not only low costing but also had high adsorption capacity along with reusability characteristics, the grafted polymer can be considered as an excellent adsorbent for the U(VI) removal from wastewater.

Acknowledgements

The authors are delighted to recognize International Atomic energy Agency (IAEA) and Bangladesh Atomic Energy Commission (BAEC) for technical support to carry out this research. The authors also would like to express sincere gratitude to the Gamma Source Division of the Institute of Food and Radiation Biology (IFRB), Atomic Energy Research Establishment (AERE), Bangladesh Atomic Energy Commission (BAEC).

DATA AVAILABILITY STATEMENT

The authors confirm that the data that supports the findings of this study are available within the article. Raw data that support the finding of this study are available from the corresponding author, upon reasonable request.

CONFLICT OF INTEREST

The authors declared no potential conflicts of interest with respect to the research, authorship, and/or publication of this article.

ETHICS

There are no ethical issues with the publication of this manuscript.

REFERENCES

[1] J. Barnes, D. Kasen, M. R. Wu, and G. Martinez-Pinedo, "Radioactivity and thermalization in the ejecta of compact object mergers and their impact on kilonova light curves," The Astrophysical Journal, Vol. 829(2), Article 110, 2016. [CrossRef]

[2] H. Arvela, M. Markkanen, and H. Lemmelä, "Mobile survey of environmental gamma radiation and fall-out levels in Finland after the Chernobyl accident," Radiation Protection Dosimetry, Vol. 32(3), pp. 177–184, 1990. [CrossRef]

[3] A. Camplani, N. Saino, and A. Pape Mø, "Carotenoids, sexual signals and immune function in barn swallows from Chernobyl," Proceedings of the Royal Society of London. Series B: Biological Sciences, Vol. 266(1424), pp. 1111–1116, 1999. [CrossRef]

[4] M. Asif, and T. Muneer, "Energy supply, its demand and security issues for developed and emerging economies," Renewable and Sustainable Energy Reviews, Vol. 11(7), pp. 1388–1413, 2007. [CrossRef]

[5] D. Copplestone, M. S. Johnson, S. R. Jones, M. E. Toal, and D. Jackson, "Radionuclide behaviour and transport in a coniferous woodland ecosystem: vegetation, invertebrates and wood mice, Apodemus sylvaticus," Science of The Total Environment, Vol. 239(1-3), pp. 95–109, 1999. [CrossRef]

[6] V. Grech, "Births and male: female birth ratio in Scandinavia and the United Kingdom after the Windscale fire of October 1957," International Journal of Risk Safety in Medicine, Vol. 26(1), pp. 45–53, 2014. [CrossRef]

[7] A. R. Oliveira, J. Hunt, N. Valverde, C. Brandao-Mello, and R. Farina, "Medical and related aspects of the Goiânia accident: An overview," Health Physics, Vol. 60(1), pp. 17–24, 1991. [CrossRef]

[8] C. Pietersen, "Analysis of the LPG-disaster in Mexico City," Journal of Hazardous Materials, Vol. 20, pp. 85–107, 1988. [CrossRef]

[9] J. Eid, and B. H. Johnsen, "Acute stress reactions after submarine accidents," Military Medicine, Vol. 167(5), pp. 427–431, 2002. [CrossRef]

[10] M. Takano, V. Romanova, H. Yamazawa, Y. Sivintsev, K. Compton, V. Novikov, and F. Parker, "Reactivity Accident of Nuclear Submarine near Vladivostok," Journal of Nuclear Science and Technology, Vol. 38(2), pp. 143–157, 2001. [CrossRef]

[11] Z. Mian, M. Ramana, and A. Nayyar, "Nuclear submarines in South Asia: New risks and dangers," Journal for Peace Nuclear Disarmament, Vol. 2(1), pp. 184–202, 2019. [CrossRef]

[12] W. M. Arkin, and J. Handler, "Naval Accidents, 1945-1988," Greenpeace, 1989.

[13] C. Tingle, "Submarine accidents a 60-year statistical assessment," Professional Safety, Vol. 54(9), 2009.

[14] D. Ball, "Nuclear war at sea," International Security, Vol. 10(3), pp. 3–31, 1985. [CrossRef]

[15] K. Maher, J. R. Bargar, and G. E. Brown Jr, "Environmental speciation of actinides," Inorganic chemistry, Vol. 52(7), pp. 3510–3532, 2013. [CrossRef]

[16] G. Sheng, X. Shao, Y. Li, J. Li, H. Dong, W. Cheng, X. Gao, and Y. Huang, "Enhanced removal of uranium (VI) by nanoscale zerovalent iron supported on Na–bentonite and an investigation of mechanism," The Journal of Physical Chemistry, Vol. 118(16), pp. 2952–2958, 2014. [CrossRef]

[17] Y. Sun, C. Ding, W. Cheng, and X. Wang, "Simultaneous adsorption and reduction of U (VI) on reduced graphene oxide-supported nanoscale zerovalent iron," Journal of Hazardous Materials, Vol. 280, pp. 399–408, 2014. [CrossRef]

[18] N. Sethy, V. Jha, P. Ravi, and R. Tripathi, "Assessment of human exposure to dissolved radon in groundwater around the uranium industry of Jaduguda, Jharkhand, India," Current Science, Vol. 109(10), pp. 1855–1860, 2015. [CrossRef]

[19] R. Konietzka, "Gastrointestinal absorption of uranium compounds–A review," Regulatory Toxicology Pharmacology, Vol. 71(1), pp. 125–133, 2015. [CrossRef]

[20] S. V. Gudkov, A. V. Chernikov, and V. I. Bruskov, "Chemical and radiological toxicity of uranium compounds," Russian Journal of General Chemistry, Vol. 86(6), pp. 1531–1538, 2016. [CrossRef]

[21] R. L. Njinga, V. M. Tshivhase, and M. Mathuthu, "Chemical toxicity of surface-based drinking water sources due to natural uranium pollutant around princess gold mine environs in Roodepoort, South Africa," Exposure Health, Vol. 8(4), pp. 457–464, 2016. [CrossRef]

[22] A. S. Saini and J. S. Melo, "Biosorption of uranium by human black hair," Journal of Environmental Radioactivity, Vol. 142, pp. 29–35, 2015. [CrossRef]

[23] L. Yuan, M. Sun, X. Liao, Y. Zhao, Z. Chai, and W. Shi, "Solvent extraction of U (VI) by trioctylphosphine oxide using a room-temperature ionic liquid," Science China Chemistry, Vol. 57(11), pp. 1432–1438, 2014. [CrossRef]

[24] A. Mellah, S. Chegrouche, and M. Barkat, "The precipitation of ammonium uranyl carbonate (AUC): thermodynamic and kinetic investigations," Hydrometallurgy, Vol. 85(2-4), pp. 163–171, 2007. [CrossRef]

[25] T. P. Rao, P. Metilda, and J. M. Gladis, "Preconcentration techniques for uranium (VI) and thorium (IV) prior to analytical determination—An overview," Talanta, Vol. 68(4), pp. 1047–1064, 2006. [CrossRef]

[26] C. Banerjee, N. Dudwadkar, S. C. Tripathi, P. M. Gandhi, V. Grover, C. P. Kaushik, and A. K. Tyagi, "Nano-cerium vanadate: A novel inorganic ion exchanger for removal of americium and uranium from simulated aqueous nuclear waste," Journal of Hazardous Materials, Vol. 280, pp. 63–70, 2014. [CrossRef]

[27] Z. Song, W. Huang, Y. Zhou, Z. Q. Tian, Z. M. Li, and D. J. Tao, "Thermally regulated molybdate-based ionic liquids toward molecular oxygen activation for one-pot oxidative cascade catalysis," Green Chemistry, Vol. 22(1), pp. 103–109, 2020. [CrossRef]

[28] W. Hui, Y. Zhou, Y. Dong, Z. J. Cao, F. Q. He, M. Z. Cai, and D. J. Tao, "Efficient hydrolysis of hemicellulose to furfural by novel superacid SO4H-functionalized ionic liquids," Green Energy Environment, Vol. 4(1), pp. 49–55, 2019. [CrossRef]

[29] D. R. Lovley, E. J. Phillips, Y. A. Gorby, and E. R. Landa, "Microbial reduction of uranium," Nature, Vol. 350(6317), pp. 413–416, 1991. [CrossRef]

[30] N. K. Gupta, A. Sengupta, A. Gupta, J. R. Sonawane, and H. Sahoo, "Biosorption-an alternative method for nuclear waste management: A critical review," Journal of Environmental Chemical Engineering, Vol. 6(2), pp. 2159–2175, 2018. [CrossRef]

[31] X. Liu, C. Cheng, C. Xiao, D. Shao, Z. Xu, J. Wang, S. Hu, X. Li, and W. Wang, "Polyaniline (PANI) modified bentonite by plasma technique for U (VI) removal from aqueous solution", Applied Surface Science, Vol. 411, pp. 331–337, 2017. [CrossRef]

[32] F. F. Chen, K. Huang, J. P. Fan, and D. Tao, "Chemical solvent in chemical solvent: A class of hybrid materials for effective capture of CO2," AIChE Journal, Vol. 64(2), pp. 632–639, 2018. [CrossRef]

[33] H. Zhao, X. Liu, M. Yu, Z. Wang, B. Zhang, H. Ma, M. Wang, and J. Li, "A study on the degree of amidoximation of polyacrylonitrile fibers and its effect on their capacity to adsorb uranyl ions," Industrial & Engineering Chemistry Research, Vol. 54(12), pp. 3101–3106, 2015. [CrossRef]

[34] X. C. An, Z. M. Li, Y. Zhou, W. Zhu, and D. J. Tao, "Rapid capture and efficient removal of low-concentration SO2 in simulated flue gas by hypercross-linked hollow nanotube ionic polymers," Chemical Engineering Journal Vol. 394, Article 124859, 2020. [CrossRef]

[35] Y. Q. Wang, Z. B. Zhang, Y. H. Liu, X. H. Cao, Y. T. Liu, and Q. Li, "Desorption of U (VI) from aqueous solution by the carboxyl-mesoporous carbon," Chemical Engineering Journal, Vol. 198, pp. 246–253, 2012. [CrossRef]

[36] W. P. Li, X. Y. Han, X. Y. Wang, Y. Q. Wang, W. X. Wang, H. Xu, T. S. Tan, W. S. Wu, H. and X. Zhang, "Recovery of uranyl from aqueous solutions using amidoximated polyacrylonitrile/exfoliated Na-montmorillonite composite," Chemical Engineering Journal, Vol. 279, pp. 735–746, 2015. [CrossRef]

[37] J. Wang, and S. Zhuang, "Removal of cesium ions from aqueous solutions using various separation technologies," Reviews in Environmental Science Bio/Technology, Vol. 18(2), pp. 231–269, 2019. [CrossRef]

[38] J. Huang, B. Huang, T. Jin, Z. Liu, D. Huang, and Y. Qian, "Electrosorption of uranium (VI) from aqueous solution by phytic acid modified chitosan: An experimental and DFT study," Separation and Purification Technology, Vol. 284, Article 120284, 2022. [CrossRef]

[39] L. Zhong, F. He, Z. Liu, B. Dong, and J. Ding, "Adsorption of uranium (VI) ions from aqueous solution by acrylic and diaminomaleonitrile modified cellulose," Colloids and Surfaces A: Physicochemical and Engineering Aspects, Vol. 641, Article 128565, 2022. [CrossRef]

[40] Y. Li, Y. Dai, Q. Tao, Z. Gao, and L. Xu, "Ultrahigh efficient and selective adsorption of U(VI) with amino acids-modified magnetic chitosan biosorbents: Performance and mechanism," International Journal of Biological Macromolecules, Vol. 214, pp. 54–66, 2022. [CrossRef]

[41] M. F. Schettini, G. Wu, and T. W. Hayton, "Synthesis and reactivity of a uranyl-imidazolyl complex," Chemical Communications, Vol. 48(10), pp. 1484–1486, 2012. [CrossRef]

[42] D. Shao, Y. Li, X. Wang, S. Hu, J. Wen, J. Xiong, A. M. Asiri, and H. M. Marwani, "Phosphate-functionalized polyethylene with high adsorption of uranium (VI)," ACS Omega, Vol. 2(7), pp. 3267–3275, 2017. [CrossRef]

[43] X. Liu, J. Li, X. Wang, C. Chen, and X. Wang, "High performance of phosphate-functionalized graphene oxide for the selective adsorption of U (VI) from acidic solution," Journal of Nuclear Materials, Vol. 466, pp. 56–64, 2015. [CrossRef]

[44] M. Rana, "Radiation Grafting of Polymers for Advanced Application," © [Master Thesis] University of Dhaka, 2022.

[45] J. Wu, K. Tian, and J. Wang, "Adsorption of uranium (VI) by amidoxime modified multiwalled carbon nanotubes," Progress in Nuclear Energy, Vol. 106, pp. 79–86, 2018. [CrossRef]

[46] D. Yuan, L. Chen, X. Xiong, L. Yuan, S. Liao, and Y. Wang, "Removal of uranium (VI) from aqueous solution by amidoxime functionalized superparamagnetic polymer microspheres prepared by a controlled radical polymerization in the presence of DPE," Chemical Engineering Journal, Vol. 285, pp. 358–367, 2016. [CrossRef]

[47] S. Shukla, and V. Skhardande, "Column studies on metal ion removal by dyed cellulosic materials," Journal of Applied Polymer Science, Vol. 44(5), pp. 903–910, 1992. [CrossRef]

[48] R. Torkaman, F. Maleki, M. Gholami, M. Torab-Mostaedi, and M. Asadollahzadeh, "Assessing the radiation-induced graft polymeric adsorbents with emphasis on heavy metals removing: A systematic literature review," Journal of Water Process Engineering, Vol. 44, Article 102371, 2021. [CrossRef]

[49] Y. Ho, J. Ng, and G. McKay, "Removal of lead (II) from effluents by sorption on peat using second-order kinetics," Separation Science Technology, Vol. 36(2), pp. 241–261, 2001. [CrossRef]

[50] N. Unlu, and M. Ersoz, "Adsorption characteristics of heavy metal ions onto a low cost biopolymeric sorbent from aqueous solutions," Journal of Hazardous Materials, Vol. 136(2), pp. 272–280, 2006. [CrossRef]

[51] R. Nazia, D. N. Chandra, S. Shahnaz, A. F. Tasneem, and M. A. Rahim, "Application of acrylic acid and sodium styrene sulfonate grafted non-woven PE Fabric in methylene blue removal," Research Journal of Chemistry Environment, Vol. 24(5), pp. 26–42, 2020.

[52] N. Dalalia, M. Kazeraninejada, and A. Akhavan, "Removal of heavy metal ions from wastewater samples using electron beam radiation in the presence of TiO2," Desalination and Water Treatment, Vol. 71, pp. 136–144, 2017. [CrossRef]

[53] M. Agarwal, and K. Singh, "Heavy metal removal from wastewater using various adsorbents: A review," Journal of Water Reuse and Desalination, Vol. 7(4), pp. 387–419, 2017. [CrossRef]

[54] M. M. Nasef, "Gamma radiation-induced graft copolymerization of styrene onto poly (ethyleneterephthalate) films," Journal of Applied Polymer Science, Vol. 77(5), pp. 1003–1012, 2000. [CrossRef]

[55] E. S. A. Hegazy, H. Kamal, N. Maziad, and A. Dessouki, "Membranes prepared by radiation grafting of binary monomers for adsorption of heavy metals from industrial wastes," Nuclear Instruments Methods in Physics Research Section B: Beam Interactions with Materials Atoms, Vol. 151(1-4), pp. 386–392, 1999. [CrossRef]

[56] E. S. A. Hegazy, H. Kamal, N. Khalifa, and G. A. Mahmoud, "Separation and extraction of some heavy and toxic metal ions from their wastes by grafted membranes," Journal of Applied Polymer Science, Vol. 81(4), pp. 849–860, 2001. [CrossRef]

[57] N. Rahman, N. Sato, S. Yoshioka, M. Sugiyama, H. Okabe, and K. Hara, "Selective Cu (II) adsorption from aqueous solutions including Cu (II), Co (II), and Ni (II) by modified acrylic acid grafted PET film," International Scholarly Research Notices, Vol. 2013(7), 2013. [CrossRef]

[58] H. Abd El-Rehim, E. Hegazy, and A. E. H. Ali, "Selective removal of some heavy metal ions from aqueous solution using treated polyethylene-g-styrene/maleic anhydride membranes," Reactive and Functional Polymers, Vol. 43(1-2), pp. 105–116, 2000. [CrossRef]

[59] H. Asamoto, Y. Kimura, Y. Ishiguro, H. Minamisawa, and K. Yamada, "Use of polyethylene films photografted with 2-(dimethylamino) ethyl methacrylate as a potential adsorbent for removal of chromium (VI) from aqueous medium," Journal of Applied Polymer Science, Vol. 133(18), 2016. [CrossRef]

[60] D. Guo, X. Song, L. Zhang, W. Chen, D. Chu, and L. Tan, "Recovery of uranium (VI) from aqueous solutions by the polyethyleneimine-functionalized reduced graphene oxide/molybdenum disulfide composition aerogels," Journal of the Taiwan Institute of Chemical Engineers, Vol. 106, pp. 198–205, 2020. [CrossRef]

[61] S. Das, Y. Oyola, R. T. Mayes, C. J. Janke, L. J. Kuo, G. Gill, J. R. Wood and S. Dai, "Extracting uranium from seawater: promising AF series adsorbents," Industrial Engineering Chemistry Research, Vol. 55(15), pp. 4110–4117, 2016. [CrossRef]

[62] M. Wei, J. Liao, N. Liu, D. Zhang, H. Kang, Y. Yang, Y. Yang, and J. Jin, "Interaction between uranium and humic acid (I): Adsorption behaviors of U (VI) in soil humic acids," Nuclear Science Techniques, Vol. 18(5), pp. 287–293, 2007. [CrossRef]

[63] M. M. Marjub, N. Rahman, N. C. Dafader, F. S. Tuhen, S. Sultana, and F. T. Ahmed, "Acrylic acid-chitosan blend hydrogel: A novel polymer adsorbent for adsorption of lead (II) and copper (II) ions from wastewater," Journal of Polymer Engineering, Vol. 39(10), pp. 883–891, 2019. [CrossRef]

[64] S. Biswas, V. Rupawate, K. Hareendran, S. B. Roy, and J. K. Chakravartty, "Novel precipitation technique for uranium recovery from carbonate leach solutions," Journal of Radioanalytical and Nuclear Chemistry, Vol. 304(3), pp. 1345–1351, 2015. [CrossRef]

[65] S. Rengaraj, J. W. Yeon, Y. Kim, Y. Jung, Y. K. Ha, and W. H. Kim, "Adsorption characteristics of Cu (II) onto ion exchange resins 252H and 1500H: Kinetics, isotherms and error analysis," Journal of Hazardous Materials, Vol. 143(1-2), pp. 469–477, 2007. [CrossRef]

[66] S. K. Yadav, D. K. Singh, and S. Sinha, "Adsorption study of lead (II) onto xanthated date palm trunk: kinetics, isotherm and mechanism," Desalination Water Treatment, Vol. 51(34-36), pp. 6798–6807, 2013. [CrossRef]

[67] S. Vukovic, L. A. Watson, S. O. Kang, R. Custelcean, and B. P. Hay, "How amidoximate binds the uranyl cation," Inorganic Chemistry, Vol. 51(6), pp. 3855–3859, 2012. [CrossRef]

[68] A. Abutaleb, A. M. Tayeb, M. A. Mahmoud, A. M. Daher, O. A. Desouky, O. Y. Bakather, and Farouq, R. "Removal and recovery of U (VI) from aqueous effluents by flax fiber: Adsorption, desorption and batch adsorber proposal," Journal of Advanced Research, Vol. 22, pp. 153–162, 2020. [CrossRef]

[69] M. A. Mahmoud, "Adsorption of U (VI) ions from aqueous solution using silicon dioxide nanopowder," Journal of Saudi Chemical Society, Vol. 22(2), pp. 229–238, 2018. [CrossRef]

[70] L. Zhang, X. Zhang, Q. Lu, X. Wu, T. Jiang, L. Mi, and Y. Peng, "Adsorption of U (VI) ions from aqueous solution using nanogoethite powder," Adsorption Science Technology, Vol. 37(1-2), pp. 113–126, 2019. [CrossRef]

[71] A. Hussein, and A. Morsy, "Uranium recovery from wet-process phosphoric acid by a commercial ceramic product," Arabian Journal of Chemistry, Vol. 10, pp. 361–367, 2017. [CrossRef]

[72] X. Zhang, T. Jiang, C. Xie, Y. Peng, M. Li, and Y. Zhong, "Preparation of a phosphate-modified flower-like α-FeOOH composite and its application for aqueous U (VI) removal," Water, Air, Soil Pollution, Vol. 229(3), pp. 1–11, 2018. [CrossRef]

Environ Res Tec, Vol. 6, Issue. 1, pp. 35–45, March 2023

Environmental Research and Technology
https://ert.yildiz.edu.tr - https://dergipark.org.tr/tr/pub/ert
DOI: https://doi.org/10.35208/ert.1222222

Environmental Research & Technology

Research Article

Sustainability improvement by utilizing polymer waste as an energy source for a diesel engine with alcohol additives

Padmanabhan SAMBANDAM[*1], Vinod Kumar THANGARAJ[2], Mahalingam SELVARAJ[3], Giridharan KRISHNAN[4], Ganesan SUBBIAH[5]

[1]*School of Mechanical and Construction, Vel Tech Rangarajan Dr. Sagunthala R & D Institute of Science and Technology, Chennai, India*
[2]*School of Mechanical Engineering, Vels Institute of Science, Technology & Advanced Studies (VISTAS), Chennai, India*
[3]*Department of Mechanical Engineering, Sona College of Technology, Salem, India*
[4]*Department of Mechanical Engineering, Easwari Engineering College, Chennai, India*
[5]*School of Mechanical Engineering, Sathyabama Institute of Science and Technology, Chennai, India*

ARTICLE INFO

Article history
Received: 27 December 2022
Revised: 13 January 2023
Accepted: 05 March 2023

Key words:
Alcohol additives; Diesel engine; Emission; Full factorial design; Polyethylene polymer; Waste to energy

ABSTRACT

Energy and fossil fuel supplies have been threatened by the depletion of fossil fuels on a global scale, as well as by the constant rise in oil prices and the continual increase in environmental degradation. On the other hand, polymer waste has increased due to its usage in a daily lifestyle because of its cheap cost, ease of production, and adaptability. Indirectly, these polymer wastes are causing some major problems for the ecosystem and other living things. By transforming waste polymers into usable energy, can address for both the non-biodegradability of polymers and the need for an alternative fuel. This research paper aims to evaluate the performance of fuel produced by the pyrolysis of polyethylene polymer. Three distinct alcohol additive blends with polymer fuel were investigated in a single-cylinder direct injection diesel engine for their performance and emission characteristics. The engine efficiency of pentanol was found to be about 3.4% higher than that of base diesel, and with 7% better fuel consumption. Additionally, alcohol additives reduced CO emissions by 3.6%–3.8% and HC emissions by 3.5%–3.8%. The results were further analysed using the design of experiment tool, "Full Factorial Design" to determine the most optimal running condition with fuel consumption of 0.4508 kg/kWh, hydrocarbon of 49 ppm and carbon monoxide 0.265% at half load conditions.

Cite this article as: Sambandam P, Thangaraj VK, Selvaraj M, Krishnan G, Subbiah G. Sustainability improvement by utilizing polymer waste as an energy source for a diesel engine with alcohol additives. Environ Res Tec 2023;6:1:35–45.

INTRODUCTION

Researchers are working around the clock to discover alternative sustainable energy sources that may address the difficulties that are occurring as a result of the depletion of non-renewable energy sources. However, a suitable waste management strategy is an additional key component of long-term success and development. Plastics are

***Corresponding author.**
*E-mail address: padmanabhan.ks@gmail.com

one of the most extensively used materials on the planet, and while they are non-biodegradable in nature, they are being employed on a variety of fronts owing to the vast variety of applications, flexibility, and cost-effectiveness that they provide. Every day, people rely on plastic for a variety of functions [1].

Due to its great demand and economic feasibility, plastic trash recycling was also pushed. Recycling plastic trash into liquid fuel also has the additional advantages of conserving resources and reducing greenhouse gas emissions [2]. In addition to reducing strain on natural resources and coping with fast industrialization and economic expansion, energy recovery from waste plastics is seen as a potential option. It has already been done commercially in certain border and industrialised countries. Because of their high combustibility and abundance in nearby areas, waste plastics are considered highly competent resources for the extraction of petro-fuels. Waste plastics may be converted into fuel using a variety of methods, depending on the nature of the material [3].

The lower viscosity of alcohol as compared to diesel allows for more efficient atomization of the fuel injected into the cylinders and better mixing with the surrounding air when alcohol is combined with diesel. A significant amount of latent heat of evaporation exists in alcohol, which means that utilizing alcohol in a diesel engine by blending it with diesel or biodiesel fuel may improve the overall volume efficiency by cooling the alcohol during the intake and compression strokes [4]. The inclusion of propane resulted in lower smoke emissions than diesel and plastic oil, but greater HC (hydrocarbon) emissions than both. Plastic oil and diesel blends with 5% Propanol by volume beat their diesel equivalents in terms of NOx (Nitrogen Oxide) emissions. More propanol mixes produced more NOx than plastic oil and diesel. The thermal efficiency of the engine improved as the quantity of propanol in the blends increased [5].

A comparison between the performance and emissions of a municipal waste plastic oil-fuelled in diesel engine in this research. Adding nano-fluids to a municipal waste plastic oil mix improves brake thermal efficiency and reduces fuel consumption. The introduction of nano-fluids decreased hydrocarbon, carbon monoxide and increased NOx emissions compared to MPO20 [6]. The research work is aimed at developing a delayed timing engine with minimal heat rejection and a combustion chamber surface that has been partially stabilised zirconia ceramic-coated. The influence of fuel injection time on the performance of waste plastic oil in low heat rejection engines was investigated in order to get a complete understanding of the performance of waste plastic oil in low heat rejection engines. In the wake of the study, performance and emission metrics have significantly improved substantially [7].

Diesel and plastic oil were used to compare the performance of coated and uncoated engines. Performance has improved and specific fuel consumption has decreased as a result of this investigation. Diesel engines covered with zirconia had lower emissions, except for NOx, than diesel engines that were not coated with zirconia [8]. Exploring the effects of variable compression ratio diesel engine performance and emissions on variable parameters such as injection pressure and time. Various proportions of ethanol and diesel are mixed with plastic oils to make test fuels. The experimental analysis shows that P90D5E5 mix has the maximum thermal efficiency, increasing by 16 and 38% over pure diesel and pure plastic oil [9].

Three high-carbon alcohols were oxygenated and their effects on emissions and performance of a diesel engine were compared. For the greatest reduction of NOx and smoke emissions while utilising the least amount of fuel, a response surface methodology-based optimization was used [10]. The performance and emissions of a diesel engine utilising waste plastic oil generated by pyrolysis using Zeolite-A as a catalyst are being investigated. Using 20% plastic oil-diesel enhances thermal efficiency and decreases brake specific fuel consumption. The NOx and HC emissions are lower at low loads and increase with load [11].

Plastic oil blends, and its distilled derivatives may be used to power the engine without requiring modification. However, both raw plastic oil and distilled plastic oil had a significant negative impact on engine performance and emission levels. A greater density and viscosity, lower cetane number, higher sulphur content and acid value were all factors contributing to this [12].

When the load rises, the thermal efficiency improves and the fuel consumption decreases due to the greater concentration of plastic oil in the mix. High in-cylinder pressure is caused by plastic oil's high heat release and delayed ignition. Oxygenated chemicals in plastic oil also aid to reduce emissions from burning. Diesel engines may utilise up to 50% plastic oil in the mix with just a minor increase in CO emissions at higher loads [13]. The combustion and performance study of the engine and the pyrolysis oil may serve as a substitute for conventional fuel. The addition of pyrolysis oil does not result in outstanding performance like diesel fuel, as shown by combustion studies such as the fuel consumption and efficiency. Adding nanoparticles to them, on the other hand, improves their performance [14].

Thermal efficiency and emission quality improve with load, compression ratio, and waste plastic oil and ethanol in diesel. ANOVA and multivariate analysis determined the optimal engine load, compression ratio, and fuel blend, boosting performance and minimizing emissions. With a compression ratio of 18.1, and 20% WPO and 20% ethanol blended diesel, braking thermal efficiency and emissions were optimized [15]. The tertiary fuel mix

Table 1. Properties of polymer oil, ethanol, pentanol and methanol

Sl. No	Fuel property	Unit	Diesel	WPO20	Ethanol	Pentanol	Methanol
1	Density, at 15 °C	(g/m^3)	0.843	0.810	0.799	0.814	0.794
2	Viscosity, at 40 °C	(cSt)	2.45	2.52	1.10	2.88	0.68
3	Calorific valve	(MJ/kg)	42.31	40.12	28.18	34.65	20.10
4	Flash point	(°C)	61	38	16	49	14
5	Cetane index	–	54	51	8	20	5

contained three WPO concentrations and ethanol. Performance, emission, and Full Factorial Design analyzed the best running condition [16]. Optimization based on the design of experiments (DoE) was used with a three-factor full factorial experimental design was used to minimize emissions while maximizing fuel economy. CO, HC, and fuel efficiency surface contour plots determined to be statistically significant [17].

This study aims to investigate the effects of three different alcohols on Waste Polymer Oil (WPO) biodiesel blends at 20% and 60% with pure diesel. The performance and emissions analysis are carried out on a single-cylinder diesel engine under varying load conditions. The results of fuel consumption, emission of hydrocarbons, and carbon monoxide were optimized for engine load and type of alcohol by the design of the experiment tool.

MATERIALS AND METHODS

Cleaner and more efficient than traditional fossil fuels, biofuels made from plastics have a low sulphur concentration. Diesel fuel with a high sulphur content is now used in many developing nations. Liquid fuels may be made from plastic trash, which reduces white pollution while also helping to ease energy constraint. In comparison to fossil diesel, waste plastic oil has comparable features, such as a greater heating value [18].

Pyrolysis yield is influenced by several factors, including the kind of plastic used, the temperature and length of operation, the catalyst type used, and any additional materials added to enhance decomposition. The pyrolysis product from each form of recycled plastic relies on the temperature maintained during pyrolysis and the time it takes to decompose to produce the liquid and gaseous fuel from the material. Incorporating a wide variety of catalysts may help improve oil yield rates. Once again, how well the catalyst works is influenced by the aforementioned variables. Therefore, in order to extract the maximum amount of liquid oil possible, the proper catalyst and operating conditions must be used. A few substances may also speed up the breakdown process [19]. The properties of Polymer oil, Ethanol, Pentanol and Methanol are tabulated in Table 1.

An increase in biodiesel evaporation, a reduction in delay time, and an improvement in secondary atomization minimise emissions when nanoparticles are combined with biodiesel. The combustion process is also made more catalytic by the addition of these activities. The capacity to store energy inside nanoscale metal particles enhances a chemical process. Though it has a higher surface area to volume ratio, nanofluid has a greater ability to improve the pace at which oxygen and fuel react, resulting in a better combustion [6].

EXPERIMENTAL DETAILS

The plastic oil sample used in this investigation was made by pyrolyzing municipal plastic waste. The pyrolysis batch reactor heats the plastic to 600 °C. The heater used in the test was driven by NiCr-based electrical resistance. The liquid nitrogen trap is required because it distributes heat evenly and generates inert conditions for pyrolysis. Unsteady heat input from an autotransformer. The reactor lasted at 500 °C for three hours before cooling down. The pyrolysis evaporated product is collected in a container. The condensed bio-oil is subsequently refrigerated by an external cooling medium. After pyrolysis, the plastic char was separated [20].

Waste Polymer Oil biodiesel blends were tested in a single-cylinder, constant-speed direct-injection engine, as shown in Figure 1 [17]. Speed is maintained regardless of load and biodiesel mix percentages in the diesel engine. The engine was coupled to an eddy current dynamometer, which was used to alter the loads from 0% to 100%. For each of the testing blends, the load is increased by 25%, 50%, 75%, and 100%, according to the 4.4 kW power output of the engine.

An eddy current dynamometer, which monitors current flow, is used to adjust the engine loads manually. The airflow rate was measured using a calibrated orifice on an air drum, and the fuel flow rate was analyzed with a calibrated burette in this investigation. Two fuel tanks were employed for the fuel flow measurement; one was filled with pure diesel and the other with esterified biodiesel, and the fuel flow was recorded. AVL software was put on the test rig, allowing for the collection of various readings and outcomes while the machine was in operation. Table 2 represents the experimental measurements, instruments and its parameters.

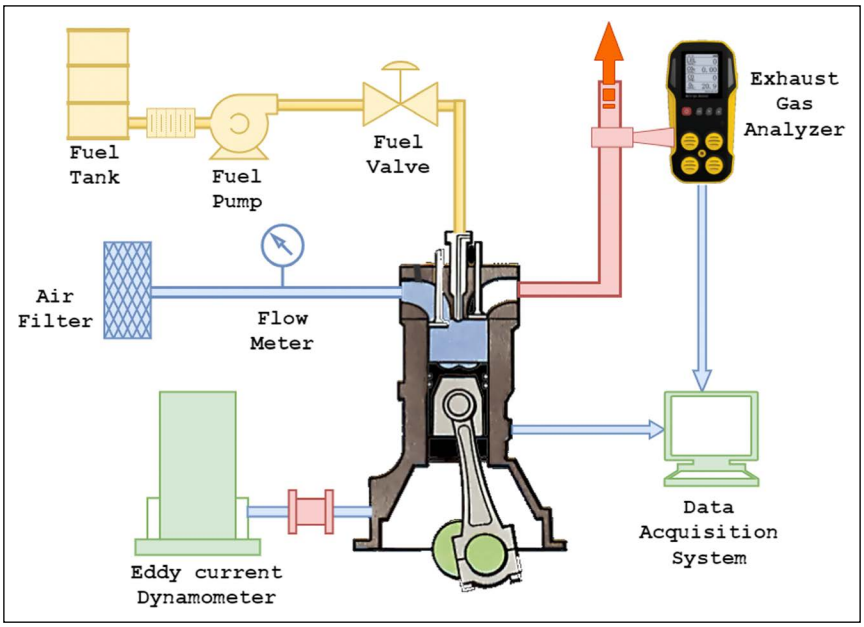

Figure 1. Experimental engine setup.

Table 2. Experimental instruments and its parameters

Sl. No	Measurement	Range	Accuracy	Instrument
1	Hydrocarbon	0 to 20000 ppm	± 10 ppm	AVL gas analyser
2	Carbon monoxide	0 to 15%	± 0.05%	AVL gas analyser
3	Nitrogen oxides	0 to 5000 ppm	± 10 ppm	AVL gas analyser
4	Engine load	–	+0.1 kg to −0.1 kg	Load cell
5	Crank speed	0–10000 rpm	± 10 rpm	Digital tachometer
6	Fuel quantity	0–50 cm^3	± 0.1 cm^3	Burette measurement

This study focuses on energy recovery from waste polymer oil as the alternative fuel source via the waste utilization approach. In this study, we used a novel mixture of shredded HDPE and LDPE in a ratio of 40:60 as the source of plastic oil extraction to use as plastic fuel. HDPE and LDPE testing needed a response time of 60 and 50 minutes, and the material was pyrolyzed into oil at 450 °C. LDPE pyrolysis products show a 60% oil yield, while HDPE pyrolysis products show a 50% oil yield, 25% wax formation, 25% gas formation, and coke formation.

Waste polymer oil obtained from the pyrolysis process of polyethylene polymer were blended with diesel at constant ratios of 20% on a volume basis, along with oxygenated additives of three different alcohols Ethanol, Pentanol and Methanol. The biodiesel fuel named WPO20E20, formed by the blends of 20% waste polymer oil biodiesel, 20% ethanol on a volume basis mixed with pure diesel of 60%. The fuel blends prepared as WPO20P20 (60% diesel + 20% WPO + 20% Pentanol), WPO20M20 (60% diesel + 20% WPO+ 20% Methanol) and WPO20 (80% diesel + 20% WPO).

RESULTS AND DISCUSSION

Brake Thermal Efficiency

The brake thermal efficiency of WPO20P20 was found to be about 3.4 % higher than that of pure diesel when tested under various load conditions (Fig. 2). Researchers found that the addition of low cetane number alcohols to blends increases the time it takes for the fuels to ignite because of the OH radicals' ability to remove hydrogen from the carbon position in most of the alcohols [5]. The efficiency of WPO over 20% has been shown to be negatively impacted. Because WPO has a greater calorific value than diesel, the WPO-diesel blend's calorific value is likewise higher than diesel. Addition of WPO to a diesel mix, however, may also cause viscosity and density increases as well as decreased heat release rates, which can have an impact on how well fuel is dispersed in the combustion process. This can lead to poorer thermal efficiency [11].

Brake Specific Fuel Consumption

By incorporating nanoparticles into the physical qualities of the fuel, as well as by providing an abundance of extra oxygen to complete the burning process, fuel consumption is re-

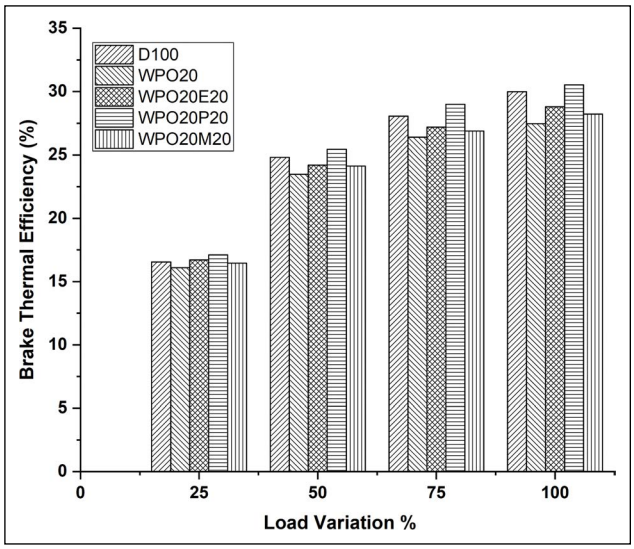

Figure 2. Variation of brake thermal efficiency on WPO.

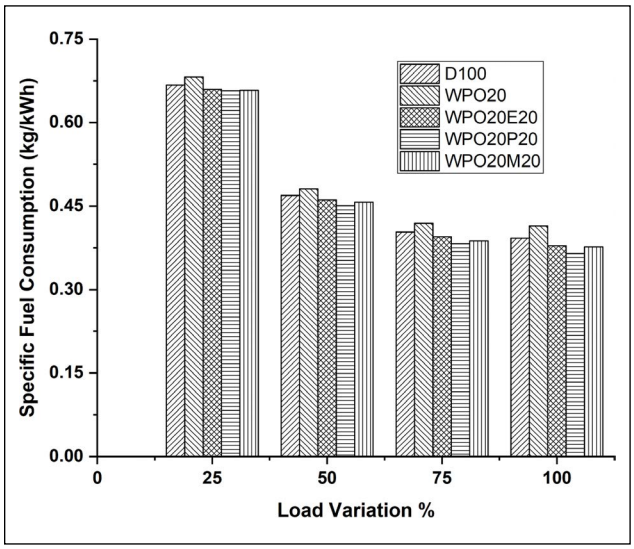

Figure 3. Variation of specific fuel consumption on WPO.

duced. There are less carbon deposits in the cylinder because of the nanoparticle treatment, which lowers the frictional power generated inside and lowers fuel consumption [6]. WPO20P20, WPO20M20 and WPO20E20 blends reached out maximum of 7%, 4% and 3.5% reduction in Specific Fuel Consumption (SFC) than diesel and WP20 blends reached out 2 to 5.5% increased fuel consumption than diesel as shown in Figure 3. As a consequence of the combustion being moved to a later stage due to a later injection timing, the pressure rises only during fast expansion, resulting in a lower effective pressure and a lower output. Combustion quality accounted for the majority of the disparity in fuel consumption across the mixes, even if the heating values were near [10].

Carbon Monoxide Emission

The blends of WPO20P20, WPO20M20 and WPO20E20 blends reached out maximum of 6.2%, 3.3% and 3.5% reduction in CO than diesel and WP20 blends reached out 2.7% increased carbon monoxide than diesel as shown in Figure 4 at various load conditions. It is due to the increased temperature of the gas that the amount of pre-mixed combustion is reduced. Because of this, the initial CO creation has been reduced in magnitude. Given its lower cetane number and greater aromatic content, WPO burns more slowly than gasoline and so burns for a shorter amount of time than gasoline [8]. High oxygen concentration means that WPO blends create fewer CO emissions than baseline fuels, which is why WPO blends have been found to be more environmentally friendly. In order to enhance combustion and reduce CO emissions, a lower viscosity and a greater latent heat of vaporisation of the mix are necessary [18].

Hydrocarbon Emission

During initial load operations, fuel with an excess of oxygen predominates inside the cylinder. This additional air decreases the quantity of fuel that travels through the cham-

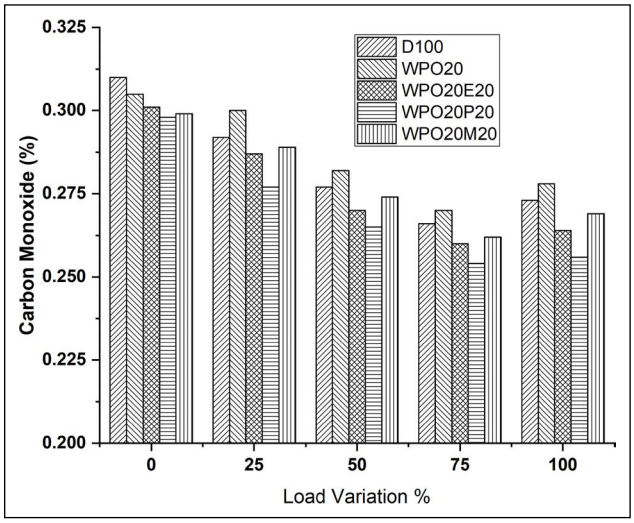

Figure 4. Variation of carbon monoxide emissions on WPO.

ber, resulting in a reduction in the amount of heat that is released. As a result, more fuel is likely to exit the chamber along with the exhaust [20].

The blends of WPO20P20, WPO20M20 and WPO20E20 blends reached out maximum of 5.8%, 3.3% and 3.8% reduction in hydrocarbon than diesel. The greater viscosity of the WPO20 blends resulted in poor vaporization, spray penetration, and greater HC emissions as a result of the process. WP20 blends reached out 11% increased HC than diesel as shown in Figure 5 at various load conditions. High viscosity reduces vapour pressure and increases droplet generation, while it exacerbates incomplete combustion. Lower air-to-fuel ratio and temperature allow HC to escape into the exhaust at lower loads and temperatures. Increasing the WPO percent fraction in the mix increases emissions due to incomplete combustion and unreacted

Table 3. Analysis of variance of fuel consumption

Source	DF	Seq SS	Contribution	Adj SS	Adj MS	F-value	P-value
Model	4	0.128787	99.97%	0.128787	0.021465	998.57	0.001
Model	4	0.128787	99.97%	0.128787	0.021465	998.57	0.001
LOAD	2	0.026706	20.73%	0.026706	0.006676	310.60	0.003
Alcohol	2	0.102052	79.21%	0.001677	0.000839	39.02	0.025
Error	4	0.00121	0.06%	0.000043	0.000021		
Total	8	-0.12997	100.00%				

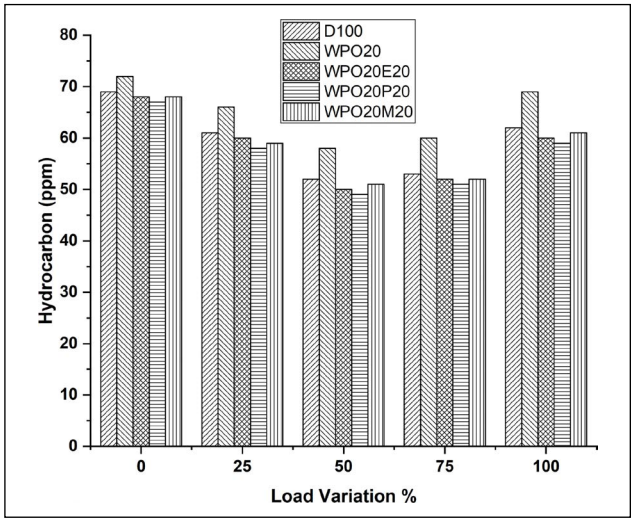

Figure 5. Variation of hydrocarbon emissions on WPO.

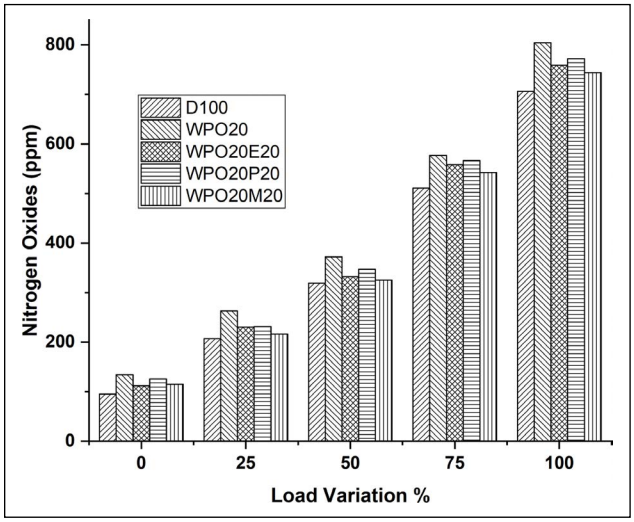

Figure 6. Variation of nitrogen oxides emissions on WPO.

hydrocarbons. PPO mixtures are connected to higher HC emissions for two reasons. Due to the lack of spreading, WPO mixes gather around walls and cracks, leaving them unburnt. Unsaturated hydrocarbons that do not burn and are ejected with the exhaust are the second major reason. Blends with high aromatic content emit more HC because they burn faster and ignite slower [13].

Nitrogen Oxide Emission

The premixed combustion phase of combustion has improved with the addition of greater alcohols to diesel, which aids in the reduction of soot emissions, as is evident. Certain instances of alcohol's evaporation enthalpy property have been claimed to have reduced NOx emissions concurrently owing to the cooling impact that occurs when alcohol evaporates [21]. As a consequence of the higher fuel use, increased engine load was blamed for the spike in NOx emissions. WPO20P20, WPO20M20 and WPO20E20 blends produce NOx at a rate of 10 %, 6 %, and 9% greater than diesel. WPO20 makes more than 15% than pure diesel. NOx emissions are produced as a consequence of a chemical interaction between oxygen and nitrogen molecules that does not occur in equilibrium in the high-temperature burned gas areas. Nitrogen dioxide and nitrogen monoxide (NO) are the primary components of NOx in tailpipe emissions. The generation of NOx is strongly reliant on the temperatures within the cylinder as well as the amount of oxygen present inside the cylinder [9].

Analysis of Variance of Fuel Consumption and Emissions

An experiment may be developed based on the results of the analysis. With varied loads and alcohol fuel mixes, the observed statistics have ramifications for fuel consumption and emissions.. In order to determine the experimental error, all potential interactions between variables may be divided into two categories using DOE. Using ANOVA tables, the researchers hope to reduce engine emissions and fuel consumption while increasing horsepower. Load variation and the kind of alcohol used are two important aspects to keep in mind while increasing efficiency and reducing expenses in this operation. Because it can handle fuel consumption variance to the extent of 99.97 percent, the model is appropriate. The model has an R-square of 99.97%, which means that it can accurately predict the response.

If the p-value is less than one, it's commonly believed that the null hypothesis must be rejected. If the p-value is less than 0.05 for the load and kind of alcohol, then the model is significant. Table 3 shows that load variation accounted for 20.73% of fuel consumption, whereas alcohol additive type

Table 4. Analysis of variance of emission

Source	DF	Seq SS	Contribution	Adj SS	Adj MS	F-value	P-value
Model	4	422.67	97.39%	422.67	105.667	37.29	0.002
Linear	4	422.67	97.39%	422.67	105.667	37.29	0.002
LOAD	2	144.67	33.33%	144.67	72.333	25.53	0.005
Alcohol	2	278.00	64.06%	278.00	139.000	49.06	0.002
Error	4	11.33	2.61%	11.33	2.833		
Total	8	434.00	100.00%				

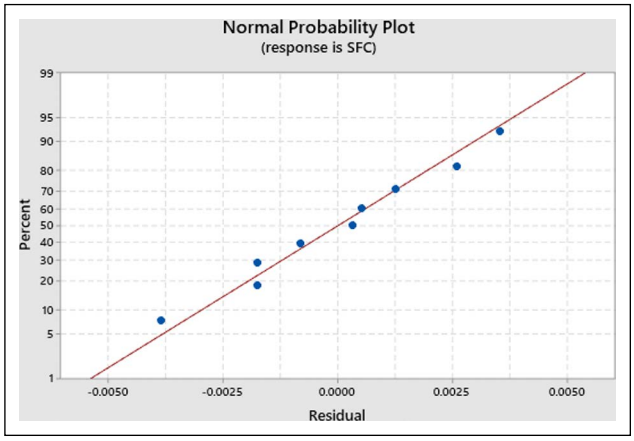

Figure 7. Normal probability of SFC.

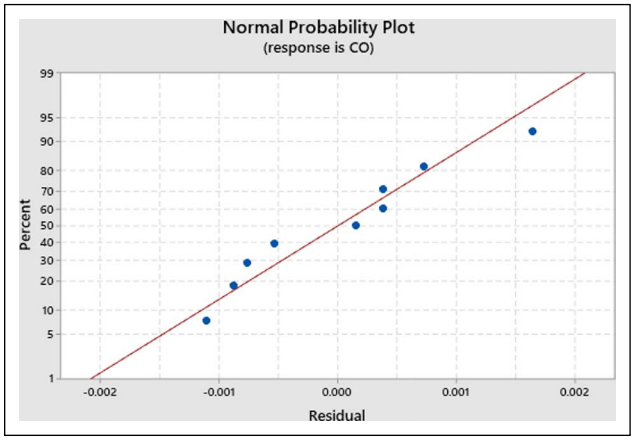

Figure 8. Normal probability of CO.

accounted for 792.1%. Additionally, the load fluctuation contributed 33.33% to emissions, while the kind of ethanol was responsible for 64.06%, as shown in Table 4.

The normal probability plot (Figures 7–9) demonstrates a normal distribution for the error terms. The residual displays have the same features as the original plot. To make acceptable assumptions, it should treat the expected and other factors as random and unstructured. Before evaluating the model, make sure the residual plot has an uneven pattern or is distributed. The normal probability plot displays the normal distribution of data and the response components. The residuals against fitted values show no change in variance. Figures 7–9 show the normal plot of residuals, which helps ensure that the residuals are normally distributed.

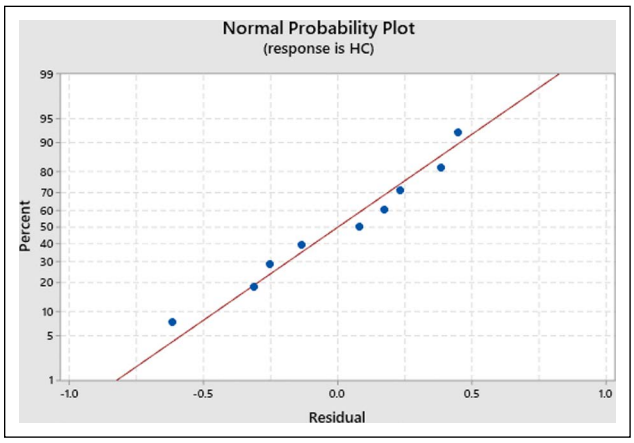

Figure 9. Normal probability of HC.

Response Optimization on Emission

Response optimization is an analytical approach that finds the optimal combination of input variable settings to maximise a single answer or a group of responses. For each variable input combination, the response optimizer function provides an optimal solution and an optimization graphic. It may be interactive. The plot's input variable values may be adjusted to obtain better optimization solutions.

Based on the response optimizer plot (Figure 10), it can be concluded that the pentanol ratio at half load condition is optimal for achieving low emission and effective fuel consumption values. As indicated in Table 5, the ideal circumstances for achieving this goal are when the engine is half loaded. Fuel consumption of 0.4508 kg/kWh, hydrocarbon of 49 ppm and carbon monoxide 0.265% are the optimum values. As depicted in Figure 10, the optimization plot reveals that the optimal load at WPO and alcohol mixes yields the lowest SFC, CO, and HC emissions at half-load conditions, with a composite desirability of 0.9285. Reducing the load will diminish all reactions. However, the impact on SFC emissions was negligible compared to CO and HC emissions. Consequently, when reducing the composite's desirability by diminishing engine

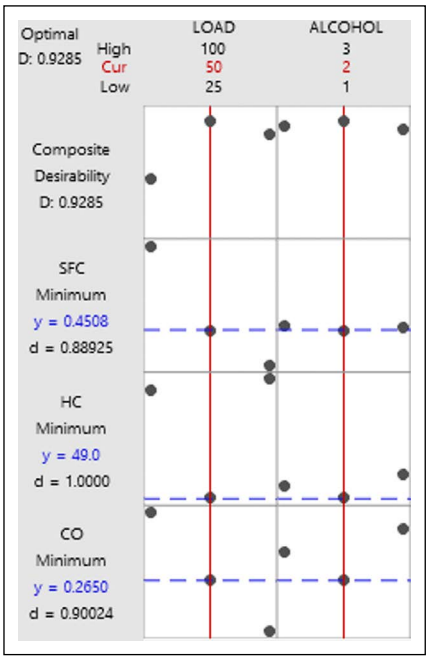

Figure 10. Optimized plot on load and alcohol.

load, the ideal values for engine load and alcohol blend in the experiment were in the half load. Increasing engine load will reduce SFC, HC, and CO emissions. This result recommends that researchers should experiment with a half-load and pentanol in order to improve engine performance.

Environmental Impact and Improvement of Bio-Economy

During the past decade, there has been a rise in investment in biofuels as sustainable alternatives to fossil fuels. These concerns have been brought about by the widespread environmental and health risks associated with the use of fossil fuels. For this reason, it is essential to properly manage the various components of the biofuel supply chain in order to successfully make the shift to a low-carbon and bio-economy. These components include the production of biomass feedstock, the logistics of transporting biomass, the production of biofuel in bio-refineries, and the distribution of biofuel to consumers [22].

A bio-economy requires the recycling of organic materials into valuable fuel and materials. Integration of recycling and bioconversion for enhanced process performance is also assessed. The goal of this work is to make it easier to recycle bio-waste for use in closed-loop systems. To commercialize and promote the use of alternative commodities, more research, market analysis, and funding are needed. To get the most out of the bio-waste, it's important to take a comprehensive, methodical approach that incorporates a wide variety of disciplines and makes use of data to refine, optimize, and introduce novel practices [23]. The circular bioeconomy can assist in solving global problems. By substituting petroleum as an industrial fuel, bioenergy and biomaterials production could reduce their environmental impact. The waste bio-refinery associated with the circular

Table 5. Optimized results on emission and fuel consumption

Load	Alcohol	SFC Fit	HC Fit	CO Fit	Composite desirability
50	2	0.450811	49	0.265	0.928528

bio-economy may aid with carbon management and greenhouse gas emissions. By minimizing greenhouse gas emissions, implementing a waste bio-refinery circular bio-economy system exhibits a low carbon economy [24].

Water-soluble, biodegradable, and quickly evaporable, ethanol may have certain safety advantages over fossil fuels. Because it can be produced in nearly any nation, ethanol fuel is the most economical alternative to traditional sources of energy. Ethanol can be made from a variety of plants, including maize, and used as a fuel. However, E10 is the most common type of ethanol utilized, and depending on where you are in the world, it may make up as much as 15% of a blend. A high ethanol fuel mix, consisting of anything from 50 to 85% ethanol, is now in use in a number of nations, including the United States and Brazil [25, 26]. The simplicity of producing ethanol results in lower production costs than those of fossil fuels. Only carbon dioxide and water are released as by products when ethanol is burned as fuel. Carbon dioxide emissions are a little contributor to the environmental crisis. But it's thought that burning ethanol made from biomass like corn and sugar cane has little impact on atmospheric carbon levels. This is because carbon dioxide is taken in by the biomass during photosynthesis, and this may offset some of the carbon dioxide released during ethanol combustion. The three main foci of the circular economy are the feedstock, the production process, and the distribution of the final product. The company never gave the proper amount of thought to the product's legacy. Not much thought has gone into how the product will be maintained once its expected lifespan has ended [23, 24, 27].

The amount of ethanol blended with gasoline in India reached 10.16 percent in 2022, greatly exceeding the country's target. Additionally, the nation has pledged to achieving a 20 percent blending rate by 2025. Similar to the successful E20 ethanol blending project in India may save the government $4 billion per year in 2020–21, when the country's net petroleum imports will be 185 Mt at $551 billion, when the country's net petroleum imports will be $551 billion [28, 29]. Prices for traditional fuels are higher, but ethanol has a lower impact on the environment. Having the ability to convert vehicles to run on E20 is both a necessity and an opportunity because of the increased availability of farmland, the rising output of food grain and sugarcane, and the widespread availability of these products. Two-wheeled vehicles reduced their CO emissions by as much as half compared to four-wheeled cars, and four-wheeled vehicles reduced their emissions by as much as thirty percent. Ethanol and gasoline together can reduce hydrocarbon emissions by about 20% [30].

The primary objective of this research was to find a way to recover energy from waste polymer while also decreasing harmful emissions from a diesel engine. The blood's ability to carry oxygen to and from tissues is compromised by carbon monoxide, making it dangerous to human health. When blood comes into contact with carbon monoxide, haemoglobin is quickly oxidized into carboxyhemoglobin. Saturation of haemoglobin with oxygen is inhibited by the presence of carbon monoxide in the lungs. It has also been shown that this hydrocarbon reduces the production of white blood cells, suppresses the immune system, and makes the body more vulnerable to infection. There's also the fact that different stages of a plant's life cycle are vulnerable to different pollutant levels in terms of phototoxicity. [31, 32].

CONCLUSION

As a potential alternative fuel source, waste polymer are examined in this research. Alcohol has a higher oxygen content, ensuring a more uniform distribution of fuel and air during combustion. More oxygen may be found in alcohol, which is also less costly. The energy industry might benefit from the use of waste polymer oil as a diesel alternative. In order to increase the thermal efficiency of polymer blends, the addition of alcohol to waste polymer fuel boosted its combustion. Additions of pentanol to WPO blends increase efficiency by 3.4% and decrease fuel consumption by 7.4% when compared to diesel. In the same manner, the use of alcohol additions may lower hazardous emissions by up to 6%. It has been shown that the optimum potential engine condition under load and fuel mix may be improved via the use of Design of Experiments. The results of response optimization have also been analysed using response optimization. Researchers found that while driving at half-load, pentanol mixed diesel consumes the most fuel and emits the least pollution.

Acknowledgements
The authors would like to thank the Vel Tech Rangarajan Dr. Sagunthala R & D Institute of Science and Technology, Chennai, India, for their excellent support for the submission of this article.

DATA AVAILABILITY STATEMENT

The authors confirm that the data that supports the findings of this study are available within the article. Raw data that support the finding of this study are available from the corresponding author, upon reasonable request.

CONFLICT OF INTEREST

The authors declared no potential conflicts of interest with respect to the research, authorship, and/or publication of this article.

ETHICS

There are no ethical issues with the publication of this manuscript.

REFERENCES

[1] V. Gnanamoorthi, and M. Murugan, "Effect of DEE and MEA as additives on a CRDI diesel engine fueled with waste plastic oil blend," Energy Sources, Part A: Recovery, Utilization, and Environmental Effects, Vol. 44(2), pp. 5016–5031, 2022. [CrossRef]

[2] P. Bridjesh, P. Periyasamy, A. V. Krishna Chaitanya, and N. K. Geetha, "MEA and DEE as additives on diesel engine using waste plastic oil diesel blends," Sustainable Environment Research, Vol. 28(3), pp. 142–147, 2018. [CrossRef]

[3] J. Gong, X. Chen, and T. Tang, "Recent progress in controlled carbonization of (waste) polymers," Progress in Polymer Science, Vol. 94, pp. 1–32, 2019. [CrossRef]

[4] H. Y. Kim, J. C. Ge, and N. J. Choi, "Effects of ethanol–diesel on the combustion and emissions from a diesel engine at a low idle speed," Applied Sciences, Vol. 10(12), Article 4153, 2020. [CrossRef]

[5] S. Ravi, and A. Karthikeyan, "Effect of propanol addition on the performance and emissions characteristics of a direct injection diesel engine fuelled with waste plastic oil," International Journal of Ambient Energy, Vol. 43(1), pp. 803–808, 2022. [CrossRef]

[6] N. Jeyakumar, and B. Narayanasamy, "Investigation of performance, emission, combustion characteristics of municipal waste plastic oil fueled diesel engine with nano fluids," Energy Sources, Part A: Recovery, Utilization, and Environmental Effects, pp. 1–22, 2020. [CrossRef]

[7] P. R. Srivathsan, P. Terrin Babu, V. N. Banugopan, S. Prabhakar, and K. Annamalai, "Experimental investigation on a low heat rejection engine," Proceeding International Conference Frontiers in Automobile and Mechanical Engineering. – Nov 25-27, FAME-2010, pp. 122–127, 2010. [CrossRef]

[8] S. Ellappan, and B. Pappula, "Utilization of unattended waste plastic oil as fuel in low heat rejection diesel engine," Sustainable Environment Research, Vol. 29(1), pp. 1–9, 2019. [CrossRef]

[9] B. Govinda Rao, Y. Datta Bharadwaz, C. Virajitha, and V. Dharma Rao, "Effect of injection parameters on the performance and emission characteristics of a variable compression ratio diesel engine with plastic oil blends – An experimental study," Energy & Environment, Vol. 29(4), pp. 492–510, 2018. [CrossRef]

[10] D. Damodharan, A. P. Sathiyagnanam, D. Rana, S. Saravanan, B. Rajesh Kumar, and B. Sethuramasamyraja, "Effective utilization of waste plastic oil in a direct injection diesel engine using high carbon alcohols as oxygenated additives for cleaner emissions," Energy Conversion and Management, Vol. 166, pp. 81–97, 2018. [CrossRef]

[11] A. K. Das, D. Hansdah, A. K. Mohapatra, and A. K. Panda, "Energy, exergy and emission analysis on a DI single cylinder diesel engine using pyrolytic waste plastic oil diesel blend," Journal of the Energy Institute, Vol. 93(4), pp. 1624–1633, 2020. [CrossRef]

[12] M. Chandran, S. Tamilkolundu, and C. Murugesan, "Characterization studies: Waste plastic oil and its blends," Energy Sources, Part A Recover. Energy Sources, Part A: Recovery, Utilization, and Environmental Effects, Vol. 42(3), pp. 281–291, 2020. [CrossRef]

[13] R. K. Singh, B. Ruj, A. K. Sadhukhan, P. Gupta, and V. P. Tigga, "Waste plastic to pyrolytic oil and its utilization in CI engine: Performance analysis and combustion characteristics," Fuel, Vol. 262, Article 116539, 2020. [CrossRef]

[14] T. R. Praveenkumar, P. Velusamy, and D. Balamoorthy, "Pyrolysis oil for diesel engines from plastic solid waste: a performance, combustion and emission study," International Journal of Ambient Energy, Vol. 43(1), pp. 1–21, 2022. [CrossRef]

[15] A. K. Das, M. R. Padhi, D. Hansdah, and A. K. Panda, "Optimization of engine parameters and ethanol fuel additive of a diesel engine fuelled with waste plastic oil blended diesel," Process Integration and Optimization for Sustainability, Vol. 4(4), pp. 465–479, 2020. [CrossRef]

[16] M. Bhargavi, T. Vinod Kumar, R. Ali Azmath Shaik, S. Kishore Kanna, and S. Padmanabhan, "Effective utilization and optimization of waste plastic oil with ethanol additive in diesel engine using full factorial design," Materials Today Proceedings, Vol. 52, pp. 930–936, 2022. [CrossRef]

[17] S. Padmanabhan, T. Vinod Kumar, K. Giridharan, B. Stalin, N. Nagaprasad, L. T. Jule, and K. Ramaswamy, "An analysis of environment effect on ethanol blends with plastic fuel and blend optimization using a full factorial design," Scientific Reports, Vol. 12(1), Article 21719, 2022. [CrossRef]

[18] D. Damodharan, K. Gopal, A. P. Sathiyagnanam, B. Rajesh Kumar, M. V. Depoures, and N. Mukilarasan, "Performance and emission study of a single cylinder diesel engine fuelled with n-octanol/WPO with some modifications," International Journal of Ambient Energy, Vol. 42(7), pp. 779–788, 2021. [CrossRef]

[19] K. Murthy, R. J. Shetty, and K. Shiva, "Plastic waste conversion to fuel: a review on pyrolysis process and influence of operating parameters," Energy Sources, Part A: Recovery, Utilization, and Environmental Effects, pp. 1–21, 2020. [CrossRef]

[20] P. Saravanan, D. Mala, V. Jayaseelan, and N. M. Kumar, "Experimental performance investigation of Partially Stabilized Zirconia coated low heat rejection diesel engine with waste plastic oil as a fuel," Energy Sources, Part A: Recovery, Utilization and Environmental Effects, pp. 1–14, 2019. [CrossRef]

[21] D. Dillikannan, J. Dilipsingh, M. V. De Poures, G. Kaliyaperumal, A. P. Sathiyagnanam, R. K. Babu, and N. Mukilarasan, "Effective utilization of waste plastic oil/n-hexanol in an off-road, unmodified DI diesel engine and evaluating its performance, emission, and combustion characteristics," Energy Sources, Part A: Recovery, Utilization, and Environmental Effects Vol. 42(11), pp. 1375–1390, 2020. [CrossRef]

[22] M. Ranjbari, Z. Shams Esfandabadi, A. Ferraris, F. Quatraro, M. Rehan, A. S. Nizami, V. K. Gupta, S. S. Lam, M. Aghbashlo, and M. Tabatabaei, "Biofuel supply chain management in the circular economy transition: An inclusive knowledge map of the field," Chemosphere, Vol. 296, Article 133968, 2022. [CrossRef]

[23] M. Xu, M. Yang, H. Sun, M. Gao, Q. Wang, and C. Wu, "Bioconversion of biowaste into renewable energy and resources: A sustainable strategy," Environmental Research Vol. 214, Article 113929, 2022. [CrossRef]

[24] H. Y. Leong, C. K. Chang, K. S. Khoo, K. W. Chew, S. R. Chia, J. W. Lim, J. S. Chang, P. L. Show, "Waste biorefinery towards a sustainable circular bioeconomy: a solution to global issues," Biotechnology for Biofuels, Vol. 14(1), Article 87, 2021. [CrossRef]

[25] G. M. K. Jesus, D. Jugend, L. A. B. Paes, R. M. Siqueira, and M. A. Leandrin, "Barriers to the adoption of the circular economy in the Brazilian sugarcane ethanol sector," Clean Technologies and Environmental Policy, Vol. 25, pp. 381–395, 2023.

[26] O. M. Butt, M. S. Ahmad, H. S. Che, and N. A. Rahim, "Usage of on-demand oxyhydrogen gas as clean/renewable fuel for combustion applications: A review," International Journal of Green Energy, Vol. 18(13), pp. 1405–1429, 2021. [CrossRef]

[27] G. Venkatesh, "Circular bio-economy—Paradigm for the future: Systematic review of scientific journal publications from 2015 to 2021," Circular Economy and Sustainability, Vol. 2(1), pp. 231–279, 2022. [CrossRef]

[28] B. Dogan, D. Erol, H. Yaman, and E. Kodanli, "The effect of ethanol-gasoline blends on performance and exhaust emissions of a spark ignition engine through exergy analysis," Applied Thermal Engineering, Vol. 120, pp. 433–443, 2017. [CrossRef]

[29] R. A. Stein, J. E. Anderson, and T. J. Wallington, "An overview of the effects of ethanol-gasoline blends on SI engine performance, fuel efficiency, and emissions," SAE International Journal of Engines, Vol. 6(1), pp. 470–487, 2013. [CrossRef]

[30] J. E. Tibaquirá, J. I. Huertas, S. Ospina, L. F. Quirama, and J. E. Niño, "The effect of using ethanol-gasoline blends on the mechanical, energy and environmental performance of in-use vehicles," Energies, Vol. 11(1), pp. 1–17, 2018. [CrossRef]

[31] S. Padmanabhan, K. Giridharan, B. Stalin, V. Elango, J. Vairamuthu, P. Sureshkumar, L. T. Jule, and R. Krishnaraj, "Sustainability and environmental impact of ethanol and oxyhydrogen addition on nanocoated gasoline engine," Bioinorganic Chemistry and Applications, Vol. 2022, Article 1936415, 2022. [CrossRef]

[32] P. Sambandam, P. Murugesan, M. I. Shajahan, B. Sethuraman, and H. M. Abdelmoneam Hussein, "Sustainability and Environmental Impact of Hydroxy Addition on a Light-Duty Generator Powered with an Ethanol–Gasoline Blend," Journal of Renewable Energy and Environment, Vol. 9(2), pp. 82–92, 2022.

Environ Res Tec, Vol. 6, Issue. 1, pp. 46–53, March 2023

Environmental Research and Technology
https://ert.yildiz.edu.tr - https://dergipark.org.tr/tr/pub/ert
DOI: https://doi.org/10.35208/ert.1226092

Environmental Research & Technology

Research Article

Effect of biomass ash vermicompost on *Sorghum bicolor* var. *saccharatum* (L.) Mohlenbr under hot and dry agro ecological condition

Güldane Aslı TURP*, Saim ÖZDEMİR

Sakarya University, Department of Environmental Engineering, Sakarya, Türkiye

ARTICLE INFO

Article history
Received: 29 December 2022
Revised: 31 January 2023
Accepted: 09 February 2023

Key words:
Biomass; Biomass ash; Brix; Sweet sorghum; Vermicompost application; Yield

ABSTRACT

Generation of the huge amount of bio-waste and their residues, including incineration ash, is a major technical and sustainability problem. To solve this problem, incorporating nutrient-rich residues into crop production has become an efficient practice to increase crop production. Vermicomposting of these wastes could be a viable option to manage both bio-wastes and their products in an environmentally friendly manner and close the material loop in bioenergy production. Therefore, the main objective of this study was to investigate the effect of vermicompost from biomass ash under hot and dry climatic conditions in summer on growth, yield and yield components of sweet sorghum (*Sorghum bicolor var. saccharatum* (L.) Mohlenbr). The high photosynthetic activity of sweet sorghum is important for biofuel production under conditions of high solar energy and water scarcity. This study provides a general overview of the feasibility of biomass ash vermicomposting processes and their potential use as a nutrient source for C4 sorghum under Bitlis ecological conditions of high solar potential and low water availability. Under Bitlis climatic conditions, the best yield was obtained when vermicompost was applied with a biomass ash content of 10.0% (T3). Plant height, plant weight, sugarcane and juice yields were reported as 133 cm, 146 g, 180 kg/da and 105 L/da, respectively.

Cite this article as: Turp GA, Özdemir S. Effect of biomass ash vermicompost on *Sorghum bicolor* var. *saccharatum* (L.) Mohlenbr under hot and dry agro ecological condition. Environ Res Tec 2023;6:1:46–53.

INTRODUCTION

The increasing demand for energy from renewable resources has led to the expansion of biomass power plants, which results in the generation of biomass ash as an end product that must be properly disposed of according to the principles of circular economy [1]. Therefore, it is critical to find new methods to recycle nutrient-rich biomass ash in a closed-loop system of crop production and energy generation to reduce waste accumulation, increase crop productivity, and reduce environmental impacts [2]. Since biomass and biofuel production generate large amounts of residues, the approach of converting them into biofertilizers to produce new fuels can overcome the net-zero CO_2 goal for developing a sustainable energy source [3]. In addition, the trend of global warming combined with chang-

***Corresponding author.**
*E-mail address: g.asliturp@gmail.com

ing rainfall regimes and high evapotranspiration for many cropping practices is destined to adapt more drought tolerant crops that are more efficient in managing nutrients and irrigation water under deficient environmental conditions [4]. A variety of waste-based, nutrient-rich organic fertilizers are being developed for recycling purposes and for fertilizing crops. Among them, vermicompost appears to be the most promising cost-effective method to convert recalcitrant biomass ash into valuable organic fertilizer for reuse in the production of biofuel feed stocks in closed-loop energy systems. Additionally, composting of organic waste stream offer the best disposal option especially in mineral resource use for crop production [5]. For instance, incorporating organic matter into the soil increases soil organic matter [6], increases the soil nutrient pool [7], minimizes soil nutrient depletion [8], acts as a slow-release fertilizer [9], improves porosity and infiltration [10], microbiological and enzymatic activity [11], and thus also improves water use efficiency of plants [12].

Among biofuels, bioethanol gains great popularity due to its numerous advantages. The sorghum plant offers a particularly high yield of biofuel under hot and dry climatic conditions [13]. The C4 sorghum plant (*Sorghum bicolor* var. *saccharatum* (L.) Mohlenbr) is characterized by high photosynthetic efficiency and high dry matter accumulation rate compared to other crops, especially under drought stress conditions. Due to its high biomass and sugar yield, it is more popular in hot and dry climates because it can withstand drought, requires lower water, fewer cultivation inputs, is easy to cultivate, and has lower fuel costs such as sugar syrup, bagasse, and grain yields. The potential to produce solid, liquid, and gaseous biofuels under conditions of high solar radiation and water deficit makes sorghum a unique, valuable crop for future challenging environmental conditions. Therefore, sweet sorghum appears to be the most promising energy crop in the hot and drought-prone regions where conventional crops with high water requirements such as corn, sugar beets, and sunflowers cannot be grown. Although sugar content in the plant stem is one of its most important characteristics, it also produces grains with high starch content and bagasse with high lignocellulose content [14], which can be fermented to produce bioethanol or solid biofuel.

Sweet sorghum is a high biomass and sugar yielding plant belonging to the C4 photosynthetic pathway. It produces plant stems up to 300 cm tall with a sugar content of 16–23% Brix, depending on the variety and agricultural inputs used. Unlike other C4 plants, it tolerates dry conditions, requires less fertilizer, and is easy and inexpensive to grow. When integrated into the cropping system, the application of vermicompost can further improve Brix content, sugar and biomass yield under high PAR (photosynthetic active radiation) and dry environmental conditions [15]. The particular advantage of sweet sorghum is its lower nitrogen requirement due to its high nitrogen use efficiency under water deficit conditions. However, yields can be increased by applying a balanced nutrient in the form of vermicompost, which copes very well with dry and hot climatic conditions due to its stress-reducing properties. It is reported that the dry biomass of sweet sorghum, grown as an alternative crop for biogas production in drought-prone areas, is 27% higher than that of maize under the experimental conditions of severe drought, which is due to the inherently deep and strong root exploitationin the subsoil [16]. On the other hand, a strong response to fertilizers is also reported. For example, in studying the effects of nitrogen and potassium fertilizers on growth parameters, it was found that an application of 180 kg urea per hectare at physiological maturity increased stem height by 12.65%, stem fresh weight by 24.57%, total weight by 78.22%, and total sugar content by 39.25%. When 50 kg of potassium sulfate was applied, the rates of increase were as follows: 24.33% in fresh stem weight, 25.44% in total weight, and 10.50% in total sugar content [17]. It is also reported that the optimum N fertilization is 59–110 kg N ha^{-1} and 200 kg N ha^{-1} for ethanol and sugar yield, respectively, which in contrast indicates lower sugar quality and ethanol yield [18].

In recent years, the focus has shifted to the use of feed stocks for biofuels, as food crops can only meet a small portion of the demand for biofuels and require intensive fertilization [19]. The main problem in biofuel production is the cost of the feed stock. As an alternative to the high demanding biofuel crops, sweet sorghum can serve as a sustainable biofuel feedstock that requires few inputs, is tolerant of environmental changes, and offers versatile processing options. As an alternative to chemical fertilizers, biofuel yields can be enhanced by sustainable nutrient resources such as vermicompost, whose nutrient content is enriched by biomass ash produced at biomass power plants. Biomass ash contains high levels of most fertilizer nutrients such as phosphorus and potassium. However, due to its high pH for agricultural use, it remains in the background in agricultural applications. Although various methods are used to recover the phosphorus contained in biomass ash in the form of apatite, the application of vermicompost can be sustainable and provide an environmentally friendly recovery [20]. Although several studies have highlighted the response of some crops to vermicompost nutrients [21] the role of biomass ash vermicompost in improving biofuel yield of sweet sorghum in hot, dry agroecosystems has not been thoroughly investigated. The results of this work could show the effects of nutrient-rich biomass ash vermicompost on biomass yield and feedstock composition of sweet sorghum in Bitlis, Turkey, which has hot summer climatic conditions with high sunshine hours.

MATERIALS AND METHODS

Vermicompost Preparation

Biomass ash is a rich source of nonvolatile plant macro- and micronutrients. Similarly, dairy manure consists of volatile nutrients abundant in nitrogen, carbon, and sulfur, which play essential roles in plant nutrition and sugar metabolism. To test the first hypothesis, the possibility of enriching vermicompost with both volatile nutrients from biowaste and non-volatile nutrients from biomass ash was examined. Therefore, vermicompost was made from a combination of dairy manure and biomass power plant ash to produce a slow-release organic biofertilizer. The biomass ash (BA) was obtained from a biomass power plant in Sakarya, Turkey. BA came from sawdust, forest residues, nut shells, and mainly poultry litter. The Turkish compost regulation specifies that the total value for N (Nitrogen), P (Phosphorus) and K (Potassium) in worm compost must not exceed 7.0%. Considering this limit, the final NPK content in vermicompost samples was 0.0% (T0 without BA), 3.5% (T1), 7.0% (T2), and 10.0% (T3), respectively [20]. The process of vermicomposting involves two phases. The first phase is performed by aerobic microbes that reduce the readily biodegradable substrate to minimize the negative effects of toxic and odorous compounds on worms. The second phase is performed by worms and gut microbes to obtain a more humified product that helps plants mobilize and absorb nutrients, but also promotes plant growth and inhibits plant pests. After homogeneously incorporating the calculated amount of BA into the dewatered cattle manure, the mixture was allowed to ferment for 21 days to prevent negative effects of volatiles and toxic substances on the vermicompost process. The vermicompost-forming materials were then incubated at room temperature and under humid conditions by spraying the surface with water in a dark environment. Processing was carried out for 60 days to allow the compost to mature [22].

Plant

The sweet sorghum plant is traditionally used as a sugar crop and is known to adapt well to dry and hot climates due to its deep proliferated root structure. Therefore, it has been shown to be competitive with conventional bifofuel crops in terms of theoretical ethanol and lignocellulosic dry matter yield. Seeds of the Gulseker Sweet Sorghum variety were obtained from the Maize Research Institute, Sakarya, Turkey. Bitlis province was selected for testing the model plant because of the high sunshine duration and the fast growth of the plants thanks to the high photosynthetic capacity of the sorghum plant.

Soil Sampling and Characterization

The experiment was conducted at directly farmers field located in Tatvan district of Bitlis province (GPS 38.509441 N, 42.341652 E, and 1690 m above sea level) in the spring summer growing season of 2021. The experimental soil was sampled from surface horizons (0–20 cm) for basic soil analysis. Some selected physicochemical properties of the soil were given in Table 1. The soil was deep silt loam, mild alkaline and low in organic matter.

Table 1. Physicochemical properties of experimental soil and bio ash [10]

Parameter	Bitlis soil	Biomass ash (BA)
pH	7.45±0.04	13.04±0.20
EC (dS m^{-1})	0.34±0.02	27.43±0.55
Organic matter (%)	1.16±0.03	1.98±0.01
Kjeldahl N (%)	0.10±0.07	ND
P (mg kg^{-1})	45.94±1.15	13212±1.56
K (mg kg^{-1})	83.66±2.40	17554±2.56
Ca (mg kg^{-1})	390.00±8.80	32724±1.23
Mg (mg kg^{-1})	180.70±2.10	5385±1.19
Fe (mg kg^{-1})	29.04±1.25	2563±2.46
Mn (mg kg^{-1})	32.38±1.87	950±1.09
Zn (mg kg^{-1})	2.94±0.16	1222±1.62
Cu (mg kg^{-1})		67±0.86

Values are the mean±standard deviation of three samples, each measured in triplicate. EC: Electrical conductivity; dS: DeciSiemens; ND: Not detected.

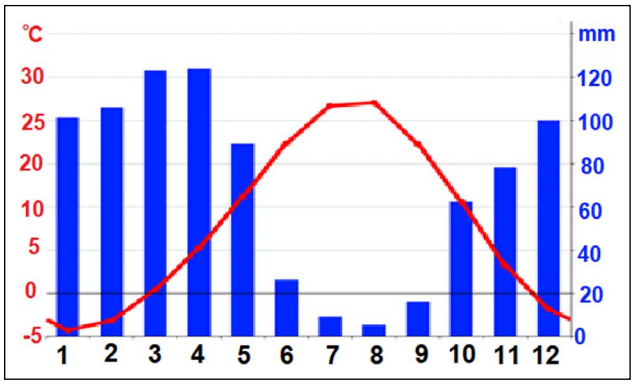

Figure 1. Long-term average precipitation, highest and lowest air temperatures for the years 1959–2021 in the province of Bitlis.

Meteorological Conditions

The experimental area is located in Bitlis province in eastern Turkey, where according to the Koeppen classification, the climate is Aas (continental dry and hot in summer), as it has high temperatures, low precipitation and relative humidity between 33 and 43% during the experimental period. The summer months are characterized by low precipitation and relatively longer hours of sunshine (12.2–13.0) per month. The average long-term monthly temperatures and precipitation for the period from 1959 to 2021 are shown in Figure 1.

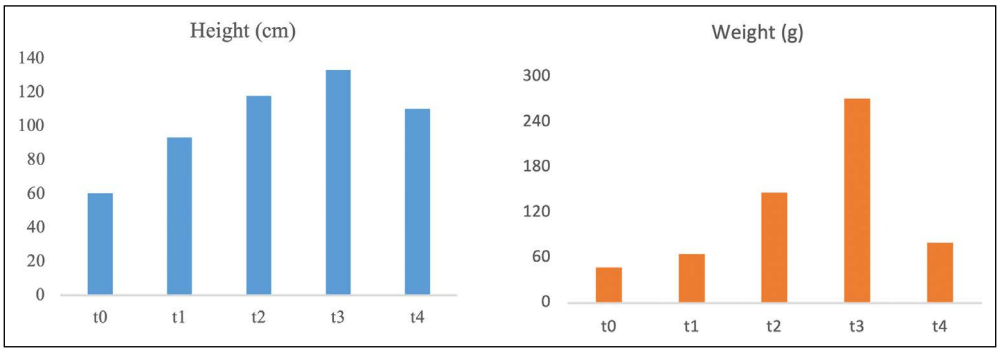

Figure 2. Biomass yield parameters of sweet sorghum plant grown in continental climate conditions with BA vermicompost application – Height and Weight (T_0=0.0%, T_1=3.5%, T_2=7.0%, T_3=10.0% biomass ash and vermicompost, T_4=fertilizer-free control).

According to the data obtained, the average amount of precipitation is 1046 mm, with most of it falling in spring and winter. The average amount of precipitation during the growing period of sweet sorghum (May-September) was 33 mm. The highest temperature during the growing season was recorded as 29.3 °C in August [23]. Rainfall during the growing season was insufficient to meet the plant's water needs. Therefore, weekly drip irrigation was applied at 10 mm per irrigation cycle.

Treatments and Field Design

Five different fertilization treatments were tested: T_0 (vermicompost, without BA); T_1 (vermicompost with BA, NPK content 3.5%); T_2 (vermicompost with BA, NPK content 7.0%); T_3 (vermicompost with BA, NPK content 10.0%); and T_4 (control, without fertilizer). Seeds were first germinated in seedling viol, and then the germinated plantlets were transplanted on the 5×3 m cultivation area at 30 cm spacing. Vermicompost was applied as basal fertilizer before sowing along the planting rows.

Brix Measurement

After plant harvest, 5 plant stems were pressed to extract the juice using a sugarcane 2-roller press. Then the Brix (%) values (Fig. 3) of juice were determined by using a hand-held refractometer. The Brix counter was set to zero with distilled water and measured by taking a small amount of juice into the counter [14]. It was assumed that the sugar content in juice was equal to 75% of Brix [24].

Calculation of Sweet Sorghum Yield Data

Sweet sorghum plants, which were harvested by leaving a stubble height of 5 cm from the planting area of the sweet sorghum plant, were weighed (Fig. 4), and then the branches and leaves were separated and the leafless stem weight was noted. The stem thickness of the plants was measured with the help of caliper from a height of 30 cm from the ground and recorded. The plant samples brought to the laboratory environment were dried in an oven at 70 °C and their dry weights were

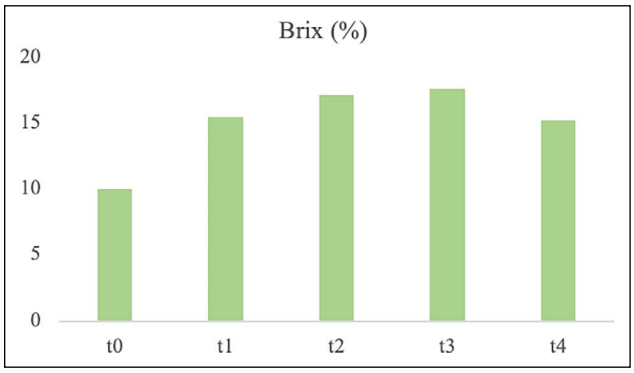

Figure 3. Biomass yield parameters of sweet sorghum plant grown in continental climate conditions with BA vermicompost application- Brix (%) (T_0=0.0%, T_1=3.5%, T_2=7.0%, T_3=10.0% biomass ash and vermicompost, T_4=-fertilizer-free control)

weighed. Calculations were made with the help of the following formulas (1), (2), (3) with the data at hand [25].

$$\text{Fluid Rate: } \frac{(Leafless\ stem\ weight\ (kg) - dry\ weight(kg))}{Leafless\ branch\ weight\ (kg)}\ x\ 100 \quad (1)$$

$$\text{Cane Yield (kg da}^{-1}\text{): } \frac{wet\ weight\ (kg)}{planting\ area(da)} \quad (2)$$

$$\text{Juice Yield (L da}^{-1}\text{): } \frac{Liquid\ Amount(L)}{planting\ area\ (da)} \quad (3)$$

Statistical Analysis

Each experiment was performed according to a completely randomized design with three replicates per amendment. The experimental data are subjected to the analysis of variance (randomize complete block design) by using the Statgraphics Centurion version of XVI (Statpoint Technologies Inc., Warrenton, VA, USA). Means that differed significantly are separated by using Tukey's Honestly Significant Difference (HSD) test at p 0.05 [3].

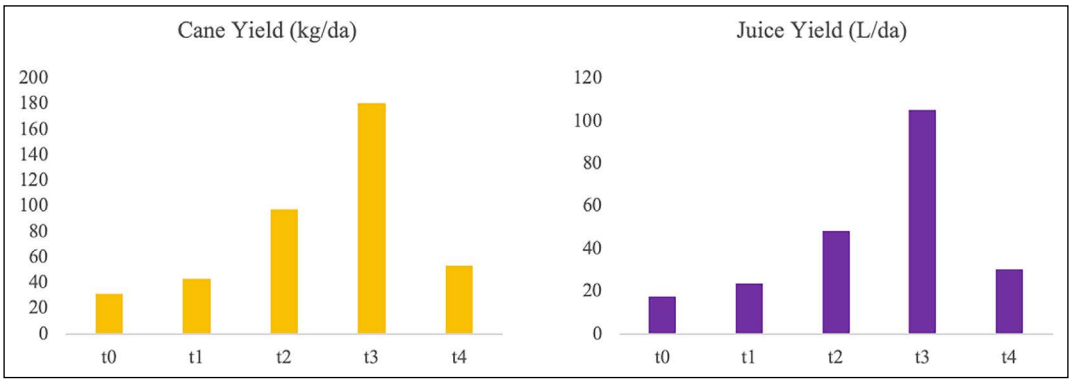

Figure 4. Biomass yield parameters of sweet sorghum plant grown in continental climate conditions with BA vermicompost application- Cane Yield and Juice Yield (T_0=0.0%, T_1=3.5%, T_2=7.0%, T_3=10.0% biomass ash and vermicompost, T_4=fertilizer-free control).

RESULTS AND DISCUSSIONS

Characterization of Biomass Ash and Experimental Soil

Total elemental composition analysis of biomass ash was done by ICP-MS. According to the analysis results, it was recorded as 32724, 17554, 13212 and 5385 mg kg^{-1} for calcium (Ca), potassium (K), phosphorus (P) and magnesium (Mg), respectively (Table 1). Biomass power plant ash includes forest waste, agricultural products and poultry bedding material as content. In previous studies, the most abundant elements in biomass ash content were recorded as calcium and potassium. Due to the presence of alkaline compounds, the pH value was recorded in the range of 12–13. The use of ash produced by biomass combustion as an additive to the composting process is envisaged as a potential solution to the most common critical problems [26].

Plant Growth Parameters

As a result of applications made for varying levels of biomass ash vermicompost, weight, height, sugar content (Brix), cane and fruit juice yield of sweet sorghum plant were examined under continental climate conditions. The averages of the parameters among the BA ratios in vermicompost applications containing BA ash in continental climate conditions are presented (Fig. 2). Brix % rates are higher than other applications as T3>T2. The Brix ratio of the plant in continental climate was brought to the range of 17–18% with BA vermicompost fertilization. Nitrogen (N) and Potassium (P) fertilized two different varieties (Rio and Keller) sweet sorghum plant obtained 18% Brix rates with different amounts of N and P applications [17].

In vermicompost applications containing BA ash, an increase in plant height was observed regardless of the ratio. The height of a sweet sorghum plant is directly proportional to its biomass yield. The plant height is between 60–133 cm and it is T3>T2>T4>T1>T0 respectively. Plant height is generally controlled by maturity and internode length. The longer the plant stays vegetative, the more leaves and height it makes. Typically, the stems contain 12–22% sugar. Although a positive relationship has been established between height and sugar accumulation, studies have shown that high sugar concentration is not only proportional to height, but it is possible to breed short and high sugar strains [27].

Height and Weight

The crop productivity of sweet sorghum plant is related to the plant population per unit area. However, wide or narrow spacing does not have a clear effect on crop performance [28]. The height of the sweet sorghum plant is mainly estimated from the maturity of the plant and the length between the nodes. Generally, late blooming plants appear to be taller than early blooming plants. Plant height of sweet sorghum is highly correlated with biomass yield [27]. The cluster that emerges while the sweet sorghum plant matures stops its lengthening. It has been reported that sugar accumulation increases after plant height stops [29]. It has been shown that 180 kg ha^{-1} urea application of the plant at physiological maturity increased the stem height by 12.65% [17]. Height and weight information of sweet sorghum plant grown in Bitlis climate conditions are given in the graphics in the figure. According to the data obtained, when the development of sweet sorghum plant is examined according to the amount of vermicompost applied, the best height is 133.33 cm in T3 (10% biomass ash and vermicompost) application. Sweet sorghum length was measured as 60.33 cm in T0 (0.0% biomass ash and vermicompost) application.

When the plant weights of the sweet sorghum plant with vermicompost application were examined, the order T3>T2>T4>T1>T0 occurred. Depending on the plant height, T3 (10% biomass ash and vermicompost) application contributed to the plant being heavier.

Brix (%)

Because of the presence of inverted sugars (glucose and fructose) the sweet sorghum juice is not commonly used for crystallized sugar production due to the difficult crystallization. However, fermentable sugars of juice offer an excellent potential for yeast fermentation to produce bioethanol. It has been reported that sugar accumulation increased rapidly after the internode elongation ceased after the sweet sorghum plant had clustered. However, the data obtained show that sugar accumulation is dependent on internode maturation rather than cluster formation [29]. When growing sweet sorghum, it is important to measure the Brix value frequently so that the growth trends of the plant can be analyzed. It helps us see how the quality of the crop improves during ripening, thus helping to find the right time to harvest the crop. Regardless of the ratio, the measured Brix remained in a narrow range of 10–17.6% in the vermicomposting application prepared with a mixture of biomass at different rates. Although positive results on plant growth were demonstrated in the previous N fertilization application, no improvement in Brix ratios was recorded [18].

Cane Yield and Juice Yield

The sugar contained in the plant is one of the most important properties of interest to growers, and research focuses on sugar accumulation and enzymes. Fermentable sugars, mainly including sucrose, glucose and fructose, are the main ingredient in sweet sorghum stalks for bioethanol production [15]. As a result of a 3-year study to determine the optimum N fertilization rate for the production of two common sweet sorghum varieties, the development of sweet sorghum was significantly affected by N application [18].

The volume of juice is a function of the stem volume depending on the stem height. Cane yield and juice yield yields are also promising in T2 and T3 applications, where the best yields in height and weight are obtained.

Transforming BA ash, which has a high plant nutrient content, into a fertilizer form that can be used by plants by the vermicompost method and fertilization at different rates, the relationship between the amount of fertilizer for the growth of sweet sorghum plant is evaluated, and T3 and T2 applications between cane and fruit juice yields are much higher than other fertilization amounts. reached

When the available data for the sweet sorghum plant, which has the ability to produce high biomass, are examined, the application of T3 (10% biomass ash vermicompost) is 70% higher than the application of T4 (without fertilizer).

CONCLUSIONS

Sweet sorghum plant, which is among sustainable green bioenergy crops, makes a potential contribution to future energy demand. With the interconnection between energy and sustainable development, sweet sorghum offers multiple benefits to both food, feed and energy security and environmental challenges such as water availability, carbon neutrality and ecosystems sustainability, if properly planned and managed. In the present study, in order to improve the existing production methods, an alternative solution was proposed in the Bitlis ecological conditions.

Biomass ash vermicompost was produced and tested as a sustainable fertilizer alternative for sweet sorghum production in Bitlis continental climate conditions. As a result of the analyzes made on the harvested stems to determine the post-harvest changes, the average best yields of different parameters were listed as T3>T2>T4>T1>T0. The plant heights were 60.33, 93, 118, 133.33, and 110 cm for the T0, T1, T2, T3, and T4, respectively. Average plant height positively correlated with the plant weights. The plant sugar yield and Brix values varied between 10–17.6% in tested treatments. Although the application of fertilizer at high rates shows positive results on sweet sorghum plant, the harms of excessive application to the environment are undeniable. It is promising that biomass yield can be improved with the application of BA vermicompost, which is preferred due to advantages such as low input requirements in Bitlis climatic conditions where the amount of dry and water is limited.

In sweet sorghum production, cane yield is 31–180 kg/da and juice yield is 17–105 L/da. Vermicompost has been investigated as an alternate source of conventional chemical fertilizer; the results revealed the significant effect of vermicompost on plant growth, yield, and quality parameters of the products. The vermicompost and crop growth experiments have shown that it is feasible to obtain nutrient-rich vermicompost by adding BA to biowaste cow dung and vermicomposting of those materials back into the production cycle of biomass energy crops solves the problem of waste disposal, thus minimizing environmental pollution.

DATA AVAILABILITY STATEMENT

The authors confirm that the data that supports the findings of this study are available within the article. Raw data that support the finding of this study are available from the corresponding author, upon reasonable request.

CONFLICT OF INTEREST

The authors declared no potential conflicts of interest with respect to the research, authorship, and/or publication of this article.

ETHICS

There are no ethical issues with the publication of this manuscript.

REFERENCES

[1] J. Zhai, I. T. Burke, and D. I. Stewart, "Beneficial management of biomass combustion ashes," Renewable and Sustainable Energy Reviews, Vol. 151, Article 111555, 2021. [CrossRef]

[2] O. H. Dede, and H. Ozer, "Enrichment of poultry manure with biomass ash to produce organomineralfertiliser," Environmental Engineering Research, Vol. 23(4), pp. 449–455, 2018. [CrossRef]

[3] S., Ozdemir, and G. A. Turp, "The impact of the pyroligneous acid-assisted biomass ash vermicompost on dry beans through climatic and agroecosystem changes," Journal of Material Cycles and Waste Management, Vol. 25, pp. 490–500, 2022. [CrossRef]

[4] B. Sen, S. Topcu, M. Turkes, B. Sen, and J. F. Warner, "Projecting climate change, drought conditions and crop productivity in Turkey," Climate Research, Vol. 52(1), 175–191, 2012. [CrossRef]

[5] L. Bilgili, and A. Y. Çetinkaya, "Application of life cycle assessment of system solution scenarios for municipal solid waste management in Turkey," Journal of Material Cycles and Waste Management, Vol. 25, pp. 324–336, 2022. [CrossRef]

[6] A., Durak, O., Altuntaş, I. K. Kutsal, R. Isık, and F. E. Karaat, "The effects of vermicompost on yield and some growth parameters of lettuce," Turkish Journal of Agriculture-Food Science and Technology, Vol. 5(12), pp. 1566–1570, 2017. [CrossRef]

[7] O. Dede, and D. Akbulut, "Analyzing the effects of biomass and coal ash for the dewatering properties of sewage sludge," Sakarya University Journal of Science, Vol. 21(5), pp. 907–914, 2017. [CrossRef]

[8] S. Sonmez, F. Okturen Asri, E. Demir, N. Ozen, and E. Kiliç, "Temporal variation of nitrogen and carbon mineralizations of different organic materials," Communications in Soil Science and Plant Analysis, Vol. 53(15), pp. 1865–1875, 2022. [CrossRef]

[9] K. Yetilmezsoy, E. Kiyan, F. Ilhan, D. Ozcimen, and A. T. Kocer, "Screening plant growth effects of sheep slaughterhouse waste-derived soil amendments in greenhouse trials," Journal of Environmental Management, Vol. 318, Article 115586, 2022. [CrossRef]

[10] S. Asghari, M. R. Neyshabouri, F. Abbasi, N. Aliasgharzad, and S. Oustan, "The effects of four organic soil conditioners on aggregate stability, pore size distribution, and respiration activity in a sandy loam soil," Turkish Journal of Agriculture and Forestry, Vol. 33(1), 47–55, 2009. [CrossRef]

[11] I. Uz, and I. E. Tavali, "Short-term effect of vermicompost application on biological properties of an alkaline soil with high lime content from Mediterranean region of Turkey," The Scientific World Journal, Vol. 2014, Article 39528, 2014. [CrossRef]

[12] Z. Demir, and C. Gülser, "Effects of rice husk compost on some soil properties, water use efficiency and tomato (Solanumlycopersicum L.) yield under greenhouse and field conditions," Communications in Soil Science and Plant Analysis, Vol. 52(9), pp. 1051–1068, 2021. [CrossRef]

[13] R. I. Nazli, "Evaluation of different sweet sorghum cultivars for bioethanol yield potential and bagasse combustion characteristics in a semiarid Mediterranean environment," Biomass and Bioenergy, Vol. 139, Article 105624, 2020. [CrossRef]

[14] M. Q. Yue, Z. Wang, B. Q. Dun, F. X. Han, and G. Y. Li, "Simplified methods of estimating fermentable sugar yield in sweet sorghum [Sorghum bicolor (L.) Moench] stems." Industrial Crops and Products, Vol. 169, Article 113652, 2021. [CrossRef]

[15] P. S. da Silva Leite, T. T. Botelho, P. C. de Oliveira Ribeiro, R. E. Schaffert, R. A. da Costa Parrella, and J. A. R. Nunes, "Intrapopulation recurrent selection in sweet sorghum for improving sugar yield," Industrial Crops and Products, Vol. 143, Article 111910, 2020. [CrossRef]

[16] S. Schittenhelm, and S. Schroetter, "Comparison of drought tolerance of maize, sweet sorghum and sorghum-sudangrass hybrids," Journal of Agronomy and Crop Science, Vol. 200(1), pp. 46 53, 2014. [CrossRef]

[17] A. Almodares, R. Taheri, M. Chung, and M. Fathi, "The effect of nitrogen and potassium fertilizers on growth parameters and carbohydrate contents of sweet sorghum cultivars," Journal of Environmental Biology, Vol. 29(6), pp. 849–852, 2008.

[18] M. J. Maw, J. H. Houx III, and F. B. Fritschi, "Sweet sorghum ethanol yield component response to nitrogen fertilization," Industrial Crops and Products, Vol. 84, pp. 43-49, 2016. [CrossRef]

[19] G. Trouche, D. Bastianelli, T. C. Hamadou, J. Chantereau, J. F. Rami, and D. Pot, "Exploring the variability of a photoperiod-in sensitive sorghum genetic panel forstem composition and related traits in temperate environments," Field Crops Research, Vol. 166, pp. 72–81, 2014. [CrossRef]

[20] G. A. Turp, S. M. Turp, S. Ozdemir, and K. Yetilmezsoy, "Vermicomposting of biomass ash with bio-waste for solubilizing nutrients and its effect on nitrogen fixation in common beans," Environmental Technology & Innovation, Vol. 23, Article 101691, 2021. [CrossRef]

[21] E. Ceotto, F. Castelli, A. Moschella, M. Diozzi, and M. Di Candilo, "It is not worthwhile to fertilize sweet sorghum (Sorghum bicolor L. Moench) with cattle slurry: Productivity and nitrogen-use efficiency," Industrial Crops and Products, Vol. 62, pp. 380–386, 2014. [CrossRef]

[22] S. Ozdemir, S. Ozdemir, and K. Yetilmezsoy, "Agro-economic and ecological assessment of poultry abattoir sludge as bio-nutrient source for walnut plantation in low-fertility soil," Environmental Progress & Sustainable Energy, Vol. 38(6), Article 13225, 2019. [CrossRef]

[23] TR Ministry of Environment Urbanization and Climate Change General Directorate of Meteorology, "Ankara," http://www.mgm.gov.tr/ Accessed on Feb 10, 2023.

[24] C. E. Vlachos, O. I. Pavli, E. Flemetakis, and G. N. Skaracis, "Exploiting pre and post harvest metabolismin sweet sorghum geno types to promote sustainable bioenergy production," Industrial Cropsand Products, Vol. 155, Article 112758, 2020. [CrossRef]

[25] C., Adiyaman, E., Erbil, A. Çelik, H., Hatipoğlu, M., Aksoy, M. Acar, and M. Dok. "Determination of some agricultural and technological characteristics of second product sweet sorghum [Sorghum bicolor (L.) Moench] in Sanlıurfa conditions," Journal of the Institute of Science and Technology, Vol. 10(4), pp. 3084–3094, 2020. [CrossRef]

[26] C. Asquer, G. Cappai, A. Carucci, G. De Gioannis, A. Muntoni, M. Piredda, and D. Spiga, "Biomass ash characterisation for reuse as additive in composting process," Biomass and Bioenergy, Vol. 123, pp. 186–194, 2019. [CrossRef]

[27] S. Shukla, T. J. Felderhoff, A. Saballos, and W. Vermerris, "The relationship between plant height and sugar accumulation in the stems of sweet sorghum (Sorghum bicolor (L.) Moench)," Field Crops Research, Vol. 203, pp. 181–191, 2017. [CrossRef]

[28] G. L. Sawargaonkar, M. D. Patil, S. P. Wani, E. Pavani, B. V. S. R., Reddy, and S. Marimuthu, "Nitrogen response and water use efficiency of sweet sorghum cultivars," Field Crops Research, Vol. 149, pp. 245–251, 2013. [CrossRef]

[29] P. S. Burks, C. M. Kaiser, E. M. Hawkins, and P. J. Brown, "Genome wide association for sugar yield in sweet sorghum," Crop Science, Vol. 55(5), pp. 2138–2148, 2015. [CrossRef]

Environ Res Tec, Vol. 6, Issue. 1, pp. 54–59, March 2023

Environmental Research and Technology
https://ert.yildiz.edu.tr - https://dergipark.org.tr/tr/pub/ert
DOI: https://doi.org/10.35208/ert.1212911

Environmental Research & Technology

Research Article

Methane yield of paper industry waste in the presence of two compounds from alcohol and aldehyde groups during thermophilic anaerobic digestion

Eda YARSUR[1], Ilona Sárvári HORVÁTH[2], Çiğdem YANGIN GÖMEÇ*[1]

[1]Department of Environmental Engineering, İstanbul Technical University, İstanbul, Türkiye
[2]Swedish Centre for Resource Recovery, University of Borås, Högskolan i Borås, Borås, Sweden

ARTICLE INFO

Article history
Received: 04 December 2022
Revised: 10 February 2023
Accepted: 07 March 2023

Key words:
Biogas; Hexanal; Inhibition; Lignocellulose; 1-octanol

ABSTRACT

In this study, effect of two chemical compounds (i.e., 1-octanol and hexanal) respectively from the alcohol and aldehyde groups on thermophilic (55±2 °C) anaerobic process digesting the waste produced at a paper industry was investigated. In this scope, possible inhibition was monitored by the cumulative methane (CH_4) yields in the batch reactors digesting the paper waste as the feedstock at concentrations of 0.005%, 0.05%, and 0.5% for each compound. Comparing the effects of the two different groups with the control reactor having only the paper waste as the substrate, the results revealed that adding 1-octanol and hexanal up to 0.05% concentrations had some synergistic effect on biogas yield (i.e., from 3% to 12% enhancement). Accordingly, the highest methane yields were 550 and 567 mL/g-VS_{fed}, respectively on average in the presence of 1-octanol and hexanal at a concentration of 0.05% while the cumulative methane yield was observed as 490 mL/g-VS_{fed} for the control reactor. With the exception of 1-octanol at 0.5%, adding both compounds at each investigated concentration was beneficial for the digestion in the batch process. Therefore, the selected alcohol and aldehyde sources did not cause the expected detrimental effect on the methanogens even at the maximum amounts added in this study. Nevertheless, since the effect of the chemical compounds on methane generation has been generally concentration-dependent, the toxic effects of 1-octanol and hexanal would be better observed at higher concentrations (>0.5%), especially when their threshold levels are exceeded in anaerobic reactors digesting paper wastes.

Cite this article as: Yarsur E, Horváth IS, Yangın Gömeç Ç. Methane yield of paper industry waste in the presence of two compounds from alcohol and aldehyde groups during thermophilic anaerobic digestion. Environ Res Tec 2023;6:1:54–59.

INTRODUCTION

Depending on the total solids (TS) content of the substrate, anaerobic digestion has been applied as wet (i.e., TS from 0.5% to 15%) or dry (i.e., TS more than 20%) processes for many decades. However, dry anaerobic digestion is particularly preferred for treating the industrial wastes in order to meet the energy demand of the facilities. In this context, since paper wastes have high carbon content and TS concentrations; these difficult degradable

***Corresponding author.**
*E-mail address: yanginci@itu.edu.tr

This paper has been presented at Sixth EurAsia Waste Management Symposium (EWMS 2022)/Istanbul, Turkiye / 24–26 October 2022.

feedstocks have been stabilized efficiently by anaerobic reactors also enabling biogas generation as one of the renewable energy sources [1–3]. However, paper industry wastes contain mostly hemicellulose and cellulose and degradation of these materials by the microorganisms are not easy. On the other hand, inhibitory substances found in paper wastes might cause process failure in bioreactors with reduced biogas yields. These inhibitory compounds are sulphuric (e.g., unionized H_2S, SO_3^{2-}, SO_4^{2-}) and chlorinated (e.g., Adsorbable Organic Halides and pentachlorophenol) compounds, wood extractives (e.g., resin acids, fatty acids, volatile terpenes, sterols, juvabiones, and tannins), and some other compounds such as H_2O_2 [4, 5]. Since paper and packaging materials are lignocellulose-based natural polymers; they release acetic acid, aldehydes, alcohol, and ester-based volatile organic compounds (VOCs) due to ageing [6]. Hence, necessary precautions against these toxic substances should be taken in order to keep the digestion process at steady-state condition for achieving an enhanced methane production. For example, some chemical compounds such as aldehydes (e.g., hexanal) and alcohols (e.g., 1-octanol) might be toxic especially to the methanogenic cultures, which adversely affect biogas yields of anaerobic processes with long lag phase periods at their increasing concentrations [3, 7]. In this context, acclimation periods generally allow the microbial cultures to adapt unfavorable conditions and inoculum adaptation plays a key role during anaerobic digestion of the inhibitory substances in bioreactors [8]. Besides available microorganisms, the impact of the chemical compounds on the stabilization process change depending on the operation parameters (e.g., pH, temperature, hydraulic retention time etc.). Moreover, it was reported that the effect of the compounds from alcohol and aldehyde groups on methane generation has been also concentration-dependent [9]. According to Jansson et al. [3], the chemical compounds that could affect biogas production in traditional wet anaerobic digestion processes were hexanal and 1-octanol which have been detected in the wastes/wastewaters of various industries such as food and paper sectors. Accordingly, the main source of odour in many paper with high wood extractives is the auto- and photo-oxidation of linoleic acid, oleic acid, linolenic acid. On the other hand, hexanal is a well-known aliphatic aldehyde and it is a predominant reaction product of linoleic acid (i.e., a fatty acid component in wood extractives) oxidation and accounts for odour nuisance in pulp and paper industry. It was also reported that hexanal was the dominating volatile aldehyde originating from pulp and paper produced for food packaging purposes. On the other hand, a large variety of other aldehydes, ketones and alcohols are also formed [10, 11]. Among them, 1-octanol, known as a fatty alcohol, is described as typical volatile oxidation compound of oleic acid which also contributes to off-flavor development and released to the environment as a metabolite of many plants [10, 12, 13]. Octanol is also found in paper industry wastewaters, due to its usage as an antifoaming agent during paper making [14]. Hence, investigation of the impact of hexanal and 1-octanol on anaerobic digestion is important owing to the fact that anaerobic treatment is mostly used to stabilize the wastes from paper industry [3, 15]. Nevertheless, these two compounds might be beneficial or detrimental to the anaerobic digestion [9]. Although hexanal and 1-octanol could be degraded by some microorganisms which are involved in anaerobic digestion process, high concentrations of these chemicals could reduce the biogas production [3]. Hence, the aim of this work was to investigate the impacts of 1-octanol and hexanal on cumulative methane yield during thermophilic (55±2 °C) anaerobic digestion of the waste from a paper industry.

MATERIALS AND METHODS

Substrate, Inoculum, and Chemical Compounds

The paper waste (PW) with a total solids (TS) and volatile solids (VS) contents of about 28% and 27% was supplied by a pulp and paper industry located in Varberg, Sweden. The inoculum was obtained from a dry anaerobic digester plant treating municipal solid waste at thermophilic conditions (Borås, Sweden). TS content of the inoculum was 3.6% with a volatile content of about 65% [16].

The chemical compounds examined were from two groups i.e. alcohol (1-octanol) and aldehyde (hexanal); all provided by Sigma-Aldrich (Germany). 1-Octanol ($C_8H_{18}O$), also known as N-octan-1-ol or capryl alcohol, is a clear and colorless liquid which is a fatty alcohol lipid molecule with a molecular weight of 130.23 g/mol [12]. Besides, hexanal ($C_6H_{12}O$) is also a clear and colorless liquid with a molecular weight of 100.16 g/mol [17]. Both chemical solutions were prepared by diluting pure liquid chemical compounds with distilled water in order to achieve concentrations of 0.005%, 0.05% and 0.5% (w/v). Hence, 0.27–27 and 0.3–30 mg COD were added to each bottle by adding hexanal and 1-octanol, respectively.

Batch Reactors and Operating Conditions

The experiments were carried out at thermophilic conditions (55±2 °C) using 118 mL serum glass bottles at which anaerobic digestion took place. The reactors were kept in an incubator and operated as batch systems. In order to measure the methane production of only the inoculum, the blank reactors were set-up with only inoculum (Control_Seed) to be incubated without the addition of substrates and chemical compounds. On the other hand, the control reactors were also set-up only with the inoculum and the used paper waste (Control_PW) with-

Table 1. The toxic concentrations of some alcohols and aldehydes in anaerobic digestion

Compound class	Value	Unit	Reference
4-Methylbenzaldehyde	4.25 (IC_{50})*	mmol/L	Sierra-Alvarez and Lettinga [20]
Benzaldehyde	5.03 (IC_{50})	mmol/L	
Formaldehyde	10	mg/L	Qu and Bhattacharya [21]
2-Phenylethanol	46.53 (IC_{50})	mmol/L	Sierra-Alvarez and Lettinga [20]
Phenylmethanol	31.74 (IC_{50})	mmol/L	
Allyl alcohol	3000	mg/L	Demirer and Speece [22]

*: The inhibitory concentration (IC_{50}) that reduces 50% of methane production.

Table 2. Average methane yields and standard deviations (mL CH_4/g-VS)

Chemical conc. (%)	Incubation time (d)							
	0	2	9	13	23	29	35	45
Inoculum (Control_Seed)								
0	0±0	13±1.0	38±1.6	89±4.0	102±4.2	107±5.4	119±7.1	128±8.8
Paper waste + Inoculum (Control_PW)								
0	0±0	34±2.5	145±10.8	461±36.3	537±89.8	581±92.3	600±93	618±92.1
Paper waste + Inoculum + 1-octanol								
0.005	0±0	39±5.1	137±1.5	400±7.8	596±13.5	628±8.9	657±12.2	675±9.1
0.05	0±0	35±4.2	133±2.3	395±14	567±36	628±13.8	655±11.8	678±12.5
0.5	0±0	34±1.1	136±8.9	381±106	527±87	563±91	583±91	599±96
Paper waste + Inoculum + Hexanal								
0.005	0±0	37±1.6	143±11	414±51.4	615±32.7	651±45	673±40.4	685±43
0.05	0±0	34±2.0	143±10	439±33.5	607±18	646±25.4	673±19.7	695±17.4
0.5	0±0	30±2.3	130±10.2	408±42.8	540±42.1	578±44.4	607±35.5	638±43.5

out the addition of chemical compounds. Only distilled water was added in the blank and control flasks. All assays were running with the substrate to inoculum ratio of 1:2 (VS basis) in reactors corresponding to 0.5 g-VS for the substrate and 1.0 g-VS for the inoculum ($VS_{substrate}$ to $VS_{inoculum}$). Besides, each serum bottle except the control ones, included 2 mL of the single selected compound. On the other hand, the control reactors were prepared with 2 mL tap water instead of hexanal or 1-octanol solution. Hence, the working volume for each reactor was about 45 mL with the headspace of about 75 mL. After the addition of all necessary components; each serum bottle was sealed with a rubber septum and with an aluminum cap. Then, the headspace of each reactor was flushed with the gas mixture of 80% N_2 and 20% CO_2 for 2 minutes to maintain anaerobic conditions inside the reactors. The reactors were then incubated at 55±2 °C while they were shaken manually once a day during the incubation period of 45 days. All experimental set-up was done in triplicates (i.e., with a total of 24 flasks) and average methane gas values were calculated.

Analytical Procedure

Gas samples were taken three times a week at the first weeks of the study, then were gradually reduced as twice a week and once a week towards the end of the digestion period. The total solids (TS) and the volatile solids (VS) of the substrate and inoculum were determined according to Standard Methods [18]. On the other hand, the biogas samples were taken from each reactor's headspace using a 250-µL pressure-lock gas syringe (VICI, Precision Sampling Inc., Baton Rouge, LA, USA). Gas measurement and analysis were conducted as described in a previous study by Teghammar et al. [19] and each methane (CH_4) by volume was obtained at standard conditions (0 °C and 1 atm). The compositions [methane (CH_4), hydrogen (H_2), carbon dioxide (CO_2)] of the produced biogas were determined using a gas chromatography (Perkin-Elmer Clarus 590, Perkin-Elmer Inc., Waltham, MA, USA) equipped with a packed column (6' x 1.8" OD, 80/100, Mesh, Perkin Elmer Inc., Waltham, MA, USA) and a thermal conductivity detector (Perkin-Elmer Inc., Waltham, MA, USA) at an inject temperature of 150 °C. The carrier gas was nitrogen operated with a flow-rate of 20 mL/min at 60 °C.

Table 3. Effect of the additions of chemical compounds on biogas production at different concentrations

Reactor content	Chemical compound	Chemical concentration (%)	Net methane yield (mL CH_4/g-VS)	Variation[a,b] (%)
Inoculum (Control_Seed)	–	0	128	–
Paper waste + Inoculum (Control_PW)	–	0	490	–
Paper waste + Inoculum	1-octanol	0.005	547	(+)9
		0.05	550	(+)10
		0.5	471	(-)3
Paper waste + Inoculum	Hexanal	0.005	557	(+)11
		0.05	567	(+)12
		0.5	510	(+)3

a: [(CH_4 produced by feedstock with chemical compound-CH_4 produced by control)/(CH_4 produced by control)x100]; b: Enhancement is indicated by (+) whereas retardation is indicated by (-) in net methane yield.

RESULTS AND DISCUSSION

Since some alcohols and aldehydes found in paper wastes might cause process failure in bioreactors; necessary precautions against these toxic substances should be taken in order to keep the digestion process at steady-state condition for achieving an enhanced methane production [7]. The toxic concentrations of some alcohols and aldehydes in anaerobic digestion are presented in Table 1.

Since Jansson et al. [3] performed a similar study with hexanal and 1-octanol at mesophilic (37±1 °C) condition; this particular study was performed in order to investigate the effects of these selected compounds on biogas production at the same concentrations at thermophilic (55±2 °C) condition. Hence, 1-octanol and hexanal were added into the reactors to achieve concentrations of 0.005, 0.05, and 0.5% (w/v). The results showed that addition of 1-octanol and hexanal at concentrations of 0.05% resulted in increased biogas production (Table 2) after 45-days incubation period. The highest net methane yields were 550 and 567 mL/g-VS_{fed}, respectively in the presence of 1-octanol and hexanal at a concentration of 0.05%. These results corresponded to about 10% and 12% enhancement in cumulative methane production, respectively compared to the control reactor (490 mL CH_4/g-VS_{fed}) digesting only the paper waste. Hence, adding both compounds to 0.05% was beneficial for the digestion process. Even at 0.5%, hexanal was somewhat beneficial; however, 1-octanol at this concentration showed a slight effect with a retardation in biogas generation of about 3% decrease. Accordingly, cumulative methane yield for 1-octanol was 471 mL CH_4/g-VS_{fed} whereas it was 510 mL CH_4/g-VS_{fed} for hexanal compared to the control reactor (490 mL CH_4/g-VS_{fed}). Hence, it could be concluded that increasing concentrations of both chemicals from 0.05% to 0.5% indicated not significantly different methane yields than that obtained from only paper waste in the control reactor. Effect of the additions of chemical compounds on net methane yields are presented in Table 3. In this context, continued

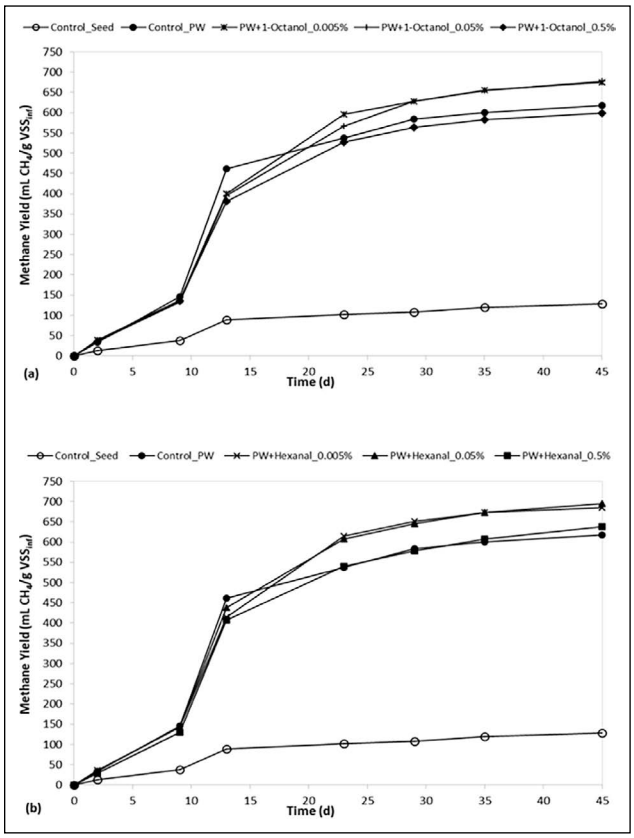

Figure 1. Biogas generation during thermophilic anaerobic digestion of paper waste with **(a)** 1-octanol and **(b)** hexanal at different concentrations in comparison to control reactors (without chemical compounds) .

biogas productions revealed the probable consumption of both chemicals up to a certain concentration by the anaerobic microorganisms available in thermophilic batch reactors. The effect of the selected compounds from alcohol and aldehyde groups on the initial digestion rate is presented in Figure 1a for 1-octanol and in Figure 1b for hexanal.

Although adding 1-octanol and hexanal did not indicate any apparent inhibition on anaerobic digestion performance of the paper waste up to 0.5% at thermophilic (55±2 °C) condition, Jansson et al. [3] who performed a similar study with the same hexanal and 1-octanol concentrations reported contrary findings at mesophilic (37±1 °C) condition. Accordingly, they reported substantial inhibition and lower methane yields at all concentrations irrespective of the chemical compound used. On the other hand, long lag phase was not observed in this particular study unlike Jansson et al. [3]. Accordingly, they previously reported more than 20 days for hexanal and 80 days for 1-octanol during mesophilic digestion of paper waste in similar batch assays at S/I ratio (VS basis) of 1.0 with a TS of 16%. Therefore, since the addition of the same alcohol and aldehyde sources up to a concentration of 0.05% improved the performance of the anaerobic process with an increase in methane yield in this particular study, it was probably due to the difference in initial VS content fed [23] into the batch reactors as well as due to higher (i.e., thermophilic) operating temperature. Meegoda et al. [24] also reported that reaction rates are increased at higher temperatures which result in a possibility of higher loading rates and improved biogas yields.

In conclusion, contrary to expectation, the selected chemical compounds did not indicate notable toxic effect on methane production in the batch assays even the concentration increased to 0.5% for 1-octanol and hexanal. However, preliminary results revealed that the toxic effects of both selected compounds would be observed at different operating conditions [3]. Moreover, higher concentrations of the chemical compounds from alcohol and aldehyde groups would exert inhibitory effect especially when their threshold levels are exceeded in anaerobic reactors digesting the wastes from industries such as food and paper facilities.

CONCLUSIONS

According to the results, cumulative methane yields measured in the batch assays showed that the degradation process was not slowed down and the externally added compounds from the alcohol (1-octanol) and aldehyde (hexanal) groups up to a concentration of 0.05% made it possible for the methanogens to produce a higher amount of ultimate biogas. Hence, addition of the selected compounds was beneficial for the digestion and improved the performance of the anaerobic process with an enhancement in methane yield of 10% for 1-octanol and 12% for hexanal. Accordingly, compared to the control reactor which only included the paper waste; net methane yield for 1-octanol was 550 mL CH_4/g-VS_{fed} whereas it was 567 mL CH_4/g-VS_{fed} for hexanal at 0.05% concentration of each compound. When it comes to the effects of the selected chemical compounds at 0.5% concentration of each, no remarkable toxic effect on methane production was observed even the concentration increased up to 0.5% for both compounds. Accordingly, methane yields indicated a slight increase for hexanal whereas a slight decrease for 1-octanol even at 0.5% concentration. Contrary to expectations, the reason why methane yields did not decrease even with increasing concentrations of both chemical compounds, was probably due to the fact that threshold levels were still not exceeded in the batch assays. In conclusion, continued biogas productions also revealed the probable consumption of both chemicals up to a certain concentration by the anaerobic microorganisms available in the reactors digesting paper waste at thermophilic temperature.

Acknowledgement
This work was financially supported by the Department of Scientific Research Projects of ITU (Project Number: MYL-2019-42365). ITU EU Centre Erasmus Office is also acknowledged. The authors are also grateful for former PhD student, Vanessa Elisa Pinheiro, for all practical help in the lab at the Swedish Centre for Resource Recovery, at University of Borås.

DATA AVAILABILITY STATEMENT

The authors confirm that the data that supports the findings of this study are available within the article. Raw data that support the finding of this study are available from the corresponding author, upon reasonable request.

CONFLICT OF INTEREST

The authors declared no potential conflicts of interest with respect to the research, authorship, and/or publication of this article.

ETHICS

There are no ethical issues with the publication of this manuscript.

REFERENCES

[1] Y. Li, S. Y. Park, and J. Zhu, "Solid-state anaerobic digestion for methane production from organic waste," Renew Sustainable Energ Review, Vol. 15, pp. 821–826, 2011. [CrossRef]

[2] J. Yi, B. Dong, J. Jin, and X. Dai, "Effect of increasing total solids contents on anaerobic digestion of food waste under mesophilic conditions: performance and microbial characteristics analysis," PLoS One, Vol. 9, pp. e102548, 2014. [CrossRef]

[3] A. T. Jansson, R. J. Patinvoh, M. J. Taherzadeh, and I. Sárvári Horváth, "Effect of organic compounds on dry anaerobic digestion of food and paper industry wastes," Bioengineered, Vol. 11, pp. 502–509, 2020. [CrossRef]

[4] T. Meyer, and E.A. Edwards, "Anaerobic digestion of pulp and paper mill wastewater and sludge," Water Research, Vol. 65, pp. 321–349, 2014. [CrossRef]

[5] S. Lacorte, A. Latorre, D. Barceló, A. Rigol, A. Malmqvist, and T. Welander, "Organic compounds in paper-mill process waters and effluents," TrAC Trends in Analytical Chemistry, Vol. 22, pp. 725–737, 2003. [CrossRef]

[6] I. Alam, and C. Sharma, "Degradation of paper products due to volatile organic compounds," Preprint (Version 1) available at Research Square [https://doi.org/10.21203/rs.3.rs-2080804/v1], 2022. [CrossRef]

[7] A. Nsair, S. Onen Cinar, A. Alassali, H. Abu Qdais, and K. Kuchta, "Operational parameters of biogas plants: A review and evaluation study," Energies, Vol. 13, pp. 3761, 2020. [CrossRef]

[8] C. Yangin-Gomec, T. Sapmaz, and S. Aydin, "Impact of inoculum acclimation on energy recovery and investigation of microbial community changes during anaerobic digestion of the chicken manure," Environmental Technology, Vol. 41, pp. 49–58, 2020. [CrossRef]

[9] H. Yanti R. Wikandari, R. Millati, C. Niklasson, and M. J. Taherzadeh, "Effect of ester compounds on biogas production: beneficial or detrimental?" Energy Science & Engineering, Vol. 2, pp. 22–30, 2014. [CrossRef]

[10] A. Fagerlund, D. Shanks, K. Sunnerheim, L. Engman, and H. Frisell, "Protective effects of synthetic and naturally occurring antioxidants in pulp products," Nordic Pulp & Paper Research Journal, Vol. 18, pp. 176–181, 2003. [CrossRef]

[11] H. Lindell, "Odour and Taste Originating from Food Packaging Board," C.F. Baker, Ed. Products of Papermaking, Trans. of the Xth Fund. Res. Symp. Oxford, Manchester: FRC, pp. 431–497, 2018.

[12] National Center for Biotechnology Information. "1-Octanol," https://pubchem.ncbi.nlm.nih.gov/compound/1-Octanol, National Center for Biotechnology Information (NCBI) website. 2020.

[13] R. Domínguez, M. Pateiro, M. Gagaoua, F.J. Barba, W. Zhang, and J. M. Lorenzo, "A comprehensive review on lipid oxidation in meat and meat products," Antioxidants, Vol. 8, pp. 429, 2019. [CrossRef]

[14] Q. Chang, Emulsion, Foam, and Gel, Q. Chang, Ed. Colloid and Interface Chemistry for Water Quality Control, Chapter 11, Academic Press, pp. 227-245, 2016. [CrossRef]

[15] C. Yangin-Gomec, E. Yarsur, and O.Y. Ozcan, "Energy recovery during anaerobic treatment of lignocellulosic wastewater with dynamic modeling and simulation results," Biomass Conversion and Biorefinery, 2021. [CrossRef]

[16] E. Yarsur, "Biogas recovery during anaerobic treatment of lignocellulose-rich pollutants with high sulfate content: an investigation via innovative applications," Master Thesis, Istanbul Technical University, Istanbul, Turkey, Feb. 2021.

[17] National Center for Biotechnology Information. "Hexenal," https://pubchem.ncbi.nlm.nih.gov/compound/Hexanal, National Center for Biotechnology Information (NCBI) website. 2020.

[18] American Public Health Association. "Standard Methods for the Examination of Water and Wastewater," 21st ed., American Public Health Association (APHA) Press, Washington, United States, 2005.

[19] A. Teghammar, J. Yngvesson, M. Lundin, M. J. Taherzadeh, and I. Sárvári Horváth, "Pretreatment of paper tube residuals for improved biogas production," Bioresource Technology, Vol. 101, pp. 1206–1212, 2010. [CrossRef]

[20] R. Sierra-Alvarez, and G. Lettinga, "The effect of aromatic structure on the inhibition of acetoclastic methanogenesis in granular sludge," Applied Microbiology and Biotechnology, Vol. 34, pp. 544–550, 1991.

[21] M. Qu, and S. K. Bhattacharya, "Toxicity and biodegradation of formaldehyde in anaerobic methanogenic culture," Biotechnology and Bioengineering, Vol. 55, pp. 727–736, 1997. [CrossRef]

[22] G. N. Demirer, and R. E. Speece, "Anaerobic biotransformation of four3-carbon compounds (acrolein, acrylic acid, allyl alcohol and n-propanol) in UASB reactors," Water Research, Vol. 32, pp. 747–759, 1998. [CrossRef]

[23] A. T. Jansson, R. J. Patinvoh, I. Sárvári Horváth, and M. J. Taherzadeh, "Dry anaerobic digestion of food and paper industry wastes at different solid contents," Fermentation, Vol. 5, pp. 40, 2019. [CrossRef]

[24] J. N. Meegoda, B. Li, K. Patel, and L. B. Wang, "A review of the processes, parameters, and optimization of anaerobic digestion," International Journal of Environment Research Public Health, Vol. 15, pp. 2224, 2018. [CrossRef]

Environ Res Tec, Vol. 6, Issue. 1, pp. 60–67, March 2023

Environmental Research and Technology
https://ert.yildiz.edu.tr - https://dergipark.org.tr/tr/pub/ert
DOI: https://doi.org/10.35208/ert.1221724

Environmental Research & Technology

Research Article

Determination of personal carbon footprint in aviation and tourism axis: Cappadocia Airport case

Selçuk GÜRÇAM*

Independent Researcher, Iğdır, Türkiye

ARTICLE INFO

Article history
Received: 20 December 2022
Revised: 06 March 2023
Accepted: 11 March 2023

Key words:
Aviation; Carbon footprint; Cappadocia Airport; Climate crisis; International agreements; Paris agreement; Tourism

ABSTRACT

Global average temperatures are increasing in direct proportion to the increase in carbon dioxide (CO_2). A significant part of this increase comprises the aviation and tourism sectors. In particular, the rapid growth of the aviation industry and its relationship with tourism development constitutes an indispensable problem for the future in the fight against the climate crisis. In this study, it has been revealed that the aviation industry is not innocent at all regarding the climate crisis when combined with tourism. The study examined flights' average personal carbon footprint to Cappadocia Airport between 2016 and 2019. The Cappadocia region stands out because it is an important tourism region of Turkiye and is located right in the middle of Turkiye. In the review, 2019 was the period with the highest emissions of 27,464.08 tons CO_2. On the other hand, 2017 was the year that emitted the least, with 8121,29 tons CO_2. The personal carbon footprint from total flights was 61,951 kg CO_2. While the individual carbon footprint was the highest in 2016 with 70,617 kg CO_2, 2019 was the year with the lowest personal carbon footprint with 56,419 kg CO_2. As a result, while there is a direct proportion between the number of flights and the total increase in CO_2, the personal carbon footprint has changed according to the number of passengers. Transportation preferences should be reviewed considering the location of the Cappadocia region and Turkiye's transportation policy.

Cite this article as: Gürçam S. Determination of personal carbon footprint in aviation and tourism axis: Cappadocia Airport case. Environ Res Tec 2023;6:1:60–67.

INTRODUCTION

Greenhouse gases (GHG) originate from various sectors. Among these, the aviation sector stands out in terms of rapid growth, although its rate is low. Between 1970 and 2019, there was a 77% improvement in passenger energy density, expressed in British Thermal Units, with improvements in the engine and design sector, efficiency in air traffic operations, denser seat configurations, and more passengers. Especially in the last 20 years, the growth in the commercial aviation sector has been more than the growth in total emissions. However, with the increased demand, the increase in destinations, the increase in the number of aircraft, and the increasing impact of the sector on global trade and economy, there has been a rapid increase in emissions from aviation [1]. According to the International Council for Clean Transport, emissions from all commercial operations increased by 29% between 2013 and 2019, reaching 918 million metric tons [2].

***Corresponding author.**
*E-mail address: selcukgrcm@gmail.com

According to the International Civil Aviation Organization, by 2050, GHG emissions from the aviation sector may increase by two to four times compared to 2015 emission levels [3]. The rapid recovery and growth in the sector after the COVID-19 epidemic, especially the increase in demand, stands as the biggest obstacle to controlling emissions in the commercial aviation sector [1]. The first of the individual measures to be implemented for this purpose is the calculation of the carbon footprint. All responsible countries and institutions, especially those that are party to the Paris Agreement, should take measures to reduce their carbon footprints. Knowing the carbon footprint, as measured by carbon dioxide (CO_2) emissions caused by human actions and understanding what it takes to minimize it is essential to combat the climate crisis individually. Airports are constantly overflowing, and the density is much higher, especially in summer. More than 1.1 billion passengers flew in the United States of America (USA) alone in 2019, both domestically and internationally. Each individual who makes these flights has left an individual carbon footprint on the climate crisis. Although people have carbon footprints because of different efforts, the carbon footprint resulting from air travel is at the top of these [4].

Another area that is intertwined with the aviation industry in terms of carbon footprint is the tourism industry. Tourism is one of the most extensive economic activities of the global economy, with 1.4 billion tourists in 2018. GHG from tourism correspond to 8% of global emissions. Improvements in the fight against the climate crisis, especially in other sectors, have not been observed in the tourism sector [5].

In this study, the aviation sector, which proliferates in terms of the climate crisis and causes global warming in direct proportion to this growth, has been examined. With the study, the personal carbon footprint originating from the aviation sector has been handled specifically for Cappadocia Airport in Turkiye. As a result of the study, it is seen that although it provides great economic, tourism, and commercial returns, it is not very innocent in terms of the environment. Cappadocia Airport was considered because its location attracts attention in terms of tourism, and it is located at a middle point that can be considered equidistant from every average region of Turkiye. This could enable the use of alternative vehicles that could result in fewer emissions. In the study, the personal carbon footprint resulting from air travel to Cappadocia Airport between 2016–2019 was determined and discussed at the political level. It is especially important to consider the years 2016–2019 in terms of revealing the real development of the aviation industry before COVID-19. In addition, this study differs from studies that only examine total emissions in terms of bringing together different disciplines in which Turkiye's transportation policy is evaluated on the axis of aviation and tourism in a single study and evaluating emissions per passenger. For example, [6] tried to determine the emission values to determine the effect of Iğdır Airport on air pollution in Iğdır province, [7] studied the emissions from total flights to Muğla Airports to studies measuring the effect of aviation on air quality [8, 9]. For this reason, this study will be a pioneer in contributing to future studies by addressing personal carbon footprints within the scope of aviation and tourism sectors.

CARBON FOOTPRINT, AVIATION AND TOURISM

The carbon footprint is generally calculated as a one-year CO_2 equivalent and is expressed as the weight in tons of CO_2 emissions produced [10]. In short, it is the number of GHG produced by human actions [11, 12]. According to Mike Berners-Lee, the author of The Carbon Footprint of Everything, it is defined as the sum of all GHG emissions necessary for producing or producing a product [13]. Youmatter [10], on the other hand, defined it as GHG that arise due to the lifestyles and actions of individuals.

The transportation sector approaches around 14% of global emissions (including non-CO_2) gases, while consumers burn fossil fuels, which account for about a quarter of CO_2 emissions [14]. In particular, the transportation sector is one of the most extensive parts of the individual carbon footprint in rich countries that use it frequently. For example, using a bicycle instead of a car for short-haul journeys reduces the carbon footprint from transportation by 75%, while using a train instead of a car for medium-haul journeys reduces the carbon footprint by 80%, and traveling by train instead of a domestic flight reduces its carbon footprint by 84% reduces. Factors such as the distance of travel, the occupancy of public transportation, and the rate of fuel used (such as fossil fuels or electric vehicles) also affect the carbon footprint when using public transportation. However, walking or cycling for short and medium-distance trips are the vehicles with the lowest carbon footprints. The electricity generation source used in a region also affects the carbon footprint. For example, if electricity is provided through nuclear energy or renewable energy, rather than a thermal power plant where electricity is produced from coal, then it is more efficient to use electric vehicles or prefer rail transportation. For example, in France, which produces 90% of its electricity from low-carbon sources (70% of nuclear energy), on average, if Eurostar rail transportation is preferred instead of traveling by plane for short distance journeys, there will be a 96% reduction in carbon footprint [15].

Traveling by plane or alone by car is the means of transportation with the most carbon impact. The distinction between the two depends on the distance traveled. For example, if traveling to a medium-distance destination is less than 1000 km, traveling by plane causes a larger carbon footprint. However, if the distance is more than 1000 km and you are traveling by car alone, then the plane causes

less carbon footprint. For example, traveling alone between London and Edinburgh with a distance of 500 km will cause around 100 kg CO_2 equivalent, while traveling by plane will have 128 kg CO_2 equivalent, and if this distance is done by train, it will have 21 kg CO_2 equivalent [15]. According to the European Environment Agency (Fig. 1), the transport sector produces the most CO_2/gram emissions per passenger kilometer of air travel.

Tourism has a share of 8% of global GHG emissions. Transportation is the main source of greenhouse gas emissions from tourism. In terms of carbon footprint, airplanes and cars produce the most CO_2 per passenger, while tour buses, ferries, and trains are other carbon footprint causes. Most of this carbon footprint from tourism consists of visitors from high-income countries, especially from the USA. More precisely, as the incentives for air travel increase, ticket prices get cheaper, and people can afford to travel, the tourism-related carbon footprint will also increase. Tourism emissions from vehicles increased by more than 60% between 2005 and 2016 [17]. The sectoral distribution of the personal carbon footprint resulting from global tourism is shown in Figure 2.

CASE STUDY: CAPPADOCIA REGION AND CAPPADOCIA AIRPORT

Cappadocia consists of a region that emerged because of the erosion of soft layers formed by ash and lava 60 million years ago by wind and rain for millions of years. This region, rich in tourism hosts millions of tourists, is a region where history and nature integrate most beautifully in the world [18, 19]. In 2019, 3 million 834 thousand 134 tourists visited the museums and ruins in Turkiye's favorite tourist region, Cappadocia. The number of people visiting the tourist centers in Cappadocia in 2019 increased by 30% compared to the previous year, which was considered the "*golden year*" in the region, 73% compared to 2017 and 157% compared to 2016 [20].

The existing airport of Cappadocia, which appeals to such a vast region, also has many valuable and important qualities. Nevşehir Cappadocia Airport is an airport that was put into service for domestic and foreign tourists in 1998 (Fig. 3). Additionally, Nevşehir Cappadocia Airport has 3500 m^2 of common-use area. In addition to this feature, there is a domestic and international terminal with an annual passenger capacity of 700,000. Additionally, there is a concrete runway of 3000x45 m, 110 PCN strength, and a concrete apron of 240x120, 110 PCN strength, with a capacity of 5 aircraft [21–23].

In addition to all this information, it will be possible to clearly say that Nevşehir Cappadocia Airport hosts hundreds of thousands of domestic and foreign tourists annually in certain periods.

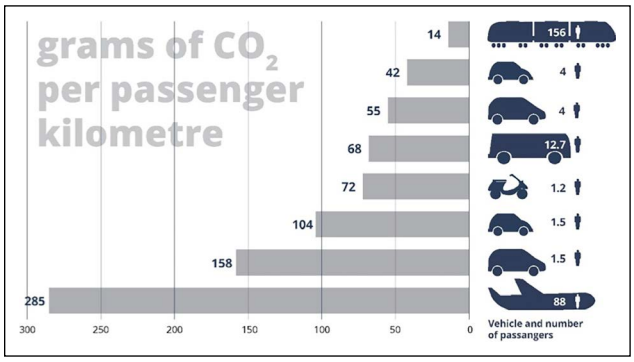

Figure 1. CO_2/gram per passenger kilometer [16].

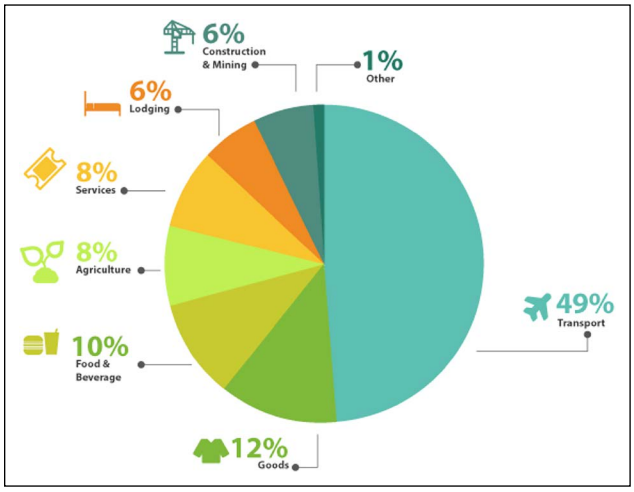

Figure 2. Carbon footprint of global tourism (2018) [17].

MATERIAL AND METHOD

In this study, all of the real-time data used to determine the average passenger carbon footprint of all flights to Nevşehir Cappadocia Airport between 2016–2019 were officially obtained from the General Directorate of Civil Aviation. Flights between 2016–2019 include both domestic and international flights. In addition, these data could not be used since there were no flights due to the renovations made at the airport between May 1 and October 31, 2017. In this study, the Tier 1 method, one of the three methods recommended by the Intergovernmental Panel on Climate Change (IPCC), was used in carbon footprint calculations. In the Tier 1 method, calculations made with the amount of fuel according to the type of fuel burned from the national energy statistics and only the assumed emission factors are sufficient. In this study, CO_2 emissions produced during the period from starting the engine to stopping are taken into account. The steps to be followed in determining the personal carbon footprint from flights are: Tj (fuel consumption), Ef (emission factor), n (number of occupied seats), and CFP (CO_2 emissions per person). Firstly, total CO_2 emission is given in equation (1), while personal carbon footprint is given in equation (2). [25–27]:

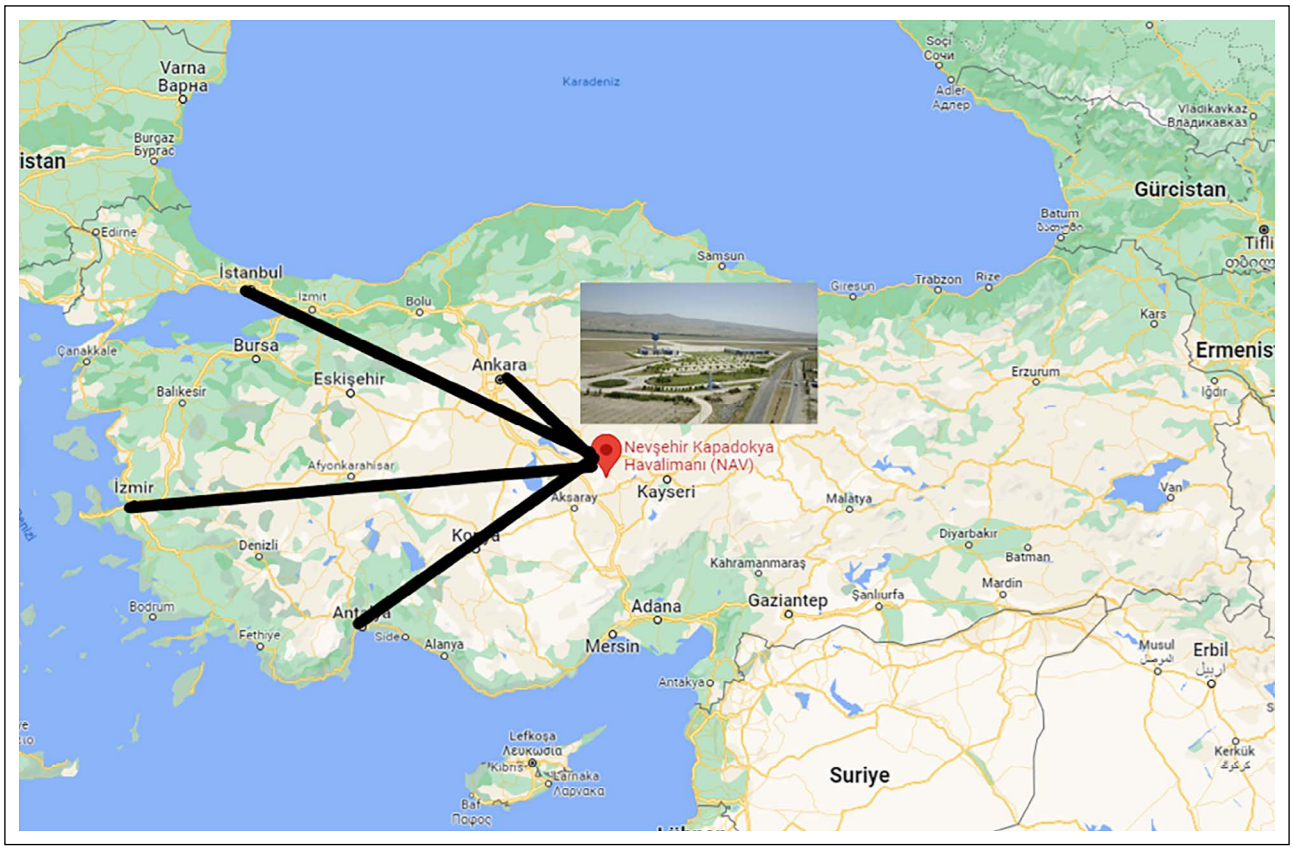

Figure 3. Location of Cappadocia Airport in Turkiye (edited using Google maps) [24].

$$\sum CO_2 = Tj \; x \; Ef \quad (1)$$

$$CFP = \frac{Tj \; x \; Ef}{n} \quad (2)$$

The emission factor here is 3.157, which refers to the CO_2 produced due to the combustion of 1 kg of fuel. That is, burning 1 kg of fuel causes 3.157 kg of CO_2 [28, 29].

RESULTS

Table 1 gives numerical data for determining the personal carbon footprint resulting from flights to Cappadocia Airport between 2016–2019.

When Table 1 was examined, the year with the highest number of flights to Cappadocia Airport between 2016–2019 was 2019, and the year with the least number of flights was 2017 when the renovation works were considered. While the month with the most flights was October 2019, with 340 flights, the month with the least flights (excluding the dates closed due to renovations) was February 2017, with 123 flights. On a total basis, it is seen that the number of flights increased between May and October. Additionally, while domestic and international flights occurred in all years, domestic flights showed a more regular distribution. While the most international flights were in 2018, with nine flights, the least was in 2017 and 2019, with seven flights. While most of the domestic flights were realized in 2019 with 3092 flights, the lowest number of domestic flights were realized in 2017 with 924.

As shown in Table 2, the year with the highest fuel consumption in flights to Cappadocia Airport between 2016–2019 was 8699.45 tons, while the minor fuel consumption was in 2017 with 2572,48 tons. The general reason that determines the maximum and minimum fuel consumption is the number of flights. Similarly, the month with the highest fuel consumption in all years was October 2019, with 922,59 tons, while the month with the lowest fuel consumption was February 2017, with 348.68 tons. Generally, there is a direct correlation between the number of flights and fuel consumption.

Table 3 tabulates the total number of passengers flying on a monthly and annual basis between 2016 and 2019. When Table 3 was examined, the highest number of passengers were transported to Cappadocia Airport in 2019, with 486,782, while the least number of passengers were carried in 2017, with 123,352. Similarly, the month with the highest number of passengers in all years was October 2019, with 53,818 passengers, while the month with the least number of passengers was February 2017, with 16,530 passengers. Generally, there is a direct proportion between the number of flights and the number of passengers.

Table 1. Total number of domestic and international flights between 2016 and 2019

	Jan	Feb	Mar	Apr	May	Jun	Jul	Aug	Sep	Oct	Nov	Dec	Tot
2016-Dom	152	192	163	251	332	297	323	309	258	210	160	170	2825
2016-Int	1	1	0	0	0	0	2	2	2	0	0	0	
2017-Dom	164	119	152	194	0	0	0	0	0	0	147	148	931
2017-Int	2	4	1	0	0	0	0	0	0	0	0	0	
2018-Dom	148	148	172	240	244	239	0	254	244	245	164	164	2271
2018-Int	2	1	3	0	0	1	0	1	1	0	0	0	
2019-Dom	182	164	192	257	286	290	272	289	317	340	263	240	3099
2019-Int	0	2	2	0	0	0	1	1	1	0	0	0	

Table 2. Average fuel consumption (tons) from monthly and annual flights between 2016 and 2019

	Jan	Feb	Mar	Apr	May	Jun	Jul	Aug	Sep	Oct	Nov	Dec	Tot
2016	436.21	553.35	427.69	689.79	886.59	777.77	899.14	870.64	730.59	575.26	440.93	450.03	7737.99
2017	464.60	348.68	415.57	524.55	0	0	0	0	0	0	403.99	415.09	2572.48
2018	426.99	431.63	516.58	666.11	663.37	672.05	0	723.94	704.10	696.09	459.38	452.15	6412.39
2019	512.20	478.01	529.53	757.64	840.81	838.63	756.49	828.47	890.31	922.59	699.97	644.80	8699.45

Table 3. The total number of passengers flying on a monthly and annual basis between 2016 and 2019

	Jan	Feb	Mar	Apr	May	Jun	Jul	Aug	Sep	Oct	Nov	Dec	Tot
2016	18.196	23.652	19.650	30.965	41.754	31.306	37.322	40.264	32.805	27.740	21.468	20.807	345.929
2017	21.935	16.530	19.328	26.226	0	0	0	0	0	0	19.629	19.704	123.352
2018	21.794	21.807	24.429	36.442	33.335	33.868	0	39.443	39.272	40.169	25.494	23.375	339.428
2019	27.165	25.161	30.279	44.672	44.796	46.435	45.736	49.353	52.373	53.818	35.294	31.700	486.782

Table 4. Average CO_2 (tons) emissions from monthly and annual flights between 2016 and 2019

	Jan	Feb	Mar	Apr	May	Jun	Jul	Aug	Sep	Oct	Nov	Dec	Tot
2016	1377.11	1746.92	1350.21	2177.66	2798.96	2455.41	2838.58	2748.61	2306.47	1816.09	1392.01	1420.74	24.428.77
2017	1466.74	1100.78	1311.95	1656.00	0	0	0	0	0	0	1275.39	1310.43	8121.29
2018	1348.00	1362.65	1630.84	2102.90	2094.25	2121.66	0	2285.47	2222.84	2197.55	1450.26	1427.43	20.243.85
2019	1617.01	1509.07	1671.72	2391.86	2654.43	2647.55	2388.23	2615.47	2810.70	2912.61	2209.80	2035.63	27.464.08

Table 5. Average personal carbon footprint CO_2 (kg) from monthly and annual flights between 2016 and 2019

	Jan	Feb	Mar	Apr	May	Jun	Jul	Aug	Sep	Oct	Nov	Dec	Yearly
2016	75.682	73.859	68.712	70.326	67.034	78.432	76.056	68.264	70.308	65.468	64.841	68.281	70.617
2017	66.867	66.592	67.878	63.143	0	0	0	0	0	0	64.974	66.505	65.838
2018	61.851	62.486	66.758	57.705	62.824	62.644	0	57.943	56.601	54.707	56.886	61.066	59.641
2019	59.525	59.976	55.210	53.542	59.255	57.016	52.217	52.995	53.666	54.119	62.611	64.215	56.419

As can be seen in Table 4, the highest CO_2 (ton) emission was realized in 2019 with 27,464.08 tons CO_2, while the lowest CO_2 (ton) emission was 8121.29 tons CO_2 in 2017. The highest CO_2 (ton) emission was in October 2019 with 2912.61 tons CO_2, while the least CO_2 (ton) emission was in February 2017 with 1100.78 tons CO_2. The results in this table show that there is a direct relationship between the number of flights and CO_2 (ton) emissions.

Within the framework of these findings, a total of 80,258.23 tons CO_2 emissions were made according to equation (1). According to equation (2), the value of 61,951 kg CO_2 per person is reached. However, annually, the highest individual average carbon footprint was 70.617 kg CO_2 in 2016, whereas the most diminutive personal average carbon footprint was 56,419 kg CO_2 in 2019. June 2016 was the month with the highest personal average carbon footprint of 78,432 kg CO_2, while the lowest private average carbon footprint was recorded in July 2019 with 52,217 kg CO_2. These carbon footprint data are given in Table 5.

DISCUSSION AND CONCLUSION

ICAO's Carbon Offset Reduction Plan for International Aviation (CORSIA) is more of a balancing program than an emission reduction. Since factors such as not taking essential steps in the Conference of the Parties (COP/26–COP/27) meetings and being away from carbon neutrality expected in 2050, alternative fuels and technological developments are the only expectations for the aviation industry in the short and medium term, the aviation industry is constantly behind a smoke screen is growing. It increases the sector's share in the climate crisis and, frankly, it cannot be stopped except for global problems. For example, the International Air Transport Association (IATA) predicts that European air travel volumes will reach pre-pandemic levels again by 2024 [30].

Although the aviation sector has a small share in the global total CO_2 emissions, it has a large share in terms of personal carbon footprint. This issue is considered one of the greatest injustices in the world. This is just like the countries with historical responsibilities with the largest climate crisis share. Because according to frequently cited estimates, 80% of people worldwide have not traveled by plane. There are also differences between the countries in terms of domestic flights. The biggest reason for this is, of course, the development indices encountered in domestic flights and the average individual carbon footprints of the countries. The use of domestic flights is increasing according to the development levels in these countries. For example, a person using domestic flights in the USA emits an average of 386 kilograms of CO_2 per year, while in Australia, 267 kg, 209 kg in Norway, 174 kg in New Zealand, and 168 kg in Canada. In most countries in Africa, Asia, and Eastern Europe, emissions per capita are less than one kg. Although this ratio is 0.8 kg on average, it is 0.14 kg in Rwanda [31].

In terms of the findings obtained in the study, although there is a direct correlation between the total emission rates and the number of flights in general, this direct ratio did not show itself in the personal carbon footprint. Having the lowest carbon footprint, especially in the year with the most flights, is an issue related to the total number of passengers rather than the total number of flights. Because as the passenger capacity of the aircraft increases, the average personal carbon footprint decreases. This is a matter of how many passengers the planes carry rather than the number of planes taking off and landing. Considering the flights to the Cappadocia region, domestic flights come to the fore. This brings Turkiye's national transportation policy to the fore in this regard. From the perspective of Turkiye or the working axis, the Turkish aviation sector is growing rapidly. This situation will rapidly increase the share of the aviation sector in the national greenhouse gas rate. Therefore, Turkiye should go through a major change in transportation preferences. As long as it maintains its air and land transport policy, it will fail to tackle the climate crisis and green transformation. Therefore, by investing in rail transport, Turkiye should determine a cleaner transportation choice as a vision in the fight against the climate crisis. This is the reason why Cappadocia airport is discussed in this study. Although the Cappadocia region is located in the heart of Turkiye (4 h from Ankara, 7.5 h from Istanbul, 11 h from Izmir, and 7.5 h from Antalya), it has adequate transportation (the nearest train station is in Kayseri) network does not have. The fact that people do not have sufficient transportation networks causes them to prefer the airline. This increases both the total emissions and the personal carbon footprint. In other words, traveling to Cappadocia from one point in Turkiye as a family or as an individual, instead of choosing an airline, is much more innocent than choosing airline transportation. Considering that most flights are made from Istanbul (759 km), traveling by car will be more beneficial in terms of both overall emissions and personal carbon footprint. Additionally, the increase in the frequency of travel with the rise in the carbon footprint of people living in developed countries and the increase in the welfare level of people living in Turkiye is the same issue. Because the level of welfare and the increase in the transportation network bring the preference for air transportation to the fore, for this reason, railroad transportation in Turkiye should be built quickly, especially in tourism regions where human flow is intense. Like a spider web, tourism regions should be connected to central cities and each other. Thus, it is inevitable that transportation preferences to change and transportation (freight) preferences change. This will enable a cleaner transport system. Otherwise, the intense human flow will continue to increase in these regions, and thus, transport emissions will increase rapidly.

For many, travel is a way of seeing the world, while for others, it is a means of transportation for work. Whatever the reason for flying, it is important to remember how it contributes to the person's overall carbon footprint and what can be done to save money. We also need to be more realistic about our contributions to the climate crisis. Especially since we cannot change the air transportation system with a magic wand, we must evaluate our duties realistically. This is both in general and in Cappadocia;

a) Choosing an airline that uses newer, more energy-efficient aircraft will contribute more to reducing its carbon footprint.

b) Airplanes use much energy during take-off and landing, which causes more emissions. Therefore, non-stop flights will save more fuel per flight and cause less carbon footprint.

c) Flying in business or private seats cause four times more carbon emissions than other economy seats. Therefore, preferring frequent-seat aircraft or flying in economy class seats will cause less carbon footprint.

d) It is also beneficial for light travel in terms of the climate crisis and personal carbon footprint. This is because the weight of the aircraft significantly affects the use of fuel to stay in the air during take-off and flight. This will affect the emissions rates.

e) Considering the location of Cappadocia, driving alone is generally more environmentally friendly than flying, especially at distances below 1000 km.

In short, traveling by plane is unsustainable, and if we can and should make more environmentally friendly choices that help make the world cleaner, it is also true that it is time to act. Passenger numbers have been increasing exponentially recently, and more and more people are using planes due to low-cost airlines' offers that allow us to reach new destinations in small quantities.

Acknowledgement
I would like to thank the General Directorate of Civil Aviation and Aviation Expert Ahmet Berkan Korkmaz for providing the necessary data for this study.

DATA AVAILABILITY STATEMENT

The authors confirm that the data that supports the findings of this study are available within the article. Raw data that support the finding of this study are available from the corresponding author, upon reasonable request.

CONFLICT OF INTEREST

The authors declared no potential conflicts of interest with respect to the research, authorship, and/or publication of this article.

ETHICS

There are no ethical issues with the publication of this manuscript.

REFERENCES

[1] J. Overton, "The growth in greenhouse gas emissions from commercial aviation," https://www.eesi.org/files/IssueBrief_Climate_Impacts_Aviation_2019rev2022.pdf Accessed on Mar 13, 2023.

[2] ICCT. (2020). CO2 Emissions from Commercial Aviation: 2013, 2018, and 2019. https://theicct.org/wp-content/uploads/2021/06/CO2-commercial-aviation-oct2020.pdf

[3] ICAO. (2022a). Environmental Trends in Aviation to 2050. https://www.icao.int/environmental-protection/Documents/EnvironmentalReports/2022/ENVReport2022_Art7.pdf

[4] Consumer Energy Alliance, "Your carbon footprint when you travel: It's a flying shame," 2022. https://consumerenergyalliance.org/2022/05/your-carbon-footprint-when-you-travel-its-a-flying-shame/ Accessed on Mar 13, 2023.

[5] P. Dorta Antequera, J. Díaz Pacheco, A. López Díez, and C. Bethencourt Herrera, "Tourism, transport and climate change: The carbon footprint of international air traffic on islands," Sustainability, Vol. 13(4), Article 1795, 2021. [CrossRef]

[6] S. Gurcam, E. Konuralp, and S. Ekici, "Determining the effect of air transportation on air pollution in the most polluted city in Turkey," Aircraft Engineering and Aerospace Technology, Vol. 93(2), pp. 354–362, 2021. [CrossRef]

[7] A. Akyuz, K. Kumas, O. Inan, and A. Gungor, "Determination of carbon footprint from airplanes: Mugla province airports," Academic Platform Journal of Engineering and Science, Vol. 7(2), pp. 291–297, 2019. [CrossRef]

[8] A. Unal, Y. Hu, M. E. Chang, M. Talat Odman, and A. G. Russell, A. G. "Airport related emissions and impacts on air quality: Application to the Atlanta International Airport," Atmospheric Environment, Vol. 39(32), pp. 5787–5798, 2005. [CrossRef]

[9] C. Grobler, P. J. Wolfe, K. Dasadhikari, I. C. Dedoussi, F. Allroggen, R. L. Speth, S. D. Eastham, A. Agarwal, M. D. Staples, J. Sabnis, and S. R.H. Barrett, "Marginal climate and air quality costs of aviation emissions," Environmental Research Letters, Vol. 14(11), Article 114031, 2019. [CrossRef]

[10] Youmatter, "Carbon footprint definition," 2020. https://youmatter.world/en/definition/definitions-carbon-footprint/ Accessed on Mar 13, 2023.

[11] The Nature Conservancy. (2022). "What is a carbon footprint?" https://www.nature.org/en-us/get-involved/how-to-help/carbon-footprint-calculator/ Accessed on Mar 13, 2023.

[12] Iberdrola, "What is the carbon footprint and why will reducing it help to combat climate change?" https://www.iberdrola.com/sustainability/carbon-footprint Accessed on Mar 13, 2023.

[13] K. Mulvaney, "What is a carbon footprint—and how to measure yours," 2022. https://www.nationalgeographic.com/environment/article/what-is-a-carbon-footprint-how-to-measure-yours Accessed on Mar 13, 2023.

[14] S. Wang, and M. Ge, "Everything you need to know about the fastest-growing source of global emissions: transport," 2019. https://www.wri.org/insights/everything-you-need-know-about-fastest-growing-source-global-emissions-transport Accessed on Mar 13, 2023.

[15] H. Ritchie, "Which form of transport has the smallest carbon footprint?," 2020. https://ourworldindata.org/travel-carbon-footprint Accessed on Mar 13, 2023.

[16] European Environment Agency, "CO2 emissions from passenger transport," 2019. https://www.eea.europa.eu/media/infographics/co2-emissions-from-passenger-transport/view Accessed on Mar 13, 2023.

[17] Sustainable Travel International, "Carbon footprint of tourism," https://sustainabletravel.org/issues/carbon-footprint-tourism/ Accessed on Mar 13, 2023.

[18] R. S. Demirkol, "Cappadocia in the context of historical environmental protection," Journal of Art and Design, Vol. 1(1), pp. 43–63, 2021.

[19] G. Erol, "A periodical investigation on domestic and foreign tourists visited Cappadocia region," Third Sector Social Economic Review, Vol. 55(3), pp. 1412–1431, 2020.

[20] Cnnturk, "Kapadokya'da turist sayısında rekor kırıldı," 2020. https://www.cnnturk.com/turkiye/kapadokyada-turist-sayisinda-rekor-kirildi Accessed on Mar 13, 2023. [Turkish]

[21] DHMI, "Şehir tarihçesi," https://www.dhmi.gov.tr/Sayfalar/Havalimani/Kapadokya/SehirTarihcesi.aspx Accessed on Mar 13, 2023.

[22] Hepfly, "Nevşehir Kapadokya Havaalanı," https://www.hepfly.com/nevsehir-kapadokya-havaalani Accessed on Mar 13, 2023. [Turkish]

[23] F. Turkoglu, (2014). "Research on environmental effects within the scope of "green aırport project" in Nevsehir international airport (Master's thesis)," Available from Kırıkkale Universtesi database.

[24] Google. "Nevşehir Kapadokya Havalimanı (NAV)," https://www.google.com/maps/place/Nevşehir+Kapadokya+Havalimanı+(NAV)/@38.8594906,34.5424931,9.5z/data=!4m5!3m4!1s0x0:0xc24176cac8c928e9!8m2!3d38.7719688!4d34.5245521 Accessed on Mar 13, 2023. [Turkish]

[25] IPCC. 2019 Refinement to the 2006 IPCC guidelines for national greenhouse gas inventories. https://www.ipcc.ch/site/assets/uploads/2019/12/19R_V0_01_Overview.pdf Accessed on Mar 14, 2023.

[26] G. Civelekoglu, and Y. Bıyık, "Calculation of carbon footprint originated from highways in ısparta province," Bilge International Journal of Science and Technology Research, Vol. 4(2), pp. 78–87, 2020.

[27] Y. Sohret, "Multi-objective evaluation of aviation-induced GHG emissions: UK domestic flight pattern," Energy & Environment, Vol. 30(6), pp. 1049–1064, 2019. [CrossRef]

[28] ICAO, "ICAO carbon emissions calculator," https://www.icao.int/environmental-protection/Carbonoffset/Pages/default.aspx Accessed on Mar 13, 2023.

[29] Oncarbon, "Methodology: flight emissions," https://oncarbon.app/methodology/flight-emissions Accessed on Mar 13, 2023.

[30] IATA, "Air traffic movement outlook – Europe," 2021. https://www.iata.org/en/iata-repository/publications/economic-reports/air-traffic-movement-outlook---europe---august-2021/ Accessed on Mar 13, 2023.

[31] H. Ritchie, "Where in the world do people have the highest CO2 emissions from flying?," 2020. https://ourworldindata.org/carbon-footprint-flying Accessed on Mar 13, 2023.

Environ Res Tec, Vol. 6, Issue. 1, pp. 68–77, March 2023

Environmental Research and Technology
https://ert.yildiz.edu.tr - https://dergipark.org.tr/tr/pub/ert
DOI: https://doi.org/10.35208/ert.1232198

Research Article

Treatment of citrus juice process wastewater with UASB and biogas production

Sevgi GÜNEŞ DURAK*[,1], Seren ACARER[2], Güler TÜRKOĞLU DEMİRKOL[2]

[1]*Department of Enviromental Engineering, Nevşehir Hacı Bektaş Veli Universirty, Nevşehir, Türkiye*
[2]*Department of Environmental Engineering, İstanbul University-Cerrahpaşa, İstanbul, Türkiye*

ARTICLE INFO

Article history
Received: 10 January 2023
Revised: 23 March 2023
Accepted: 26 March 2023

Key words:
Biogas; Citrus juice process wastewater; COD; Methane; Organic loading rate; UASB reactor

ABSTRACT

A lab-scale up-flow anaerobic sludge blanket (UASB) reactor was used for biogas production from the citrus juice process wastewater (CPWW). The volume of the reactor was 11.5 L. During 200 days of the reactor, the organic loading rate (OLR) value changed from 1.8-21.9 kgCOD./m^3.d, upflow velocities (Vup) 0.1–5.2 m/h and hydraulic retention time (HRT) changed from 0.042 to 4.16 days. The reactor showed a stable performance at all organic loadings. Experimental chemical oxygen demand (COD) removal efficiencies were 71.5±21% and 83.3±16.3% for total COD (TCOD) and soluble COD (SCOD), respectively. The acetic acid concentration changed from 135 to 650 mg/L. The temperature was kept in the range of 35.1±1.4 °C, the pH in the range of 6.6±0.2, and the alkalinity was controlled daily and kept in the range of 411±273 $CaCO_3$ mg/L. After anaerobic reactions, 6283±3476 m^3/d biogas was produced and the methane concentration in the biogas was 65.5±11.5%. Depending on the methane production, the annual energy value potential that can be obtained from the existing UASB reactor is estimated as 48,768 kWh.

Cite this article as: Durak SG, Acarer S, Türkoğlu Demirkol G. Treatment of citrus juice process wastewater with UASB and biogas production. Environ Res Tec 2023;6:1:68–77.

INTRODUCTION

The fruit juice processing industry consists of 3 parts: the clear part where fruits such as apples and cherries are processed, the blurred part where fruits such as peaches and apricots are processed, and the citrus part where fruits such as oranges, lemons, tangerines, grapefruit, limes, bergamot, and lemons are processed [1, 2]. It is common for the citrus line to consume large quantities of water, and wastewater is produced in direct proportion to this consumption. In the citrus juice process facilities, water is used in many stages such as during the transportation of the products, washing, rinsing, pressing the fruits, washing the glass bottles, container washing, filtration, and grinding of the juice [3]. During all of these processes, wastewater is produced in large quantities. The continuous use of clean water at various stages of citrus processing is common. However, the total amount of wastewater is more than 10 times the volume of citrus juice produced [4–6].

***Corresponding author.**
*E-mail address: sgdurak@nevsehir.edu.tr

This paper has been presented at Sixth EurAsia Waste Management Symposium (EWMS 2022)/Istanbul, Turkiye / 24–26 October 2022.

In general, CPWW can be thought of as dilute solutions of citrus juice. Wastewater from citrus processing has a high water (80–90%) and organic matter (95%) content [7]. Numerous treatment processes have been applied for citrus processing waste and wastewater from the past to the present. These include ponding and chemical flocculation, spreading, spray irrigation, artificial aeration, yeast production, anaerobic ponding, trickle filtration and activated sludge, anaerobic digestion, and membrane filtration [8]. Due to its high organic matter content and the growth of the microbial mass, biological treatment has been applied in the treatment of CPWW in recent years [9]. Because treatment plants based on physical and chemical treatment are expensive and rarely reliable and efficient, it has limited use for CPWW. For example, the removal of CPWW by evaporation creates a high energy requirement. A disadvantage is the removal of dissolved and total suspended solids (TSS) by flocculation and the high cost of flocculation materials as well as low removal efficiency. The CPWW's contents make biological treatment suitable [2]. Anaerobic treatment is preferred over biological treatment methods. Facultative and anaerobic microorganisms convert organic materials into carbon dioxide (CO_2) and methane (CH_4) in the absence of oxygen [5]. Also, thanks to anaerobic digestion, there is less sludge production, more energy gain, and, above all, less cost [10]. Biogas produced after anaerobic treatment can be used for steam production in boilers and meets the energy demands of the unit [11].

Factors such as temperature, OLR, alkalinity, pH and HRT affect the performance of the bacteria and the yield of the biogas produced [5]. In particular, OLR and HRT are important factors in the set-up phase, as they allow the decision to be made on the amount of feed to the reactor. These two factors determine the final amount of hydrolysis and methanogenesis in the UASB reactor. OLR is an important parameter that must be kept under control for maximum biogas production and high COD removal [12]. The occurrence of anaerobic reactions at lower HRT is an advantage over other digestion methods [13]. Along with all these advantages, the anaerobic digestion of citrus residues makes it possible to reduce wastewater disposal problems. In addition, since it has a high phosphorus content as a final product, it can be applied directly to the soil as a fertilizer or organic substance. The high rate of methane production compared to other industries is the reason why anaerobic methods are preferred for CPWW [2].

Some anaerobic treatment methods applied for CPWW are two-stage anaerobic sequencing batch reactors [8, 14–16], upflow anaerobic sludge bed reactors [17–19], lab-scale completely stirred tank reactor [20], thermophilic downflow stationary fixed film anaerobic reactor [21], anaerobic hybrid reactor [22], anaerobic sequencing batch reactor [23], lab-scale horizontal flow anaerobic immobilized biomass reactor [24], two-stage anaerobic digestion [25] and pilot-scale upflow anaerobic sludge blanket reactor [26] methods.

Table 1. Citrus juice wastewater characterization

Parameter	Wastewater
SCOD (mg/L)	7.760±0.02
TCOD (mg/L)	12.926±0.09
TKN (mg/L)	29.3±1.3
TP (mg/L)	9.7±0.01
pH	4.64±0.3
VFA (as acetic acid) (mg/L)	27.5±1.7
TSS (mg/L)	1.442±0.05
Conductivity (mS/cm)	1.35±0.02

This study aimed to present the results obtained by anaerobic digestion of citrus process wastewater to achieve high biogas production and COD removal. Moreover, the amount of biogas produced was used to estimate the electrical energy potential.

MATERIALS AND METHODS

Wastewater Characteristics

In this study, treatment efficiency and biogas production performance were investigated by using UASB reactor for CPWW treatment. Wastewater was supplied from a fruit juice production facility with a total fruit processing capacity of 125,000 tons. There is an annual inflow of 75,000 tons of citrus fruit to the facility, and the amount of freshwater entering the facility for production is 720,908 m^3 per year on average. The amount of wastewater coming out of the facility is 127 m^3 per day on average.

SCOD, TCOD and volatile fatty acids (VFAs) (as acetate) concentrations, total Kjeldahl nitrogen (TKN), total phosphorous (TP) and TSS concentrations, pH and electrical conductivity values of CPWW are given in Table 1.

The Experimental Setup

The lab-scale UASB reactor in the study was made of plexiglass, with a diameter of 0.12 m, a length of 1.5 m, and an effective volume of 11.5 L (Fig. 1). There was a gas/liquid/solid separator at the top of the reactor. The gas was collected at the upper point as separated and the gas flow was measured with a wet gas meter. Liquid products, on the other hand, were taken to the collection container by weirs from the upper part (Fig. 1-Part 5). The temperature in the reactor was kept constant in the range of 35.1±1.4 °C.

Operating Conditions

Feed solutions were added to the reactor daily. 3 L of 11.5 L was inoculum and the remaining volume was as citrus juice waste. Alkalinity, SCOD, TCOD, OLR, biogas, methane and TSS were measured once in two days; BOD_5, TKN, TP, pH, VFAs, electrical conductivity and temperature parameters

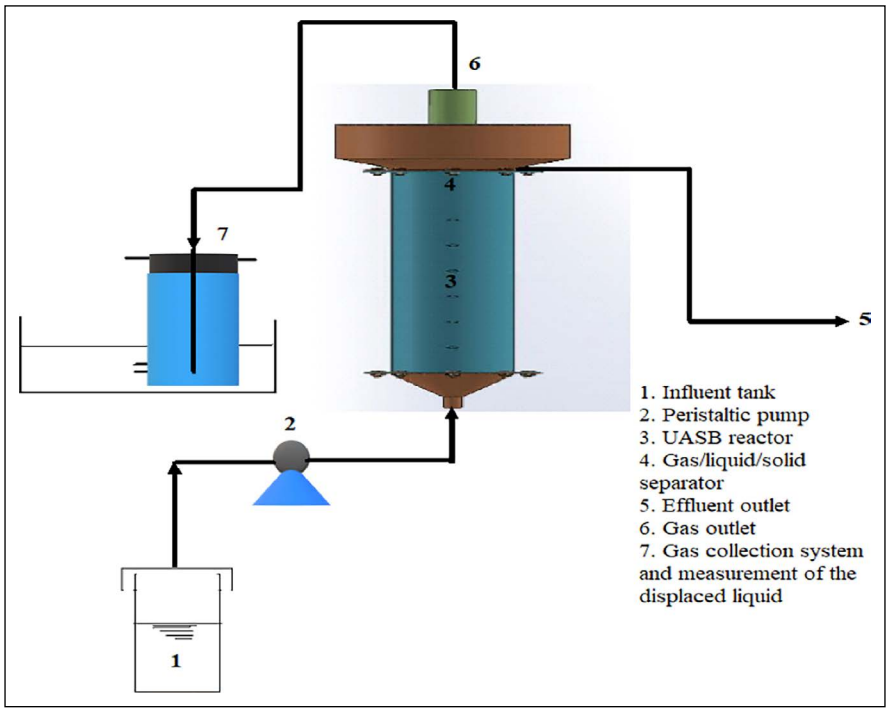

Figure 1. Schematic view of the lab-scale UASB reactor.

were measured as required. The analyzes were carried out to determine the SCOD and TCOD removal efficiency, the amount of biogas produced, and the proportional distribution of the gases in the biogas. The initial HRT value was 0.85 days and the average value of the initial total COD was 7356 mg/L. The OLR varied between 1.8 and 21.9 kgCOD/m^3. d. The alkalinity value at the inlet is 720 $CaCO_3$ mg/L. To keep the COD/N/P ratio around 300/5/1, nutrient was added to the wastewater with ammonium chloride (NH_4Cl) and disodium phosphate (Na_2HPO_4). To provide sufficient alkalinity in the reactor and to buffer CO_2 and volatile acids, 3.3 g/L $NaHCO_3$ was added. According to the alkalinity measurement results, this amount was increased when necessary. A variable-speed peristaltic pump was used to pump feed from a vessel to the reactor every day for 60 days. After the adaptation was achieved, a 200-day operating period was started.

COD analyzes were performed using COD Reactor CR25, DragonLab MX-F, and Spectroquant Colorimeter Picco COD/CSB Merck instruments by EPA 410.4 and ISO 15705 standards [27, 28]. HQ40D Portable pH/Dissolved Oxygen Meter Dual-Channel Multimeter was used for pH and electrical conductivity measurements. TKN, TP, BOD_5 and TSS analyzes were performed using Standard Methods [29].

VFAs parameter was measured by Anderson and Yang [30] method and alkalinity measurements were measured with standard methods 2320 B [31]. Gas measurements were made with the liquid displacement method, 2 days a week during the 200-day operating period. Methane gas was obtained by separating carbon dioxide from biogas by passing it through a liquid containing 3% NaOH, and the amount of methane gas was measured using Draeger X-am® 2500.

Possible Energy Values

The daily produced energy (DPE) that can be obtained from biogas production is calculated by Eq. 1 [32].

$$DPE = C_V \times \%CH_4 \times PB \quad (1)$$

where DPE is the energy produced daily (kJ/d); CV, the theoretical calorific value of methane (35.75 kJ/L) (at 1 atm. pressure and 273 K); The value of methane produced in $\%CH_4$ biogas, PB, is expressed as the measured amount of biogas (L/d) (1 atm. pressure and 273 K temperature).

Eq. 2 is used to calculate the daily energy used (DUE) to produce biogas [32]:

$$DUE = C_P \times \Delta T \times Q \quad (2)$$

where DUE is the energy required for the combustion of biogas (kJ/d); C_p is the specific heat capacity of the wastewater (3.8 kJ/L °C); ΔT is the temperature rise (°C) affecting the reactor due to heating and Q is the average flow rate (L/d) of the UASB reactor.

Heating efficiency is calculated by Eq. 3 [32]:

$$Heating\ Efficiency = \frac{DUE}{DPE} \times 100 \quad (3)$$

To calculate the energy outputs (NEY, kJ/d) in the daily produced energy content, the daily used energy is subtracted from the daily produced energy (Eq.4) [32].

$$NEY = DPE - DUE \quad (4)$$

Table 2. Wastewater characteristics of UASB reactor

Parameter	Unit	Influent	Effluent
SCOD	mg/L	5.466±1.542	610±437
TCOD	mg/L	7.356±1.756	1500±875
BOD5	mg/L	2462.5±374	662±324
TP	mg/L	13.8±0.9	12.9±8.3
TKN	mg/L	51.0±27.0	12±9.1
Temperature	°C	35.1±1.4	33.3±0.7
pH	–	6.6±0.2	6.5±0.5

Table 3. The operation conditions of the UASB reactor

Parameter	Value
OLR (kgCOD/m³.d)	8.63±5.0
HRT (d)	1.15±0.91
Alkalinity as $CaCO_3$ (mg/L)	411±273
VFA as acetic acid (mg/L)	319±160
Biogas production (m³/d)	6.283±3.476
Flow (m³/d)	1.386±868

Eq. 5 is used to determine the energy potential of CPWW [32].

$$EP_{CPWW} = \frac{PB \times \%\, CH_4}{OLR^{S}_{rem} \times V_R} \times SCOD \times SCOD - RE \times C_V \quad (5)$$

EP_{CPWW}, energy potential (kJ/m³$_{CPWW}$); OLR^{s}_{rem} removed dissolved organic loading rate (kg-SCOD /m³.d), V_R, reactor volume (m³); SCOD is SCOD entering the reactor (g-SCOD /L_{CPWW}) and SCOD-RE is SCOD removal efficiency (%). Descriptions of other parameters are given in the explanation of Eq. 1.

RESULTS AND DISCUSSION

In the study, using the lab-scale UASB reactor, the treatment of CPWW for 200 days and the biogas content formed by the reactor were monitored. At the end of 60 days, the reactor reached to steady-state, and granular sludge formation started. The characteristics of the wastewater and the operation conditions of the UASB reactor are given in Table 2 and Table 3.

SCOD and TCOD Removal in UASB Reactor

The OLR parameter was initially kept at 7 kgCOD/m³.d and an attempt was made to operate without reducing it below 4.2 kgCOD/m³.d (approximately 60%). The OLR increased to OLR of 10 kgCOD/m³.d approximately in two weeks. According to the results obtained, the effluent TCOD concentrations varied from 41 mg/L to 4,590 mg/L during the monitoring period. The TCOD removal efficiency changed from 51% to 93%, respectively (Fig. 2). SCOD removal concentrations ranged from 20 mg/L to 1,853 mg/L, and SCOD removal efficiencies ranged between 67% and 99.6% (Fig. 3). It is also seen from Figure 2 and 3 that as the influent concentration increases, the removal efficiency increases [33].

Effect of OLR on UASB Reactor

OLR is important for microorganisms to perform their vital activities. Because it is the amount of organic matter required for the growth and reproduction of microorganisms in a system [34]. The treatment efficiency increased with the increase of OLR in many wastewaters. However, in case of an excessive increase, problems such as excessive foaming at the gas-liquid interface in the sludge blanket, its flotation and gas-liquid-solid separator, and accumulation of undigested components arise [35]. In steady-state conditions, the OLR reached 21.9 kg COD/m³.d, and the TCOD removal efficiency was 54% and the SCOD removal efficiency exceeded 89% [10, 36]. Hajiabadi et al. [37] (2009) states that high OLR provides high TCOD removal. However, in the current study, as the OLR increased, there was a decrease in the removal efficiency of TCOD (Fig. 4). While the TCOD removal efficiency was 90% when the OLR was 1.8 kg/m³, there was a general decrease in the TCOD removal efficiency as the OLR increased.

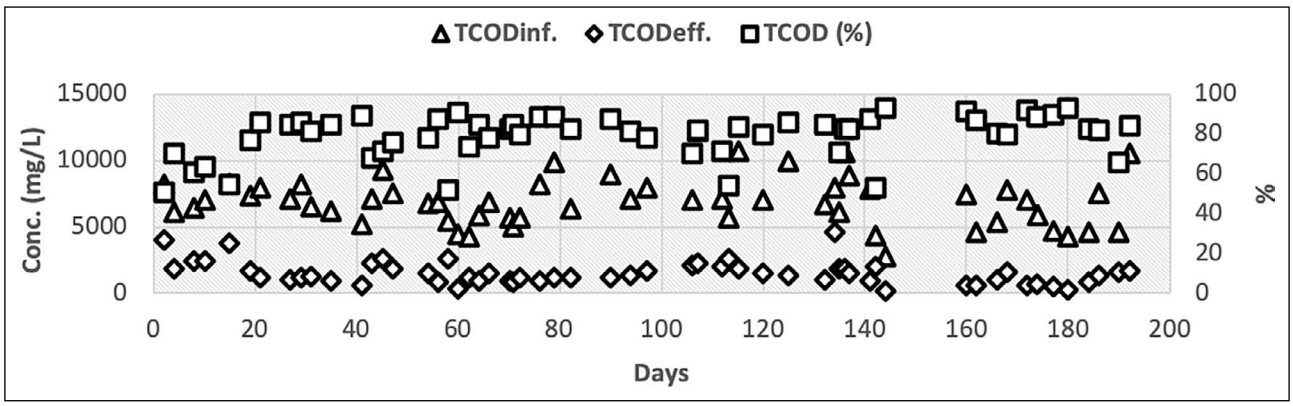

Figure 2. TCOD influent and effluent concentrations, and removal efficiencies.

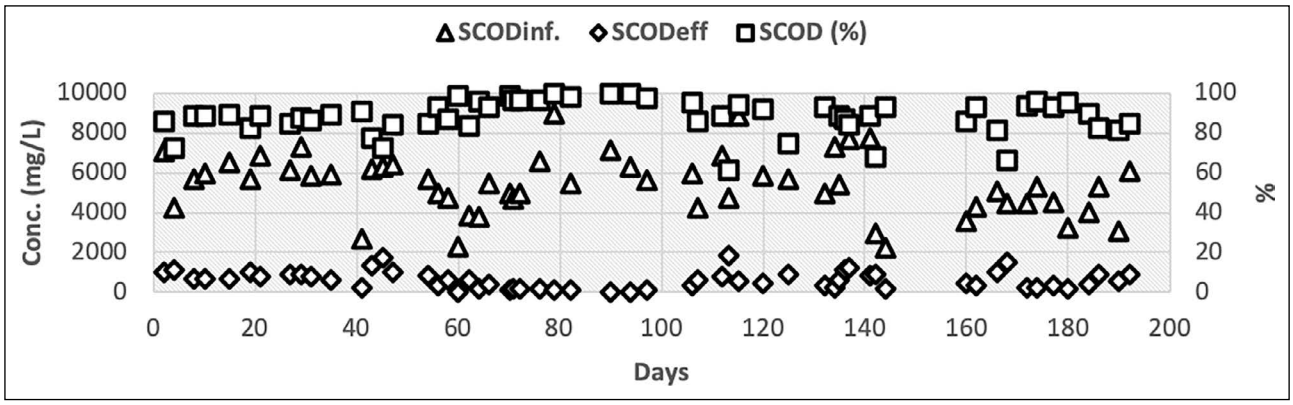

Figure 3. SCOD influent and effluent concentrations, and removal efficiencies.

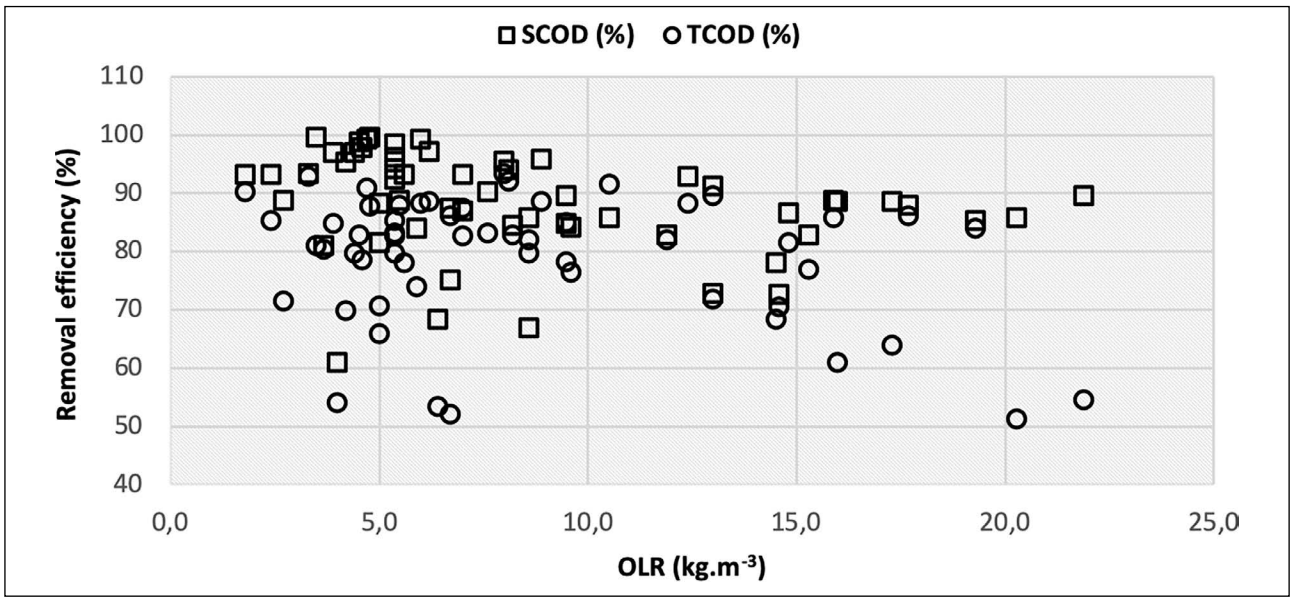

Figure 4. Variation of SCOD and TCOD removal efficiencies according to OLR.

The Effect of Alkalinity on the UASB Reactor

Low pH slows down anaerobic degradation. The VFA concentration is a function of pH. In acidic conditions, the amount of VFAs increases [38]. When Figure 5 is examined, the amount of VFA (acetic acid) is low in conditions where alkalinity is high, and the amount of VFA is high in conditions where it is low [39]. In the study, the amount of propionic acid and butyric acid was ignored as they were in trace amounts.

The Impact of Upflow Velocity on the UASB Reactor

HRT can cause compaction and coalescence of solids in the sludge blanket as a result of its relationship to the V_{up} and the solid's contact time in the reactor [35, 40]. V_{up} is the main factor affecting reactor efficiency. It affects sludge retention and is the basis of the settling characteristic. Increasing the V_{up} increases the collision rate between suspended particles and sludge, and increases the removal efficiency [35, 41–43].

Table 4. Approximate energy values that can be obtained from the UASB reactor

Parameter	UASB reactor
DPE (kWh)	71,715
DUE (kWh)	2,633.4
Heating efficiency (%)	3.67
NEY (kWh)	69,081.6
EP_{CPWW} (kJ/m^3_{CJIW})	3,859

When sufficient contact time between the sludge and wastewater is provided, the biomass is separated from the gas [44]. With the increase in V_{up}, HRT and removal efficiency also decrease [35, 45]. HRT, which was determined as 69.3 hours at 0.1 m/h V_{up} speed, decreased to 9.7 hours when V_{up} reached 1.9 m/h. In addition, as shown in Figure 6, TCOD removal efficiency decreased as HRT decreased [44, 46, 47].

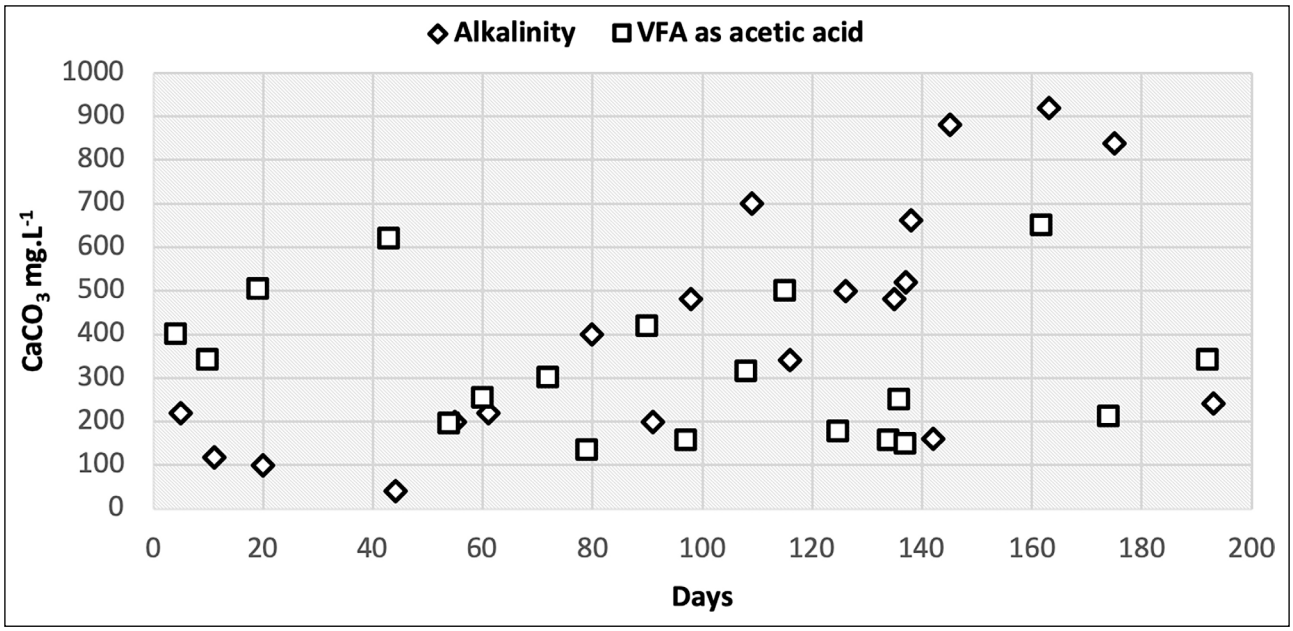

Figure 5. Variation of Alkalinity and VFAs concentration during operation.

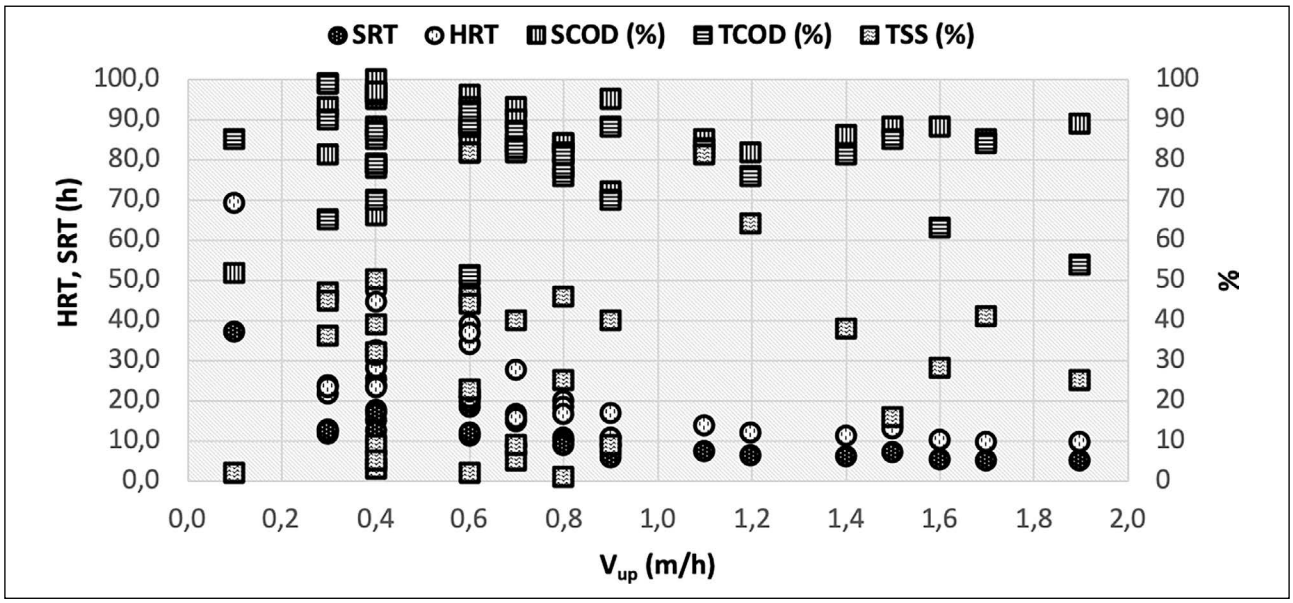

Figure 6. The effect of upflow velocity and variation of HRT and SRT on SCOD, TCOD, and TSS removal efficiencies.

Biogas Production and Composition in the UASB Reactor

Produced biogas values are given in Figure 6 and Figure 7. The biogas production amount is 6283±3476 m^3/d on average. The biogas content consists of methane gas at a high rate (Fig. 7). On average, biogas contains 62% CH_4, 32% CO_2, and traces of H_2S. The studies show similarities with the available data. Accordingly, it is possible to obtain from 54% to 77% methane [47–50] and 30–50% CO_2 [51] from biogas and convert methane into energy.

While there was more biogas production at the beginning, as time passed, a decrease in biogas production occurred. The formation of granular sludge is essential for efficient biogas production. The diameter of the granules is small at the beginning but increase over time. The decrease in biogas production after day 143 can be explained by the increase in granule size. However, the amount of CH_4 in the biogas content is also higher in the initial phase and decreases similar to the decrease in biogas production. When Figure 5 and Figure 7 are examined, it is seen that there is a similar change between VFA amount and biogas production [39].

The amount of biogas production varied between 6283±3476 m^3/d and there was a directly proportional in-

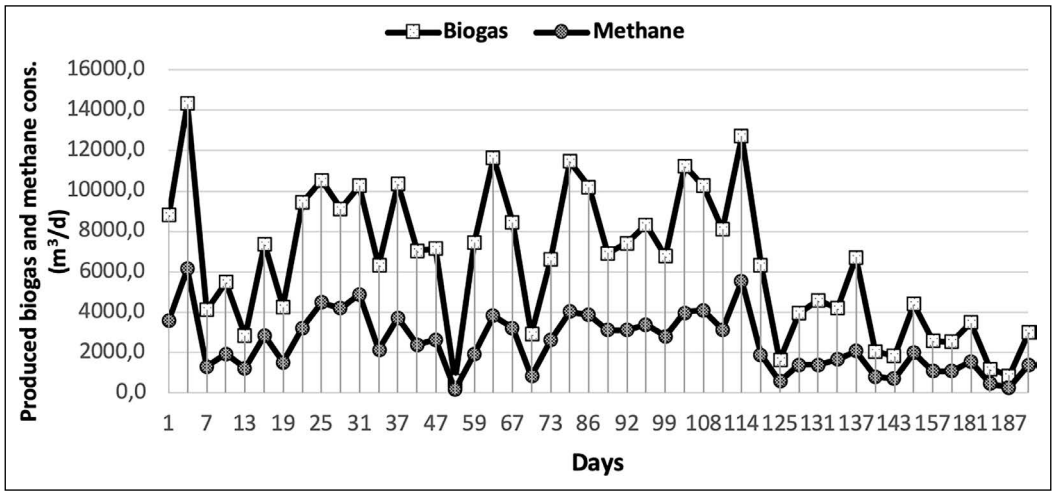

Figure 7. Biogas, and the amount of methane production in biogas' content.

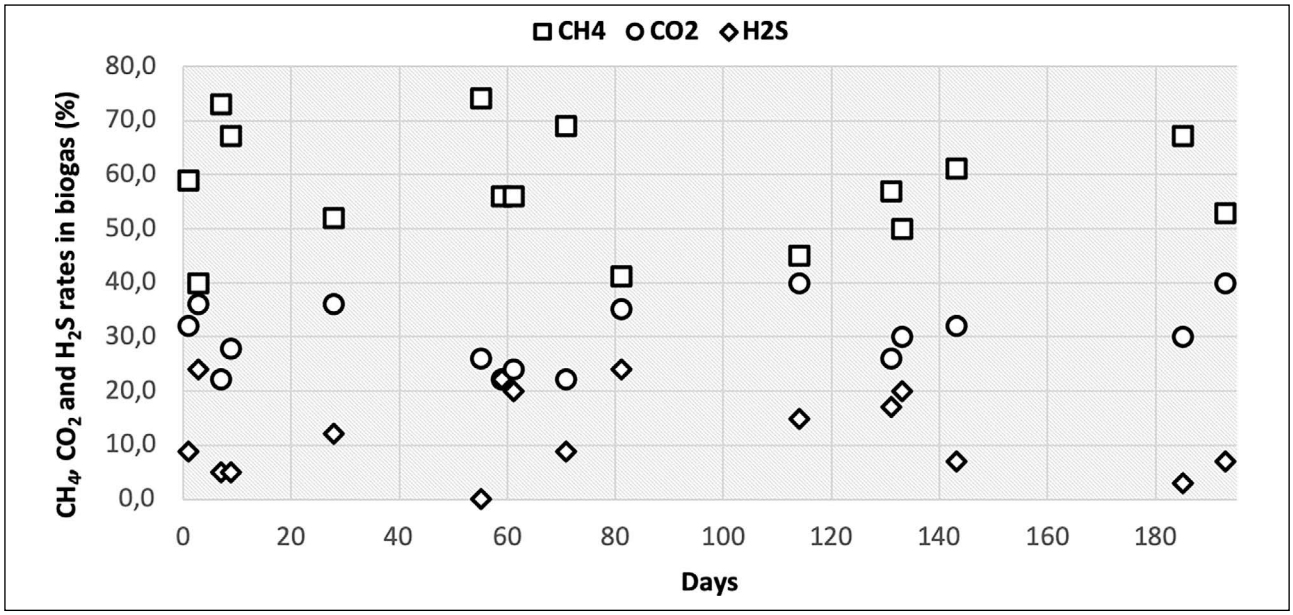

Figure 8. The amount of biogas formation and the percentage of gases.

crease in biogas production as OLR increased (Fig. 9). The linear regression showed a high R^2 coefficient (0.8405).

When calculations are made with the equations given in the possible energy values section, DPE, DUE, Heating Efficiency, NEY, and EPCPWW values are given in Table 4.

The daily energy produced under operating conditions is more than the average daily energy use. The lower the DUE, the higher the heat losses. NEY represents 96.3% of the DPE from the UASB reactor (71,715 kWh). This result shows that the reactor is a useful system. EPCPWW has been calculated considering the operating parameters of the reactor. The increase in temperature increased the EP, accordingly biogas production and anaerobic biomass activity increased. The amount of wastewater released from citrus juice production is approximately 127 m^3 per day (3,800 m^3 per month). The efficiency of a potential power source produces 3,859 kJ/m^3 CPWW (3.85 MJ/m^3 CPWW) can reach 14,630 MJ or 4,064 kWh per month. The annual amount may correspond to 48,768 kWh. In addition, the heat generated while the biogas is converted into electricity can be directed to the reactor, as the efficiency of the reactor will increase if the temperature is high. This increases both the biogas production and the NEY value.

CONCLUSION

With the increase of OLR, biogas production also increased. It is possible to say that the interaction of the particles deteriorates after a certain speed for the V_{up}. HRT and SRT decreased significantly with increasing V_{up} rates.

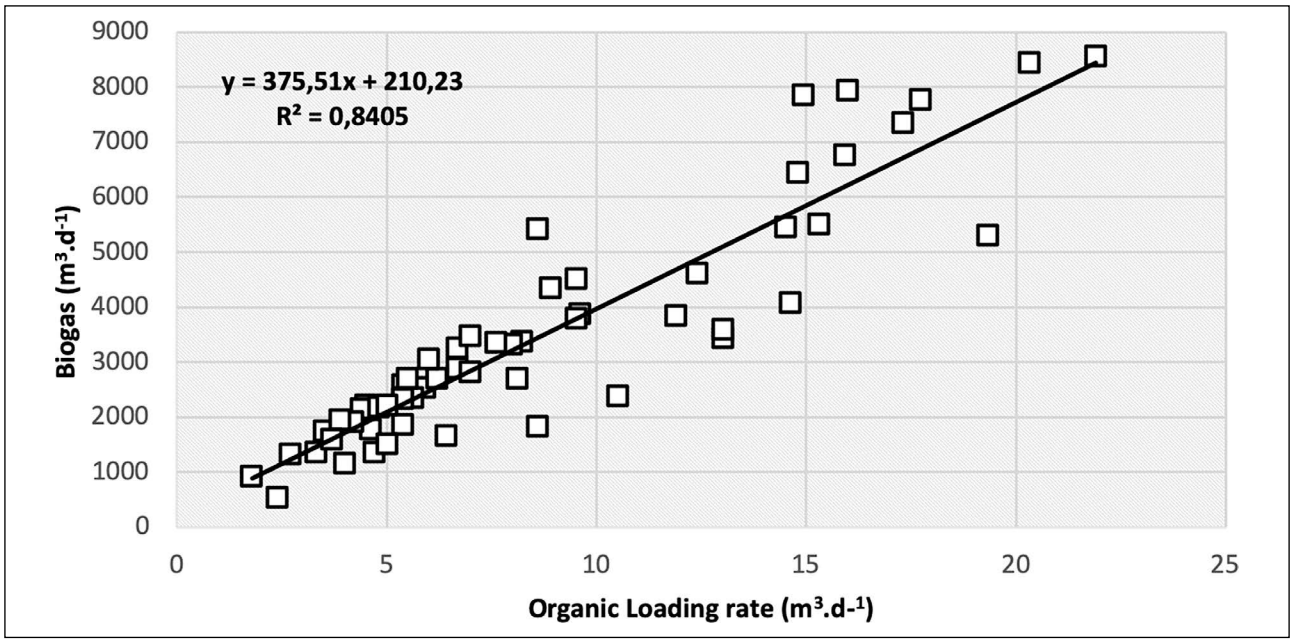

Figure 9. Change of biogas production amount according to organic loading rate.

According to the analysis results, it is possible to say that there is a negative correlation between VFA as acetic acid and alkalinity. When the energy values are examined, it is possible to obtain 48,768 kWh of energy annually from the system. This energy can be used to increase the temperature of the reactor and accordingly increase biogas production. Due to the high organic matter content of citrus juice wastewater, it appears that using UASB reactors is an appropriate option because of their ability to generate energy. In some citrus juice units, increasing the wastewater fed to the UASB reactor and therefore its volumetric capacity can satisfy the required energy needs by generating electricity. Further, considering that the average household consumption of electricity is 238 kWh per month, the energy obtained monthly can serve approximately 17 households. The removal efficiencies of the SCOD and TCOD parameters indicate that the treated wastewater from the UASB reactor can be reused in appropriate sections of the appropriate industries (cooling towers, ash irrigation, flue gas scrubbing, etc.).

DATA AVAILABILITY STATEMENT

The authors confirm that the data that supports the findings of this study are available within the article. Raw data that support the finding of this study are available from the corresponding author, upon reasonable request.

CONFLICT OF INTEREST

The authors declared no potential conflicts of interest with respect to the research, authorship, and/or publication of this article.

ETHICS

There are no ethical issues with the publication of this manuscript.

REFERENCES

[1] E. Akdağ, "Turkey Fruit Juice etc. Products Industry Report", İstanbul, 2011.

[2] D. A. Zema, P. S. Calabro, A. Folino, V. Tamburino, G. Zappia, and S. M. Zimbone, "Wastewater Management in Citrus Processing Industries: An Overview of Advantages and Limits", *Water 2019*, Vol. 11 (12), pp. 2481–2481, 2019. [CrossRef]

[3] S. Güneş-Durak, T. Ormancı-Acar, and N. Tüfekci, "Effect of PVP content and polymer concentration on polyetherimide (PEI) and polyacrylonitrile (PAN) based ultrafiltration membrane fabrication and characterization", *Water Science and Technology*, Vol. 2017 (2), pp. 329–339, 2018. [CrossRef]

[4] H. Elif, G. Akbay, C. Akarsu, and H. Kumbur, "Treatment of fruit juice concentrate wastewater by electrocoagulation: Optimization of COD removal", *International Advanced Researches and Engineering Journal*, Vol. 2 (01), pp. 53–057, 2018.

[5] M. Garg, "Treatment and Recycling of Wastewater from Beverages/The Soft Drink Bottling Industry", Springer, Singapore, pp. 333–361, 2019. [CrossRef]

[6] K. Özdemir, "Meyvesuyu fabrikası atıksularının elektrokimyasal olarak arıtılması, Ulusal Tez ve Araştırma Merkezi - Akademik Tezler ve Araştırmalar", 2005.

[7] J. Ángel Siles López, Q. Li, and I. P. Thompson, "Biorefinery of waste orange peel", Vol. 30 (1), pp. 63–69, 2010. [CrossRef]

[8] R. J. TeKippe, "Treatment and Disposal of Citrus Fruit Processing Wastes", *Journal (Water Pollution Control Federation)*, Vol. 44 (10), pp. 2001–2012, 1972.

[9] L. K. Wang, N. K. Shammas, and Y.-T. Hung, "Advanced Biological Treatment Processes", *Advanced Biological Treatment Processes*, 2009. [CrossRef]

[10] M. A. Musa, S. Idrus, C. M. Hasfalina, and N. N. N. Daud, "Effect of organic loading rate on anaerobic digestion performance of mesophilic (UASB) reactor using cattle slaughterhouse wastewater as substrate", *International Journal of Environmental Research and Public Health*, 2018. [CrossRef]

[11] T. Nandy, S. Shastry, and S. N. Kaul, "Wastewater management in a cane molasses distillery involving bioresource recovery", *Journal of Environmental Management*, Vol. 65 (1), pp. 25–38, 2002. [CrossRef]

[12] M. A. Latif, R. Ghufran, Z. A. Wahid, and A. Ahmad, "Integrated application of upflow anaerobic sludge blanket reactor for the treatment of wastewaters", *Water Research*, Vol. 45 (16), pp. 4683–4699, 2011. [CrossRef]

[13] M. Mainardis, M. Buttazzoni, and D. Goi, "Up-Flow Anaerobic Sludge Blanket (UASB) Technology for Energy Recovery: A Review on State-of-the-Art and Recent Technological Advances", *Bioengineering*, Vol. 7 (2), pp. 43–43, 2020. [CrossRef]

[14] M. H. Dougherty, "Activated Sludge Treatment of Citrus Waste", *Journal (Water Pollution Control Federation)*, Vol. 36 (1), pp. 72–79, 1964.

[15] M. H. Dougherty, R. W. Wolford, and R. R. Mcnary, "Citrus Waste Water Treatment of Activated Sludge", Vol. 27 (7), pp. 821–826, 1955.

[16] R. R. McNary, R. W. Wolford, and M. H. Dougherty, "Pilot Plant Treatment of Citrus Waste Water by Activated Sludge", *Sewage and Industrial Wastes*, Vol. 28 (7), pp. 894–905, 1956.

[17] M. Elnekave, S. Ö. Celik, M. Tatlier, and N. Tufekci, "Artificial Neural Network Predictions of Up-Flow Anaerobic Sludge Blanket (UASB) Reactor Performance in the Treatment of Citrus Juice Wastewater", *Pol. J. Environ. Stud.*, Vol. 21 (1), pp. 49–56, 2012.

[18] M. P. Jiménez-Castro, L. S. Buller, A. Zoffreo, M. T. Timko, and T. Forster-Carneiro, "Two-stage anaerobic digestion of orange peel without pre-treatment: Experimental evaluation and application to São Paulo state", *Journal of Environmental Chemical Engineering*, Vol. 8 (4), pp. 104035–104035, 2020. [CrossRef]

[19] Lukitawesa, R. Wikandari, R. Millati, M. J. Taherzadeh, and C. Niklasson, "Effect of effluent recirculation on biogas production using two-stage anaerobic digestion of citrus waste", Vol. 23 (12), pp. 3380–3380, 2018. [CrossRef]

[20] M. de los Á. M. Santos, J. Á. S. López, A. F. C. Pérez, and A. M. Martín, "Modelling the anaerobic digestion of wastewater derived from the pressing of orange peel produced in orange juice manufacturing", *Bioresource Technology*, Vol. 101 (11), pp. 3909–3916, 2010. [CrossRef]

[21] A. Koppar and P. Pullammanappallil, "Anaerobic digestion of peel waste and wastewater for on site energy generation in a citrus processing facility", *Energy*, Vol. 60, pp. 62–68, 2013. [CrossRef]

[22] E. S. Rosas-Mendoza, J. M. Méndez-Contreras, A. Martínez-Sibaja, N. A. Vallejo-Cantú, and A. Alvarado-Lassman, "Anaerobic digestion of citrus industry effluents using an Anaerobic Hybrid Reactor", *Clean Technologies and Environmental Policy*, Vol. 20 (7), pp. 1387–1397, 2018. [CrossRef]

[23] L. D. M. Torquato, R. Pachiega, M. S. Crespi, M. G. Nespeca, J. E. de Oliveira, and S. I. Maintinguer, "Potential of biohydrogen production from effluents of citrus processing industry using anaerobic bacteria from sewage sludge", *Waste Management*, Vol. 59, pp. 181–193, 2017. [CrossRef]

[24] B. C. G. Rodrigues, B. S. de Mello, B. F. da Silva, E. Pozzi, P. C. F. de Lima Gomes, and A. Sarti, "Limonene removal using a horizontal-flow anaerobic immobilized biomass bioreactor", *Journal of Water Process Engineering*, Vol. 43, pp. 102225–102225, 2021. [CrossRef]

[25] B. Eryildiz, Lukitawesa, and M. J. Taherzadeh, "Effect of pH, substrate loading, oxygen, and methanogens inhibitors on volatile fatty acid (VFA) production from citrus waste by anaerobic digestion", *Bioresource Technology*, Vol. 302, pp. 122800–122800, 2020. [CrossRef]

[26] W. D. Machado, M. N. Russo, C. F. Molina, E. A. Quaia, and L. A. N. Recio, "Granulation of dispersed anaerobic sludges fed with lemon industry effluent", *Rev. Ind. y Agríc. de Tucumán Tomo*, Vol. 96 (1), pp. 55–63, 2019.

[27] ISO 15705:2002, "Water quality — Determination of the chemical oxygen demand index (ST-COD) — Small-scale sealed-tube method", 2002.

[28] USEPA, "Method 410.4, Revision 2.0: The Determination of Chemical Oxygen Demand by Semi-Automated Colorimetry", 1993.

[29] APHA, AWWA, and WEF, "Standard method 6232B. Trihalomethanes and chlorinated organic solvents: liquidliquid extraction gas chromatographic method", *Standard Methods for the Examination of Water and Wastewater*, (6000), pp. 40, 46–40, 46, 1998.

[30] G. K. Anderson and G. Yang, "Determination of Bicarbonate and Total Volatile Acid Concentration in Anaerobic Digesters Using a Simple Titration on JSTOR", *Water Environment Research*, Vol. 64 (1), pp. 53–59, 1992. [CrossRef]

[31] A. D. Eaton, L. S. Clesceri, and A. E. Greenberg, Standard methods for the examination of water and wastewater. 19th ed. Supplement. Washington, D.C.: American Public Health Association; American Water Works Association; *Water Environment Federation*, 1995.

[32] S. Alcaraz-Ibarra, M. A. Mier-Quiroga, M. Esparza-Soto, M. Lucero-Chávez, and C. Fall, "Treatment of chocolate-processing industry wastewater in a low-temperature pilot-scale UASB: Reactor performance and in-situ biogas use for bioenergy recovery", *Biomass and Bioenergy*, Vol. 142, pp. 105786–105786, 2020. [CrossRef]

[33] K. Wang, "Integrated anaerobic and aerobic treatment of sewage", *Environmental Technology*, WIMEK 1994.

[34] A. Torkian, A. Eqbali, and S. J. Hashemian, "The effect of organic loading rate on the performance of UASB reactor treating slaughterhouse effluent", *Resources, Conservation and Recycling*, Vol. 40 (1), pp. 1–11, 2003. [CrossRef]

[35] N. Mahmoud, G. Zeeman, H. Gijzen, and G. Lettinga, "Solids removal in upflow anaerobic reactors, a review", *Bioresource Technology*, Vol. 90 (1), pp. 1–9, 2003. [CrossRef]

[36] V. Del Nery, I. R. De Nardi, M. H. R. Z. Damianovic, E. Pozzi, A. K. B. Amorim, and M. Zaiat, "Long-term operating performance of a poultry slaughterhouse wastewater treatment plant", *Resources, Conservation and Recycling*, Vol. 50 (1), pp. 102–114, 2007. [CrossRef]

[37] H. Hajiabadi, M. R. A. Moghaddam, and S. H. Hashemi, "Effect of sludge retention time on treating high load synthetic wastewater using aerobic sequencing batch reactors", *Iranian Journal of Environmental Health Science & Engineering*, Vol. 6 (4), pp. 217–222, 2009. [CrossRef]

[38] R. Gökçe, Y. Çinçin, and O. N. Ağdağ, "Besi çiftliği atıksularının anaerobik/aerobik yöntemlerle arıtılabilirliği", Vol. 25 (8), pp. 922–928, 2019. [CrossRef]

[39] R. Borja and C. J. Banks, "Response of an anaerobic fluidized bed reactor treating ice-cream wastewater to organic, hydraulic, temperature and pH shocks", *Journal of Biotechnology*, Vol. 39 (3), pp. 251–259, 1995. [CrossRef]

[40] G. Zeeman and G. Lettinga, "The role of anaerobic digestion of domestic sewage in closing the water and nutrient cycle at community level", *Water Science and Technology*, Vol. 39 (5), pp. 187–194, 1999. [CrossRef]

[41] R. F. Gonçalves, "Primary fermentation of soluble and particulate organic matter for wastewater treatment PDF", *Water Science and Technology*, Vol. 30 (6), pp. 53–62, 1996. [CrossRef]

[42] L. Metcalf, H. P. Eddy, and G. Tchobanoglous, *Wastewater energy: treatment and reuse*. McGraw-Hill, 2004.

[43] W. M. Wiegant, "Experiences and potential of anaerobic wastewater treatment in tropical regions", *Water Science and Technology*, Vol. 44 (8), pp. 107–113, 2001. [CrossRef]

[44] H. Rizvi, N. Ahmad, F. Abbas, I. H. Bukhari, A. Yasar, S. Ali, T. Yasmeen, and M. Riaz, "Start-up of UASB reactors treating municipal wastewater and effect of temperature/sludge age and hydraulic retention time (HRT) on its performance", *Arabian Journal of Chemistry*, Vol. 8 (6), pp. 780–786, 2015. [CrossRef]

[45] M. R. Peña, D. D. Mara, and G. P. Avella, "Dispersion and treatment performance analysis of an UASB reactor under different hydraulic loading rates", *Water Research*, Vol. 40 (3), pp. 445–452, 2006. [CrossRef]

[46] H. H. P. Fang and H. Q. Yu, "Effect of HRT on Mesophilic Acidogenesis of Dairy Wastewater", *Journal of Environmental Engineering*, Vol. 126 (12), pp. 1145–1148, 2000. [CrossRef]

[47] M. Hernández and M. Rodríguez, "Hydrogen production by anaerobic digestion of pig manure: Effect of operating conditions", *Renewable Energy*, Vol. 53, pp. 187–192, 2013. [CrossRef]

[48] W. Qiao, X. Yan, J. Ye, Y. Sun, W. Wang, and Z. Zhang, "Evaluation of biogas production from different biomass wastes with/without hydrothermal pretreatment", *Renewable Energy*, Vol. 36 (12), pp. 3313–3318, 2011. [CrossRef]

[49] S. Zerrouki, R. Rihani, F. Bentahar, and K. Belkacemi, "Anaerobic digestion of wastewater from the fruit juice industry: experiments and modeling", *Water Science and Technology*, Vol. 72 (1), pp. 123–134, 2015. [CrossRef]

[50] S. Zerrouki, R. Rihani, K. Lekikot, and I. Ramdhane, "Enhanced biogas production from anaerobic digestion of wastewater from the fruit juice industry by sonolysis: experiments and modelling", *Water Science and Technology*, Vol. 84 (3), pp. 644–655, 2021. [CrossRef]

[51] O. I. Maile, H. Tesfagiorgis, and E. Muzenda, "The potency of monoethanolamine in biogas purification and upgrading", 2017. [CrossRef]